LUND UNIVERSITY
Faculty of Science

# Unified theory and experimental approach for measuring restricted diffusion and water exchange

Arthur Simbarashe Chakwizira

Thesis submitted for the degree of Master of Science
Project duration: 5 months

Supervised by Markus Nilsson and Filip Szczepankiewicz

Department of Medical Radiation Physics

May 2020

**Abstract**

Fifteen million people lose their lives to stroke and cancer every year. This amounts to one in every four deaths worldwide, making these among the deadliest diseases affecting humankind. Fruitful attempts at containing stroke- and cancer-related mortality hinge on early detection. Diffusion MRI (dMRI) is an imaging modality that is sensitive to tissue microstructure, and therefore unveils tissue changes before they become visible on morphological images. Maps of the apparent diffusion coefficient (ADC) find routine clinical use for cancer and stroke diagnosis. More detailed microstructural information is obtained by time-dependent dMRI, which probes the diffusion of water restricted within cells and exchanging between cellular environments. Measurements of water restriction and exchange yield estimates of cell size and permeability, respectively. Tracking these features may be important for reliable tumour characterisation and evaluation of treatment response. Estimating cell size and permeability is a challenge because the phenomena of restriction and exchange have opposing effects on the diffusion-weighted signal. With increasing diffusion time, restriction elevates the signal while exchange decreases it. Restriction and exchange can therefore not be disentangled by solely varying the diffusion time in a dMRI experiment. Typical models assume that restriction is prevalent at short time scales while exchange is dominant at long time scales. Estimates of size and exchange are made independently by doing experiments in different time regimes. Nevertheless, previous research has highlighted that this approach may induce inaccuracy in estimated diffusion metrics. In light of this, the objective of this thesis work was to develop a unified theoretical framework and experimental approach for measuring restriction and exchange at all time scales. Extending previous work, a commonly used model of exchange within dMRI - the Kärger model - was generalised to accommodate arbitrary gradient waveforms. By incorporating the restriction information contained in the diffusion spectrum, this thesis work derived a general unified model of restriction and exchange that is valid for all time scales, gradient waveforms and b-values. In other words, the proposed model is an exact solution to the problem at hand. With the aim of deriving a complementary theory more informative for experimental design, an alternative approach employing the relation between the particle velocity autocorrelation function and the diffusion spectrum was also explored. This yielded a second-order signal representation applicable to any gradient waveform, all time scales and moderate b-values. Monte-Carlo simulations were performed on a synthetic structure to validate the developed theory. Excellent agreement between simulated and estimated parameters was observed. Numerically optimised gradient waveforms improved precision in parameter estimates by a factor of 2 in relation to standard pulsed-gradient sequences. In a word, this thesis work presents a general, unified theoretical framework describing the effects of restricted diffusion and water exchange on the diffusion-weighted signal. The results pave the way for future research involving optimisation of experiments to minimise scan times, which is a crucial step towards clinical implementation.

## Popular abstract (Swedish)

Drygt femton miljoner människor avlider av cancer och stroke varje år, vilket gör dem till några av de svåraste sjukdomarna som vi drabbas av. Dödligheten hos dessa sjukdomar påverkas främst av när dem upptäcks. Ju tidigare sjukdomen diagnostiseras, desto högre blir sannolikheten för att den botas. Tidig upptäckt kräver känsliga diagnostiska metoder, särskilt de som kan detektera förändringar i vävnaden innan de visas på vanliga anatomiska bilder. Diffusions MR (dMRI) är en bildgivande metod som är känslig mot vävnadens mikroskopiska struktur och funktion. dMRI kan således detektera förändringar innan de syns på konventionella medicinska bilder. Mätningar av diffusionshastigheten hos vattenmolekyler används rutinmässigt inom kliniken för att diagnostisera cancer och stroke. Mer information om vävnadens mikrostruktur utöver diffusionshastigheten kan bidra till diagnos och karakterisering av tumörer, samt utvärdering av respons på behandling. Sådan information kan erhållas med hjälp av så kallad tidsberoende dMRI, vilket möjliggör mätning av cellernas storlek och genomsläpplighet. Dessa cellegenskaper är dock svåra att mäta på grund av att de har motsatta effekter på den insamlade MR signalen. En minskning av signalen kan antingen bero på att cellen har blivit större eller att genomsläppligheten har ökat, vilket gör det svårt att särskilja de två effekterna. Befintliga modeller inom dMRI antar att cellstorleken är viktig endast vid korta tidskalor, och genomsläpplighet är relevant endast vid långa tidskalor. Genom att utföra experiment på olika tidskalor kan man erhålla uppskattningar av cellstorlek och genomsläpplighet. Det har dock visats att denna metod kan införa osäkerheter i de uppmätta egenskaperna. Syftet med detta examenarbete var därmed att utveckla en teori och experimentell metod för att kunna mäta cellstorlek och genomsläpplighet utan att göra de ovan beskrivna antaganden. Detta gjordes genom att generalisera och kombinera befintliga teorier som beskriver effekterna av cellstorlek och genomsläpplighet på MR-signalen. Den generaliserade teorin gör det möjligt att designa, optimera och utföra experiment som ger pålitliga mätningar av cellstorlek och genomsläpplighet. Datorsimuleringar utfördes för att validera den utvecklade teorin. Teorin visade god överensstämmelse med simuleringarna. Detta arbete utgör ett viktigt tillägg i forskningsområdet dMRI. Resultaten kan användas som utgångspunkt för framtida forskning inom optimering av experiment för att minimera undersökningstider. På så sätt kan metoden eventuellt implementeras i kliniken.

# List of abbreviations and acronyms

| | |
|---|---|
| SDE | Single Diffusion Encoding |
| DDE | Double Diffusion Encoding |
| dMRI | Diffusion Magnetic Resonance Imaging |
| ADC | Apparent Diffusion Coefficient |
| VA | Velocity Autocorrelation |

# Contents

# 1 Introduction

Cancer and stroke remain among the leading causes of death worldwide [1]. In 2018 alone, cancer single-handedly claimed just shy of ten million lives. Stroke affects fifteen million people every year, killing five million and permanently crippling just as many [1]. Notwithstanding recent surges in medicine towards battling these diseases, they pose a dire threat to human health. Innovation of more sensitive diagnostic tools lies at the heart of successfully alleviating cancer- and stroke-related mortality.

The prognosis of any disorder is greatly improved by early detection. As regards cancer and stroke, magnetic resonance imaging (MRI) has proved a vastly potent instrument in the arsenal of modern imaging techniques. MRI owes its success to the ability to deliver high resolution diagnostic data without exposing the patient to ionising radiation. The ample quantity of water and the delicate transport of its molecules in the body are exploited instead. Conventional MRI provides morphological images that are invaluable for the diagnosis and treatment planning of brain tumours [2]. However, a greater head start is offered by a diagnostic tool capable of revealing tissue alterations before they manifest on anatomical images. This demands an imaging modality that is sensitive to tissue micro-architecture and molecular function. Diffusion MRI (dMRI), by virtue of its immaculate sensitivity to the random displacement of water molecules, provides a non-invasive marker of tissue microstructure [3, 4, 5, 6]. Indeed, diffusion-weighted images show an elevated signal, and correspondingly reduced apparent diffusion coefficient (ADC), in ischaemic tissue almost immediately after onset. T2-weighted images, by comparison, only show the corresponding tissue change hours following onset [3, 7].

Prospects of early detection and eventual eradication of pathology increase with the amount of information that can be reliably inferred from registered images. The ADC - although highly sensitive - does not communicate microstructural features such as cell sizes and membrane permeability [4, 8]. Capturing the temporal dynamics of these quantities enables non-invasive tumour characterisation and assessment of treatment response [9]. Alterations in cell size are indicative of cell proliferation or therapy-induced cell death, while permeability is a direct reflection of membrane integrity [10, 11]. In the same breath, explicitly treating cells as objects of finite size bounded by permeable membranes gives more accurate estimates of ADC [11, 12]. The need for knowledge of cell sizes and permeability necessitates time-dependent diffusion MRI. Water molecules restricted within cells demonstrate time-dependent rates of diffusion that are characteristic of the geometry of confinement [12, 13, 14]. The rate of exchange of water molecules between cellular environments is proportional to membrane permeability [12]. Hence, probing restriction and exchange using time-dependent dMRI provides estimates of cell size and permeability.

Measuring restriction and exchange is rendered a non-trivial challenge by the conflicting influences that the two phenomena have on the diffusion-weighted signal. As the diffusion time increases, the effect of exchange is to deplete the registered signal, while restriction acts to the contrary by raising it [15]. Consequently, any dMRI experiment that endeavours to probe time-dependence by varying the diffusion time fails to disentangle the two effects. Exchange estimates are invariably confounded by restriction, and the converse is true of size estimates.

To date, restriction and exchange are measured via the assumption that the two effects prevail in distinct time regimes. Particularly, cells are treated as impermeable enclosures at short time scales, enabling a size estimation while neglecting exchange. On the opposite end of the spectrum - long time scales - exchange is inferred by regarding cells as components devoid of geometry [12]. It goes without saying that a just reflection of reality would be a theory encompassing both restriction and exchange phenomena at all time scales. This presents a research gap in the field of dMRI and an attempt at addressing the void was the central aim of this thesis work. The project builds on the work of Nilsson et al. [15], who developed a unified model of restriction and exchange that is applicable to systems with slow exchange, short time scales and moderate b-values. Nilsson demonstrated the superiority of numerically optimised gradient waveforms over conventional pulsed-gradient spin-echo (PGSE) sequences. The present work aimed at addressing the shortcomings of the unified model and building a general and robust theory of restriction and exchange. Flexibility of experimental design was maintained by ensuring that the theory could accommodate arbitrary gradient waveforms.

# 2 Background

The discovery of the nuclear magnetic resonance phenomenon dates back to 1938 when Isidor Isaac Rabi observed the emission of radio waves at well-defined frequencies from a beam of molecules traversing a magnetic field [16]. His work earned him the 1944 Nobel Prize in Physics. Felix Bloch and Edward Mills Purcell later demonstrated the phenomenon in solids and liquids, providing the first experimental description in 1946 [17, 18, 19] and receiving the 1952 Nobel Prize in Physics. Already in 1971, Raymond Damadian highlighted the potential of differences in relaxation rates for differentiating between healthy and cancerous tissue [20]. Paul C Lauterbar [21] showed in 1973 that nuclear magnetic resonance could be used to generate an anatomical image, receiving the 2003 Nobel Prize in Physiology or Medicine together with Sir Peter Mansfield [16]. These pioneering breakthroughs saw the dawn of a cascade of research and clinical applications of magnetic resonance. This section provides a succinct review of the fundamental principles of MRI, the physics of diffusion and the foundation of diffusion MRI. In addition, models

used to describe restricted diffusion and water exchange in the field of dMRI are briefly discussed.

## 2.1 Principles of MRI

Hydrogen nuclei bear a non-zero net spin and therefore possess a net magnetic moment [22]. Unperturbed, the spin vectors exhibit random orientations in matter, giving rise to zero net magnetisation. Exertion of a strong static magnetic field induces spin precession about the direction of the field. The precession frequency - directly proportional to the field strength - is called the Larmor frequency and is a physical quantity of paramount importance. In the presence of the field, a measurement of the magnetisation of an individual proton would yield one of two results: spin-up (parallel to the field) or spin-down (anti-parallel) [23]. However, an MRI experiment registers signal from ensembles of interacting spins, leading to a largely isotropic distribution of spin orientations. There is, nevertheless, a slight skewing of the distribution in the direction of the field, giving rise to a net magnetisation vector. In equilibrium, this vector is stationary, but otherwise precesses about the static magnetic field at the Larmor frequency [23].

The energy difference between the spin-up and spin-down states corresponds to the energy of electromagnetic radiation in the radio-frequency (RF) regime. Radio waves can thus be utilised to influence the magnetisation vector. Indeed, as perceived from a rotating frame of reference, the effect of an RF pulse in resonance with the precession is to rotate the magnetisation vector into a plane perpendicular to the static field. In this plane, the precession of the magnetisation vector becomes rotational motion. This produces a time-varying magnetic field capable of inducing a current in a conducting coil. The induced current is the MR signal [17, 22].

Exposure of the magnetisation to an RF pulse perpendicular to the static field is called excitation. Once the excitation pulse is terminated, relaxation commences forthwith to return the system to equilibrium. Longitudinal restoration of the magnetisation occurs due to energy loss to the lattice and is characterised by the time-constant $T_1$. Transverse relaxation is driven by spin dephasing either due to interaction with neighbouring spins or inhomogeneities in the static field (time constant $T_2$ or $T_2^*$, respectively). The transverse net magnetisation thus decays over time and so does the registered MR signal [17, 22].

All the phenomena described above can be encapsulated into the Bloch equation [18], which reads

$$\frac{d\boldsymbol{M}}{dt} = \gamma \boldsymbol{M} \times \boldsymbol{B} - \frac{M_x + M_y}{T_2} - \frac{M_z - M_0}{T_1} \tag{1}$$

where $\boldsymbol{M} = (M_x \ M_y \ M_z)^T$ is the magnetisation vector, $\gamma$ is the gyromagnetic constant, $\boldsymbol{B}$ is the external magnetic field, $M_0$ is the equilibrium magnetisation and $T_1$ and $T_2$ are time constants for longitudinal and transverse relaxation, respectively. The gist of equation 1 is that the magnetisation is given rise to by the magnetic field $\boldsymbol{B}$ and dissipated both longitudinally and transversely. A solution of equation 1 provides a description of the time-evolution of the MR signal as a function of $T_1$ and $T_2$. Note that equation 1 (and all experimental designs based on it) assumes that spins are stationary.

An MRI experiment involves - in addition to the static magnetic field and the RF - a combination of spatially varying magnetic fields (gradients) whose purpose is to localise the registered MR signal to a given voxel [17, 22]. The blend of gradients consists of a frequency-encoding ($G_x$), phase-encoding ($G_y$) and slice-selection ($G_z$) component. An elucidative illustration of the function of these components is the basic spin-echo experiment shown in Figure 1. Excitation is done by the 90° pulse while the 180° is a refocusing

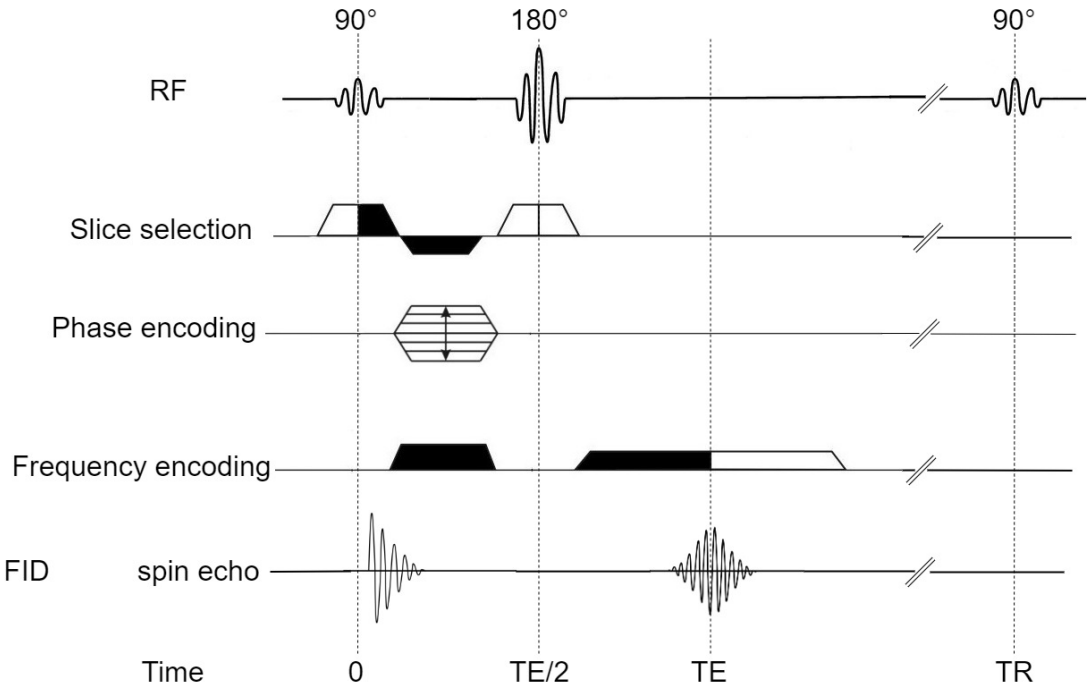


Figure 1: Spin-echo experiment. The 90° excitation RF pulse is followed by the 180° refocusing pulse. Slice-selection gradients restrict the effect of the RF pulses to a specific slice. The phase-encoding and frequency-encoding gradients localise signal vertically and horizontally, respectively. All gradients save the phase-encoding are balanced to eliminate undesired signal loss. The FID (Free Induction Decay) is the signal directly preceded by the 90° pulse. The echo used for image generation is registered at the echo-time (TE). The experiment is repeated after a repetition time (TR).

pulse that eliminates the effects of inhomogeneities in the static field. The slice-selection gradient localises the excitation (and refocusing) to a desired slice of the imaged volume. The negative gradient shown in black serves to reverse the spin dephasing (and consequent signal loss) caused by the section of $G_z$ shaded black. Signal localisation in the vertical axis ($y$) is enabled by the phase-encoding gradient which is applied in that direction. While on, the gradient changes both the precession frequency and phase of the spins, but the frequency is restored when the gradient is switched off. On the contrary, the induced position-dependent phase changes persist until the signal is registered at the echo time (TE). The frequency-encoding gradient is applied along the horizontal ($x$) axis and localises the signal in this direction based on the induced position-dependent precession frequencies. A preparation pulse shown in black in the time interval [0 TE/2] reverses spin dephasing due to the section of $G_x$ leading up to TE. Note that the axes $x, y$ and $z$ are used here to indicate the relative orientations of the gradients, but their actual directions in the imaged volume can be chosen arbitrarily. Signal arising directly after the 90° pulse is termed the free induction decay (FID) and the signal used to generate the MR image is the echo. The time taken to repeat the experiment in Figure 1 is called the repetition time (TR).

## 2.2 Principles of diffusion

Brownian motion was first observed in 1827 by Robert Brown, who noticed the incessant oscillation of pollen grains suspended in water [24]. Adolf Fick hypothesised in 1855 that the flux through a boundary is proportional to the concentration gradient across it, arriving at what is now recognised as Fick's first law of diffusion [25]:

$$J = -D \cdot \nabla C \tag{2}$$

where $J$ is the flux, $C$ is the concentration and $D$ is the diffusion coefficient. Note that equation 2 is valid in isotropic media. If this condition is not met, $D$ becomes a tensor that may be represented by the matrix [26]:

$$\boldsymbol{D} = \begin{bmatrix} D_{xx} & D_{xy} & D_{xz} \\ D_{yx} & D_{yy} & D_{yz} \\ D_{zx} & D_{zy} & D_{zz} \end{bmatrix} \tag{3}$$

The continuity equation for $C$ dictates that the rate of change of particle concentration in a given volume must be equal to the net flux across the boundaries. Assuming that there is no source inside the volume, this relation can be expressed

$$\frac{\partial C}{\partial t} = -\nabla \cdot J \tag{4}$$

Combining equations 2 and 4 provides Fick's second law of diffusion:

$$\frac{\partial C}{\partial t} = D\nabla^2 C \tag{5}$$

Fick's laws predict a zero net flux in the absence of a concentration gradient, disregarding diffusion driven by thermal fluctuations (so-called self-diffusion). Einstein introduced a probabilistic interpretation of Fick's laws and arrived at an expression for the mean-square-displacement of a diffusing particle from its starting position [27]:

$$\langle [\boldsymbol{r}(t) - \boldsymbol{r}(0)]^2 \rangle = 2nDt \tag{6}$$

where $n$ is the number of spatial dimensions and $\boldsymbol{r}$ is the particle position vector. Equation 6 can also be interpreted as the variance of the individual step lengths taken by the particle, with time $t$ being replaced by the duration of steps ($\Delta t$). Self-diffusion can thus be described by a propagator ($P(x_1|x_0, t)$), which is a probability density function that gives the probability of finding the particle at position $x_1$ given that it started at $x_0$ and diffused for a time $t$ [14, 28]. An expression for the propagator may be obtained by solving Fick's second law and replacing the concentration $C$ with probability density $P$ to obtain:

$$P(x_1|x_0, t) = \frac{1}{\sqrt{2\pi \cdot 2Dt}} \cdot \mathrm{e}^{-\frac{(x_1 - x_0)^2}{2 \cdot 2Dt}} \tag{7}$$

which is a Gaussian distribution with variance equal to the right-hand-side of equation 6. The generalisation of equation 7 to higher spatial dimensions is straightforward.

### 2.2.1 On the diffusion spectrum

The motion of a particle diffusing in a confinement can be resolved into frequency components, giving rise to a spectrum of diffusivities [29]. A heuristic but useful interpretation is that a confinement renders the particle displacement perfectly sinusoidal in time. The maximum amplitude of the oscillations is dictated by the size of the confinement. A constraint on displacement at a given frequency translates to a restraint on the velocity at that frequency. Motion at high frequency may attain the maximum possible particle velocity (the intrinsic value). On the contrary, the velocity at low frequency is determined by the confinement size. The result is a diffusion spectrum whose shape is characteristic of the geometry of confinement. This interpretation holds even in a more realistic scenario where restricted diffusion is not oscillatory [29].

Generally, the diffusion spectrum is defined as the Fourier transform of the velocity autocorrelation function [14, 29, 30]:

$$D(\omega) = \int_{-\infty}^{\infty} \langle v(0)v(t) \rangle \mathrm{e}^{-i\omega t} dt \tag{8}$$

Stepisnik [14] derived $D(\omega)$ for parallel planes, cylinders and spherical geometries. For ease of reference, the result for cylinders is given below

$$D(\omega) = \sum_n B_n \cdot \frac{a_n D_0 \omega^2}{a_n^2 D_0^2 + \omega^2} \tag{9}$$

where $D_0$ is the intrinsic diffusivity and

$$B_n = \frac{2(R/\mu_n)^2}{\mu_n^2 - 1} \tag{10}$$

and

$$a_n = \left(\frac{\mu_n}{R}\right)^2 \tag{11}$$

where $\mu_n$ are the roots of $J_1'(\mu) = 0$ and $J_1'$ is a Bessel function of the first order and kind. $R$ is the radius of the cylinder.

## 2.3 Principles of diffusion MRI

As earlier alluded to, the Bloch equation describing the MRI experiment makes no provision for spin transport. Rather, water molecules are assumed to be fully *in situ*. Motion may be incorporated into the Bloch equation by considering the continuity equation for the magnetisation $\boldsymbol{M}$ [31]:

$$\frac{\partial \boldsymbol{M}}{\partial t} = R(t) - \nabla \cdot J(\boldsymbol{M}) \tag{12}$$

where $R(t)$ represents a source-sink process (the right-hand-side of the Bloch equation) and $J(\boldsymbol{M})$ is a flux term denoting an arbitrary mode of spin transport (such as diffusion or flow). The solution of equation 12 depends on the choice of the flux term $J$. In fact, different choices of $J$ yield distinct MRI techniques. $J = 0$ gives T1/T2-weighted imaging [31]. Torrey [32] defined $J$ according to Fick's first law (equation 2) arriving at the renowned Bloch-Torrey equation:

$$\frac{\partial \boldsymbol{M}}{\partial t} = \gamma \boldsymbol{M} \times \boldsymbol{B} - \frac{M_x + M_y}{T_2} - \frac{M_z - M_0}{T_1} - \nabla \cdot (D \nabla \boldsymbol{M}) \tag{13}$$

Diffusional motion can be encoded into the MR signal by the introduction of additional gradient pulses into the spin-echo experiment (Figure 1). A pedagogical illustration is the Stejskal-Tanner experiment, shown schematically in Figure 2 [33, 34].

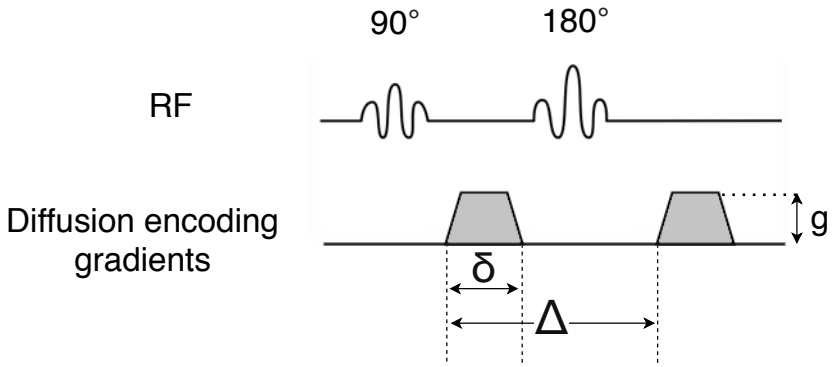


Figure 2: The Stejskal-Tanner experiment (single diffusion encoding). Two gradient pulses are added to the spin-echo sequence of Figure 1, on either side of the 180° pulse. In the absence of incoherent spin motion, the gradients cause no net dephasing and have no effect. Incoherent motion such as diffusion leads to phase dispersion and consequent signal loss. $\delta$, $\Delta$ and $g$ represent the pulse duration, interval and amplitude, respectively.

This sequence is also referred to as Single Diffusion Encoding, stemming from the fact that a single pair of gradient pulses are used to probe diffusion. One gradient pulse is applied following the excitation RF-pulse, and another after the refocusing RF-pulse. What transpires between the cessation of the first pulse and the onset of the second is the backbone of diffusion MRI. The essence of the experiment is that, in the absence of incoherent motion between the two pulses, the spin dephasing due to the first pulse is exactly reversed by the second pulse. Consequently, the diffusion-encoding gradients have no influence on the MR signal and a T2-weighted image is obtained. Nevertheless, should spins migrate incoherently (as by diffusion), the second pulse does not fully eliminate the dephasing due to the first pulse. A phase dispersion ensues and manifests itself as an attenuation of the MR signal [34, 35]. The phase change following exposure to a magnetic field gradient $\boldsymbol{g}(t) = [g_x(t)\ \ g_y(t)\ \ g_z(t)]$ for a time $T$ is given by

$$\phi(T) = \gamma \int_0^T \boldsymbol{g}(t) \cdot \boldsymbol{r}(t) dt \tag{14}$$

where $\boldsymbol{r}(t)$ is the particle position vector [14]. Note that the functional form of $\boldsymbol{g}(t)$ is referred to as the gradient waveform. Let $f_\phi$ denote the probability density function of the phase $\phi$. The signal attenuation due to phase dispersion can then be described by

$$S = \int_{-\infty}^{\infty} \mathrm{e}^{-i\phi} f_\phi d\phi \equiv \langle \mathrm{e}^{-i\phi} \rangle \tag{15}$$

where the average is taken over all contributing spins. An intuitive interpretation of equation 15 is that there is no signal attenuation when there is no spin dephasing, and for arbitrarily large phase changes, the signal vanishes.

An alternative signal representation employs the propagator formalism introduced in equation 7. Assuming gradient pulses of short duration, the diffusion-weighted signal can be approximated by the Fourier transform of the averaged diffusion propagator [28, 36, 37, 38]:

$$S(q) = \int \overline{P}(x, t_d) \cdot e^{-iq \cdot x} dx \tag{16}$$

where $x := x_1 - x_0$, $t_d$ is the diffusion time and $q$ is the magnitude of an important quantity called the q-vector, related to the gradient waveform through:

$$\boldsymbol{q} = \frac{\gamma}{2\pi} \delta \boldsymbol{g} \tag{17}$$

where $\delta$ is the pulse width as shown in Figure 2. In the case of free diffusion in homogeneous media, the average diffusion propagator is described by the Gaussian [36, 37, 38]

$$\overline{P}(x, t_d) = \frac{1}{\sqrt{4\pi D t_d}} \cdot e^{-\frac{x^2}{4Dt_d}} \tag{18}$$

Substituting equation 18 into equation 16 gives

$$S(q) = e^{-4\pi^2 q^2 D t_d} \tag{19}$$

where $t_d = \Delta$ (the pulse spacing) assuming arbitrarily narrow gradient pulses. Stejskal and Tanner [34] showed that, for any pulse duration, the diffusion time is given by $t_d = \Delta - \delta/3$. Equation 19 can be written

$$S(b) = e^{-bD} \tag{20}$$

where

$$b = 4\pi^2 q^2 \cdot (\Delta - \delta/3) \tag{21}$$

is called the b-value and captures the amount of diffusion encoding performed by the gradient $\boldsymbol{g}$. Equation 20 is a highly important result.

Note that $q$ has been treated as a constant in the formalism above, and this is only true under the assumption of narrow gradient pulses. A more general definition of the q-vector can be expressed [35]

$$\boldsymbol{q}(t) = \gamma \int_0^t \boldsymbol{g}(\tau) d\tau \tag{22}$$

and the corresponding general definition for $b$ becomes

$$b = \int_0^T q^2(t) dt \tag{23}$$

where $T$ is the total diffusion encoding time. The apparent diffusion coefficient, $D$, is equal to the bulk diffusivity ($D_0$) in the case of free diffusion. Given a sample with a distribution of diffusivities, denoted $P(D)$, the signal attenuation can be written as the average value

$$S(b) = \int e^{-bD} P(D) dD \equiv \langle e^{-bD} \rangle \tag{24}$$

Diffusion in inhomogeneous media is not free and is more appropriately described by a time-dependent diffusivity, $D(t)$. Expressions for $D(t)$ in specific time regimes for PGSE experiments have been presented pedagogically elsewhere [12, 13, 28]. Worth highlighting is that the problem of time-dependent diffusion has solutions for short time scales and times approaching the tortuosity limit. The form of $D(t)$ in the intermediate time regime has at best been estimated via interpolation between the solutions in the two extremes. To compound the challenge, there is no general solution for time-dependence with arbitrary gradient waveforms on any time scale [28]. A common approach is to use the diffusion spectrum introduced in Section 2.2.1 to arrive at the signal representation [14, 28, 30]:

$$\ln S \approx -\frac{1}{2\pi} \int_{-\infty}^{\infty} D(\omega) |Q(\omega)|^2 d\omega \tag{25}$$

where $Q(\omega)$ is the Fourier transform of $q(t)$:

$$Q(\omega) = \int_{-\infty}^{\infty} q(t) \cdot e^{-iwt} dt \tag{26}$$

## 2.4 Biophysical models and the cumulant expansion

The complexity of biological systems is projected onto any biophysical model that purports to capture the salient features of such systems. While suitable for forward modelling, the resulting mathematical descriptions may not offer insights that are valuable for experimental design. A remedy worth introducing is the mathematical instrument called the cumulant expansion. Its objective is to approximate sophisticated model representations with intuitive expressions whose terms bear fundamental physical significance. Although liable to inaccuracy due to its approximative nature, the benefits entailed by the cumulant expansion are considerable.

### 2.4.1 Principles of moments and cumulants

Given a random variable $X$ with probability density function $f_X$, the $n$-th moment of the probability distribution of $X$, $\mu_n$, is given by

$$\mu_n = \langle X^n \rangle = \int_{-\infty}^{\infty} x^n f_X(x) dx \tag{27}$$

where $\langle\cdot\rangle$ denotes an expectation value. Evaluating moments using the integral in equation 27 poses a growing challenge as the order $n$ increases. A common strategy is to introduce the so-called moment-generating function which is defined by [39, 40]

$$M(t) = \langle \mathrm{e}^{tx} \rangle = \int_{-\infty}^{\infty} \mathrm{e}^{tx} f_X(x) dx \tag{28}$$

where $t$ is a dummy variable. The moment-generating function is considered to exist if there exists a positive real number $\xi$ such that the integral in equation 28 converges for all $t \in [-\xi, \xi]$. Performing a Taylor series expansion of equation 28 yields

$$M(t) = \left\langle 1 + tx + \frac{t^2x^2}{2!} + \frac{t^3x^3}{3!} + ... \right\rangle = \int_{-\infty}^{\infty} \left( 1 + tx + \frac{t^2x^2}{2!} + \frac{t^3x^3}{3!} + ... \right) f_X(x) dx \tag{29}$$

Hence, the moment-generating function can be expressed as a polynomial of the moments of the distribution of $X$ [39, 40]:

$$M(t) = \langle 1 \rangle + t\langle x \rangle + \frac{t^2\langle x^2 \rangle}{2!} + \frac{t^3\langle x^3 \rangle}{3!} + ... = 1 + t\mu_1 + \frac{t^2\mu_2}{2!} + \frac{t^3\mu_3}{3!} + ... \tag{30}$$

The power of exploiting the moment-generating function is that, contrary to evaluating the $n$-th order moment via the integral in equation 27, it is now given by the $n$-th derivative of $M(t)$ evaluated at $t = 0$. That is

$$\mu_n = \left. \frac{d^n M(t)}{dt^n} \right|_{t=0} \tag{31}$$

The cumulant-generating function is defined as the logarithm of the moment-generating function [39, 40]

$$C(t) := \ln M(t) = \ln \left( 1 + t\mu_1 + \frac{t^2\mu_2}{2!} + \frac{t^3\mu_3}{3!} + ... \right) \tag{32}$$

and can also be expressed as a polynomial in cumulants of the distribution of $X$, $c_n$:

$$C(t) = tc_1 + \frac{t^2c_2}{2!} + \frac{t^3c_3}{3!} + ... \tag{33}$$

Taylor-expanding equation 32 and comparing coefficients of $t^n$ with those in equation 33 yields relationships between the cumulants and moments of the distribution of $X$:

$$\begin{aligned} c_1 &= \mu_1 \\ c_2 &= \mu_2 - \mu_1^2 \\ c_3 &= \mu_3 - 3\mu_1\mu_2 + 2\mu_1^3 \\ c_4 &= \mu_4 - 4\mu_1\mu_3 + 12\mu_1^2\mu_2 - 3\mu_2^2 - 6\mu_1^4 \\ &\vdots \qquad\qquad\qquad \vdots \end{aligned} \tag{34}$$

A general expression relating the $n$-th order cumulant to the moments has been provided by Zheng [39] and Rodriguez and Tsallis [40].

### 2.4.2 Applications in diffusion MRI

The convenience brought by the cumulant expansion is made apparent by applying the principles described above to the following signal representation

$$S/S_0 = \langle \mathrm{e}^{-i\phi} \rangle \tag{35}$$

which describes the signal attenuation due to diffusion-induced spin dephasing averaged over all contributing spins. In the absence of flow, the distribution of $\phi$ may be assumed symmetric, implying that all moments of odd order are zero. To fourth order, equation 35 can be written

$$\ln(S/S_0) \approx -\frac{1}{2}c_2 + \frac{1}{24}c_4 \tag{36}$$

Using the relations between cumulants and moments in 34, the following approximation is obtained

$$\ln(S/S_0) \approx -\frac{1}{2}\langle\phi^2\rangle + \frac{1}{24}(\langle\phi^4\rangle - 3\langle\phi^2\rangle^2) \tag{37}$$

Equivalently, the signal equation

$$S(b)/S_0 = \langle \exp(-bD) \rangle \tag{38}$$

can be approximated with

$$\ln(S(b)/S_0) \approx -b \cdot \langle D \rangle + \frac{b^2}{2} \cdot \left[ \langle D^2 \rangle - \langle D \rangle^2 \right] \tag{39}$$

which is linear in the mean and variance of the diffusivities.

## 2.5 Water exchange

The theory presented in preceding sections deals with a single pool or continua of spins. Tissue models typically include two distinct compartments arbitrarily associated with the names “intracellular” and “extracellular”. The Bloch-Torrey equation can be transformed into a coupled system of differential equations representing the communication between two pools of spins (labelled 1 and 2 below) [31]:

$$\begin{aligned} \frac{\partial \boldsymbol{M}_1(t)}{\partial t} &= R_1(\boldsymbol{M}_1) - \nabla J_1(\boldsymbol{M}_1) - E_{12}\boldsymbol{M}_1 + E_{21}\boldsymbol{M}_2 \\ \frac{\partial \boldsymbol{M}_2(t)}{\partial t} &= R_2(\boldsymbol{M}_2) - \nabla J_2(\boldsymbol{M}_2) - E_{21}\boldsymbol{M}_2 + E_{12}\boldsymbol{M}_1 \end{aligned} \tag{40}$$

where $E_{12}$ denotes the exchange rate from compartment 1 to 2, and similarly for $E_{21}$. The net magnetisation is given by the superposition of the individual magnetisations in the two compartments:

$$\boldsymbol{M} = \boldsymbol{M}_1 + \boldsymbol{M}_2 \tag{41}$$

These equations lead to a prominent model of exchange within diffusion MRI: the Kärger model [41]. It assumes two well-mixed pools occupying the entire available voxel volume. The two pools are associated with signal fractions $f_1$ and $f_2$ satisfying $f_1 + f_2 = 1$. Relaxation characteristics are assumed identical, allowing the Bloch terms in equation 40 to be neglected. Further, Gaussian diffusion is assumed in both pools, permitting constant diffusivities. Exchange is represented by a constant rate matrix, implicitly implying that the exchange probability is independent of time or position. In one dimension, the Kärger model is described by

$$\frac{\partial}{\partial t}\begin{pmatrix} M_1 \\ M_2 \end{pmatrix} = [K - Dq^2]\begin{pmatrix} M_1 \\ M_2 \end{pmatrix} \tag{42}$$

where $K$ (the rate matrix) and $D$ (a diagonal matrix of diffusivities) are given by

$$K = \begin{bmatrix} -k_{12} & k_{21} \\ k_{12} & -k_{21} \end{bmatrix} \quad ; \quad D = \begin{bmatrix} D_1 & 0 \\ 0 & D_2 \end{bmatrix}$$

Note that $q$ in equation 42 is constant. Noteworthy derivatives of the Kärger model include FEXI (Filtered Exchange Imaging) and CG (constant gradient) [43], both of which have demonstrated sensitivity to transcytolemmal water exchange (labelled $k_{12}$ above). It is vital to mention that all these exchange models do not account for the geometry of restriction. Diffusion is assumed to be free everywhere - an assumption supported by the finding that time-dependent diffusion dominates only at short time scales. In addition, the models demand specific pulse sequences and make no room for arbitrary gradient waveforms. The latter issue has been addressed by Ning et al. [44] using a cumulant expansion of the phase distribution which was introduced in section 2.4. Herein, the theory developed by Ning et al. will be referred to as the Ning model.

The Ning model shares the same assumptions as the Kärger model, with the exception of the demands on the gradient waveform. Arbitrary gradient waveforms are accommodated by the Ning model via the following generalisation of the Kärger equations:

$$\frac{\partial}{\partial t}\begin{pmatrix} S_1 \\ S_2 \end{pmatrix} = [K - Dq(t)^2]\begin{pmatrix} S_1 \\ S_2 \end{pmatrix} \tag{43}$$

where $S_1$ and $S_2$ are signals from pools 1 and 2, respectively, and $q(t)$ needs not be constant. In cases where $q(t)$ is constant (SDE with narrow pulses) or piecewise constant (DDE with narrow pulses), analytical solutions to the system in equation 43 exist and are given by

$$S_{SDE}(q, T) = \mathbb{1} \cdot \exp([K - Dq^2]T) \cdot F \tag{44}$$

$$S_{DDE}(q_1, q_2, \Delta_1, \Delta_2, t_m) = \mathbb{1} \cdot \exp([K - Dq_2^2]\Delta_2) \cdot \exp(Kt_m) \cdot \exp([K - Dq_1^2]\Delta_1) \cdot F \quad (45)$$

where $\mathbb{1} = [1\ \ 1]$, $F = [f_1\ \ f_2]'$, $T$ is the total encoding time, the subscripts 1 and 2 on $q$ and $\Delta$ represent the first and second pair of pulses in a DDE sequence and $t_m$ is the mixing time. A closed-form solution of this kind does not exist when $q(t)$ is a smooth function of time (that is, for arbitrary gradients). Using a stochastic calculus approach, Ning et al. evaluated the cumulants of the phase distribution in equation 37 and arrived at the following signal representation

$$\ln S \approx -\overline{D}b + \frac{1}{2}\mathrm{Var}(D)h(\cdot)b^2 \quad (46)$$

where $h(\cdot)$ is the exchange-weighting function given by

$$h(\cdot) = \frac{2}{b^2}\int_0^T e^{-kt} q_4(t)dt \quad (47)$$

where

$$q_4(t) = \int_0^T q^2(t_1)q^2(t_1 + t)dt_1 \quad (48)$$

and $k = k_{12} + k_{21}$ is the sum of the exchange rates between the two pools. If the product $kT$ is small enough to allow the approximation $e^{-kt} \approx 1 - kt$, the Ning model can be written

$$\ln S \approx -\overline{D}b + \frac{1}{2}\mathrm{Var}(D)(1 - k\Gamma)b^2 \quad (49)$$

where

$$\Gamma = \frac{2}{b^2}\int_0^T tq_4(t)dt \quad (50)$$

is the effective exchange weighting time that depends on the gradient waveform and the diffusion time.

## 2.6 Restricted diffusion

Numerous techniques have been proposed for probing restricted diffusion. Early approaches computed the diffusion propagator by taking the inverse Fourier transform of the measured signal in equation 16. An estimate of compartment diameter was obtained as the FWHM of this propagator [45]. Note that this is valid assuming short gradient pulses. In scenarios where the diffusion time is long, and diffusion is restricted by compartments of equal size, the function $S(q)$ takes the form of a diffraction pattern from which the compartment size can be estimated [45]. Other prominent models include

IMPULSED (imaging microstructural parameters using spectrally edited diffusion), POMACE (pulsed and oscillating gradient MRI for assessment of cell size and extracellular space) and VERDICT (vascular, extracellular and restricted diffusion for cytometry in tumours). IMPULSED and POMACE assume two compartments (intracellular and extracellular), while VERDICT assumes an additional vascular compartment. All three models are based on multiple PGSE and/or OGSE acquisitions and have shown promising results in *in vivo* studies [12].

Nilsson et al. [46], exploiting the geometry information carried by the diffusion spectrum, derived the following signal representation for cylindrical geometries:

$$S \approx \exp\left(-\frac{bV_\omega c d^4}{D_0}\right) \tag{51}$$

where $d$ is the cylinder diameter, $c$ is a geometry-dependent constant which has the value $7/1536$ for cylinders, $D_0$ is the bulk diffusivity and $V_w$ is a gradient waveform-dependent parameter with the definition

$$V_\omega = \frac{\int g^2(t)dt}{\int q^2(t)dt} = \frac{1}{2\pi b}\int \omega^2 |Q(\omega)|^2 d\omega \tag{52}$$

Equation 51 is valid for low frequencies where the diffusion spectrum can be approximated by the second-order polynomial:

$$D(\omega) \approx \frac{c d^4 \omega^2}{D_0} \tag{53}$$

The theory above will be referred to as the Nilsson model. A notable strength of the Nilsson model is its ability to accommodate arbitrary gradient waveforms: equation 52 places no restrictions on the shape of $q(t)$ or $g(t)$. However, none of the restriction models presented in this section take cell permeability (and therefore exchange) into account. Cells are modelled as impermeable spheres (or cylinders in the case of the Nilsson model).

## 2.7 Unification of restriction and exchange theory

Previous chapters clarified the existence of two classes of models for measuring restriction and exchange: one that describes exchange while disregarding restriction, and another that captures restriction while neglecting exchange. Negative effects of this approach on parameter estimation have been noted [11, 12, 13, 44]. The scarcity of literature on models describing both restricted diffusion and water exchange is indicative of the non-triviality of the problem.

In the short-time limit, Sen [47] provided an expression for time-dependent compartment diffusivities incorporating compartment radius of curvature and permeability. In

the long-time regime, an effective medium theory approach was proposed by Latour et al. [48] describing the effects of permeability on diffusion in this time scale. An accurate estimate of the permeability of yeast cells was obtained using this model. Models called "empirical permeable plane/spheres" also exist. Rather than directly measuring permeability, they account for its effect on the measured diffusivities using empirical formulae. Also worth the mention is the random permeable barrier model (developed by Novikov et al. [49]) which treats membranes as randomly oriented flat planes. This model has been used to estimate cell size and permeability *in vivo*.

Recently, Nilsson et al. [15] united the Ning model of exchange with the Nilsson model of restriction to arrive at a unified model capturing restriction and exchange effects to second order:

$$\ln S \approx -b \cdot E + \frac{1}{2} b^2 \cdot V \cdot (1 - k\Gamma) \tag{54}$$

where the mean term $E$ is given by

$$E = \overline{D} + \frac{V_\omega}{b} \overline{R} \tag{55}$$

where

$$R = \frac{cd^4}{D_0} \tag{56}$$

and the variance term $V$ is defined

$$V = \mathrm{Var}(D) + \frac{V_\omega}{b} \mathrm{Cov}(D, R) + \left( \frac{V_\omega}{b} \right)^2 \mathrm{Var}(R) \tag{57}$$

where $\mathrm{Cov}(\cdot)$ denotes covariance. The theory presented here will be referred to as the unified model. Monte-Carlo simulation-based validation by Nilsson et al. showed capacity to disentangle size and exchange. Numerically optimised gradient waveforms proved superior to traditional pulsed-gradient sequences. Note must be made, nonetheless, that this unified model is valid for moderate b-values since it is derived from a cumulant expansion. This limitation is strictly a restriction on the size of the product $bD$, but will be referred to simply as a restraint on b-value because this is the parameter that can be influenced by experiment. Further, the unified model requires that the exchange rate scaled by the total encoding time ($kT$) be small, because the approximation of the exchange-weighting term as $1 - k\Gamma$ is otherwise invalid. As noted for the b-value, this limitation will be termed a restriction on time scale since $T$ is the experimental parameter. As highlighted earlier, the unified model is based on an approximation of the diffusion spectrum with a second-order polynomial, which is well-grounded only at low frequencies. Eliminating all these weaknesses constitutes the substance of later chapters.

# 3 Theory

Theory developed during the thesis work is presented in this section. Its aim is to address the two major limitations associated with the unified framework by Nilsson et al. [15]: inaccuracy at high b-values and long time scales and invalidity at high frequencies in the diffusion spectrum. The former is tackled by generalising the Kärger model to accommodate arbitrary gradient waveforms, and the latter by proposing the use of the full diffusion spectrum as opposed to its low-frequency approximation. Aiming to derive an approximative signal representation to aid the extraction of insights from the developed theory, the velocity autocorrelation function is employed to evaluate cumulants of the phase distribution. The outcome is a signal equation capturing both restriction and exchange effects to second order.

## 3.1 Generalising the Kärger model

It is worth reiterating that, while the unified model describes the effects of exchange and restriction for any gradient waveform, it veers off truth at high b-values due to its foundation in cumulant space. Furthermore, the definition of the exchange weighting time ($\Gamma$) introduces inaccuracy as the product $kT$ grows. Both of these hurdles could be circumvented by using the closed-form solutions of the Kärger equations for SDE and DDE (equations 44 and 45) to describe exchange. However, while placing no restrictions on the magnitude of $b$ or $T$, these equations do demand that $q(t)$ be constant or piecewise constant. Eliminating this last restriction to obtain an exchange representation valid for any b-value, $T$ and $q(t)$ was the objective of this section of the thesis work.

The premise is that a given gradient waveform may be divided into a series of impulses of arbitrarily short duration. Let $\Delta t$ denote the duration of a pair of such impulses. The resulting q-vector becomes piece-wise constant, having a fixed value in every time interval $\Delta t$ as shown in Figure 3. Recall that the coupled Kärger differential equations (43) have analytical solutions for constant $q$. Integrating these equations in every $\Delta t$ leads to the following generalised discretised solution.

$$S(q,N) = \begin{bmatrix}1 & 1\end{bmatrix} \cdot \prod_{i=1}^{N} \exp\left( \begin{bmatrix}-k_{12} & k_{21} \\ k_{12} & -k_{21}\end{bmatrix} \Delta t - \begin{bmatrix}D_1 & 0 \\ 0 & D_2\end{bmatrix} q_i^2 \Delta t \right) \cdot \begin{bmatrix}f_1 \\ f_2\end{bmatrix} \tag{58}$$

where $N = \frac{T}{\Delta t}$ is the number of discretisation points, $k_{mn}$ is the exchange rate from pool $m$ to $n$ and $D_m$ and $f_m$ are the diffusivities and signal fractions of pool $m$, respectively. The b-value is defined through

$$b = \sum_{i=1}^{N} q_i^2 \Delta t \tag{59}$$

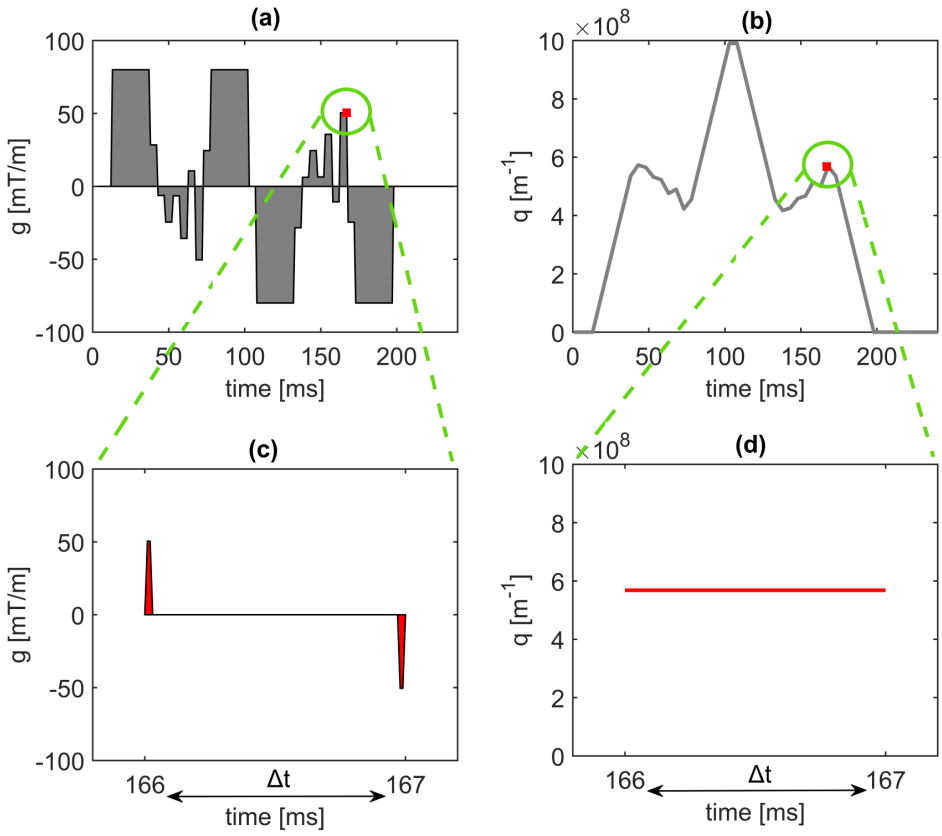


Figure 3: Generalisation of the Kärger model of exchange. (a): An arbitrary gradient waveform. The point highlighted in red lies at 166 ms and has a value of 50 mT/m. (b): The q-vector corresponding to the gradient waveform in (a). The point marked in red is the integral of the gradient waveform over [0 166] ms. (c): Theoretical treatment of the red point in (a) as a pair of impulses of amplitude 50 mT/m and time interval $\Delta t$. (d): q-vector corresponding to the impulses in (c). Note that the red point in (a) has been chosen arbitrarily. Following the same procedure for every point on the waveform results in a q-vector that is piecewise constant, having a constant value in every time-step $\Delta t$. This entails that a closed-form solution to the Kärger equations (43) can be obtained in every $\Delta t$, yielding the expression in equation 58.

which is the discrete version of equation 23. The generality of equation 58 renders it potentially useful for model fitting and parameter inference. Be that as it may, the equation is a product of a possibly large number of matrix exponentials, which depletes its informative capacity towards experimental design. Alleviating this limitation by providing an enlightening approximate formulation of the generalised exchange model is the subject matter of the following section.

## 3.2 Cumulant expansion of the generalised exchange model

Section 2.4 accentuated the critical role played by the cumulant expansion in unveiling insights within biophysical model representations that may appear a contraption at first glance. Needless to say, the cumulant expansion is an apt tool for analysing the generalised exchange model in equation 58. Approximate but readable expressions are provided in this section with two-fold intent: extracting insights from the signal equation and comparing it to the Ning model. To this end, a fourth-order multivariate Taylor series expansion of the logarithm of equation 58 was taken around $q_i = 0\ , i = 1, 2, 3, ..., N$. The expansion was performed for a few values of $N$ and then generalised to the following:

$$\ln(S) \approx -\left(\sum_{i=1}^{N} q_i^2 \Delta t\right) \cdot \overline{D} + \frac{\mathrm{Var}(D)}{k^2} \cdot \left[\sum_{j=1}^{N}\left(e^{-j\cdot k\Delta t}\left(\sum_{i=1}^{N-(j-1)} q_i^2 q_{i+(j-1)}^2 - 2\sum_{i=1}^{N-j} q_i^2 q_{i+j}^2 + \sum_{i=1}^{N-(j+1)} q_i^2 q_{i+(j+1)}^2\right)\right) - (1 - k\Delta t)\cdot\sum_{i=1}^{N} q_i^4 + \sum_{i=1}^{N-1} q_i^2 q_{i+1}^2\right] \quad (60)$$

where $\overline{D} = f_1 D_1 + f_2 D_2$ is the mean diffusivity, $\mathrm{Var}(D) = f_1 f_2 (D_1 - D_2)^2$ is the variance of diffusivities and $k = k_{12} + k_{21}$ is the sum of the exchange rates between the two pools. The full derivation of equation 60 is provided in Appendices A1 and A2. Tedious algebraic manipulations were executed in Maple [50]. A compact representation of equation 60 may be written

$$\ln(S) \approx -\overline{D}b + \frac{1}{2}\mathrm{Var}(D)h(\cdot)b^2 \quad (61)$$

where

$$h(\cdot) = \frac{2}{b^2 \cdot k^2} \cdot \left[\sum_{j=1}^{N}\left(e^{-j\cdot k\Delta t}\left(\sum_{i=1}^{N-(j-1)} q_i^2 q_{i+(j-1)}^2 - 2\sum_{i=1}^{N-j} q_i^2 q_{i+j}^2 + \sum_{i=1}^{N-(j+1)} q_i^2 q_{i+(j+1)}^2\right)\right) - (1 - k\Delta t)\cdot\sum_{i=1}^{N} q_i^4 + \sum_{i=1}^{N-1} q_i^2 q_{i+1}^2\right] \quad (62)$$

The stark contrast between equations 61 and 58 illustrates the remarkable utility of the cumulant expansion. Exchange in equation 61 is controlled by the function $h(\cdot)$, which is

reminiscent of equation 47 from Ning et al. [44]. It is relevant to note that, for the case of single-diffusion encoding where $q(t)$ is constant in time, $h(\cdot)$ takes the form

$$h(\cdot) = 2 \cdot \frac{(e^{-kT} - (1 - kT))}{(kT)^2} \tag{63}$$

which has the following intuitive limiting behaviour:

$$h(\cdot) = \begin{cases} 0 & T \to \infty \\ 1 & T \to 0 \end{cases} \tag{64}$$

The derivation of equation 63 can be found in Appendix A4. In the more general case where $q(t)$ is smooth in time (equation 62), the functional form of $h(\cdot)$ is not easily interpreted. This necessitates an approximate form of equation 62 in which the exponential terms are expanded to third order. That is, where

$$e^{-jk\Delta t} \approx 1 - jk\Delta t + \frac{j^2k^2\Delta t^2}{2} - \frac{j^3k^3\Delta t^3}{6} \qquad ; \qquad j = 1, 2, 3, ...N \tag{65}$$

The choice of order 3 in equation 65 is not arbitrary; expansion to second order would result in $h(\cdot) = 1$ and first order would yield $h(\cdot) = 0$. These facts can be readily inferred from equation 63. Furthermore, it is not necessary to choose an order higher than 3 because, in all relevant cases, $\Delta t$ is small. Equipped with equation 65, the signal representation becomes (consult Appendices A1 and A3 for derivation):

$$\ln(S) \approx -b \cdot \overline{D} + \frac{\mathrm{Var}(D)}{6} \cdot \left[ 3b^2 - k \cdot \left[ \sum_{i=1}^{N} (q_i^4 \Delta t^2)\Delta t + \sum_{j=1}^{N-1} \left( 6j \cdot \sum_{i=1}^{N-j} q_i^2 q_{i+j}^2 \Delta t^2 \right) \Delta t \right] \right] \tag{66}$$

which can be reformulated

$$\ln(S) \approx -\overline{D}b + \frac{1}{2}\mathrm{Var}(D) \left[ 1 - k \cdot \left( \frac{Q_4}{3b^2} \right) \right] b^2 \tag{67}$$

where

$$Q_4 := \sum_{i=1}^{N} (q_i^4 \Delta t^2)\Delta t + \sum_{j=1}^{N-1} \left( 6j \cdot \sum_{i=1}^{N-j} q_i^2 q_{i+j}^2 \Delta t^2 \right) \Delta t \tag{68}$$

At this juncture, a generalised exchange-weighting time ($\Gamma$) can now be defined in a fashion similar to the work by Ning et al. [44] :

$$\Gamma := \frac{Q_4}{3b^2} \tag{69}$$

This allows the signal representation in equation 67 to be rewritten as

$$\ln(S) \approx -\overline{D}b + \frac{1}{2}\mathrm{Var}(D)(1 - k\Gamma)b^2 \tag{70}$$

which corresponds to equation 61 with the exchange-weighting function approximated by

$$h(\cdot) = 1 - k\Gamma \tag{71}$$

It is worth noting that, in the SDE case with infinitely short pulses (where q is constant), the exchange-weighting time, $\Gamma$, is given by

$$\Gamma_{SDE} = \frac{T}{3} \tag{72}$$

which is also the result by Ning et al. Appendix A5 contains the derivation of the result above.

This section has demonstrated that the proposed generalisation of the Kärger model can be brought to intuitive forms consistent with the results of Ning et al. [44]. It is key to stress that the formulae derived in this section serve as a guide towards conceptual understanding. They must not be regarded as a tool for forward modelling, since this would defeat the purpose of the generalised exchange model in equation 58. That said, it is at this point appropriate to reiterate the objective of this thesis work: develop a unified framework for modelling and measuring exchange and restriction. It can be submitted to the reader that the exchange part has been dealt with in a comprehensive manner. Fusing the exchange theory with restriction forms the substance of the next chapter.

## 3.3 Generalising the unified model

Although affording flexibility in terms of gradient waveform choice, the generalised exchange model (equation 58) is still grounded on the fundamental assumptions of the Kärger model. Particularly, there exists two infinite well-mixed spin-carrying exchanging pools within which Gaussian diffusion takes place. In other words, the underlying geometry is neglected. Herein - following the work of Nilsson et al. [15] - restriction-induced time-dependent diffusion is introduced into the generalised exchange model by way of the diffusion spectrum. The goal is to arrive at a generalisation of the unified model that addresses all the weaknesses discussed in Section 2.7.

Equations 20 and 25, which represent a stationary and time-dependent signal description, can be used to formulate appropriate expressions for the diffusivities in the generalised

model. The attenuation factors in these equations are juxtaposed here for clarity.

$$bD(\cdot) = \frac{1}{2\pi}\int_{-\infty}^{\infty} D(\omega)|Q(\omega)|^2 dw \tag{73}$$

where the diffusivity $D(\cdot)$ is now defined as a function of compartment geometry as a generalisation of the derivation by Nilsson (2017) for cylinders [46]. Equation 73 permits the definition

$$D(\cdot) = \frac{1}{2\pi b}\int_{-\infty}^{\infty} D(\omega)|Q(\omega)|^2 dw \tag{74}$$

Incorporating equation 74 into the generalised exchange model yields the expression

$$S(q,N) = \begin{bmatrix}1 & 1\end{bmatrix} \cdot \prod_{i=1}^{N} \exp\left( \begin{bmatrix}-k_{12} & k_{21}\\ k_{12} & -k_{21}\end{bmatrix}\Delta t - \begin{bmatrix}D_1(\cdot) & 0\\ 0 & D_2(\cdot)\end{bmatrix} q_i^2 \Delta t\right) \cdot \begin{bmatrix}f_1\\ f_2\end{bmatrix} \tag{75}$$

where $D_1(\cdot)$ and $D_2(\cdot)$ are given by equation 74. While not a prerequisite for the model presented here, it is routine practice to assume Gaussian diffusion in the extracellular space. That is, $D_2(\cdot) := D_2$. Equation 75 proposes a theory potentially capable of capturing size and exchange phenomena at all time scales, for any range of b-values and with any gradient waveform. Note that this theory will be referred to as simply the generalised model.

It must, nonetheless, be emphasised that equation 75, although free of the weaknesses of the original unified model, is not as easily interpreted. The expression is a product of a large number of matrix exponentials embedding the experimental parameter $q_i$. It is a real challenge to use equation 75 to determine how to design $q_i$ to influence an experiment towards a desired outcome. A possible solution is to take the cumulant expansion of equation 75 in the same manner as was done for the case of exchange without restriction (equation 60). However, the derivation involves discouragingly tedious algebra. An alternative approach employing the particle velocity autocorrelation function is explored in the coming section. An added advantage of this method is that it innately involves both restriction and exchange, thus obviating the need for the post-combination of a restriction-neglecting exchange theory and an exchange-neglecting restriction theory.

## 3.4 Velocity autocorrelations towards restriction and exchange

A generalised, unified theoretical framework describing both restriction and water exchange was presented in the preceding chapters. This section derives a signal representation that is easier to interpret than the generalised model, and therefore offers more insights towards experimental design. The generalised model was arrived at by way of

generalising, modifying and uniting independent restriction and exchange theories. Although this does not in itself constitute a weakness, the approach proposed in this section demonstrates that it is possible to build a theory whose foundation needs not consist of two complementary pillars: one disregarding restriction and the other overlooking exchange. Notwithstanding these advantages, it must be noted that the theory developed in this section is an approximate signal representation valid within a limited range of b-values. The approach is based on the velocity autocorrelation function. The motivation is that this function can be related to the diffusion spectrum, which in turn provides a link to the underlying geometry. Cumulants of the phase distribution are evaluated using these velocity autocorrelations, yielding a theory describing both exchange and restriction.

The definition of phase change ($\phi(T)$) in terms of the product of the gradient waveform and spin position (equation 14) can be reformulated to include particle velocity using integration by parts. Define

$$\xi := \boldsymbol{r}(t) \implies d\xi = d\boldsymbol{r}(t) = \boldsymbol{v}(t)dt$$

and

$$d\sigma := \gamma \boldsymbol{g}(t)dt \implies \sigma = \gamma \int_0^t \boldsymbol{g}(\tau)d\tau = \boldsymbol{q}(t)$$

where the last equality follows from the definition of the q-vector. The above gives

$$\phi(T) = \gamma \int_0^T \boldsymbol{g}(t) \cdot \boldsymbol{r}(t)dt = \xi \cdot \sigma - \int \sigma d\xi = \left[\boldsymbol{r}(t)\gamma \int \boldsymbol{g}(t)dt\right]_0^T - \int_0^T \boldsymbol{q}(t) \cdot \boldsymbol{v}(t)dt \quad (76)$$

The spin-echo condition imposes $\int_0^T \boldsymbol{g}(t)dt = 0$, which brings equation 76 to the form

$$\phi(T) = -\int_0^T \boldsymbol{q}(t) \cdot \boldsymbol{v}(t)dt \quad (77)$$

which has also been presented by Stepisnik [14]. As discussed in earlier sections, the second order signal approximation in equation 37 demands the evaluation of the second- and fourth-order moments of the phase distribution. Given equation 77, these moments take the forms

$$\langle \phi(T)^2 \rangle = \int_0^T \int_0^T \boldsymbol{q}(t_1)\boldsymbol{q}(t_2)\langle \boldsymbol{v}(t_1)\boldsymbol{v}(t_2)\rangle dt_1 dt_2 \quad (78)$$

and

$$\langle \phi(T)^4 \rangle = \int_0^T \int_0^T \int_0^T \int_0^T \boldsymbol{q}(t_1)\boldsymbol{q}(t_2)\boldsymbol{q}(t_3)\boldsymbol{q}(t_4)\langle \boldsymbol{v}(t_1)\boldsymbol{v}(t_2)\boldsymbol{v}(t_3)\boldsymbol{v}(t_4)\rangle dt_1 dt_2 dt_3 dt_4 \quad (79)$$

It is worth reiterating that the velocity autocorrelation function is defined formally as the inverse Fourier transform of the diffusion spectrum [14, 28, 30, 51]:

$$\langle \boldsymbol{v}(t_1)\boldsymbol{v}(t_2)\rangle = \frac{1}{\pi}\int_{-\infty}^{\infty} \boldsymbol{D}(\omega)\mathrm{e}^{i\omega(t_2-t_1)}d\omega \tag{80}$$

where $\boldsymbol{D}(\omega)$ is a tensor whose elements represent the Fourier transforms of the correlations between the velocity components. In three dimensions, $\boldsymbol{D}(\omega)$ has the matrix representation

$$\boldsymbol{D}(\omega) = \begin{bmatrix} D_{xx}(\omega) & D_{xy}(\omega) & D_{xz}(\omega) \\ D_{yx}(\omega) & D_{yy}(\omega) & D_{yz}(\omega) \\ D_{zx}(\omega) & D_{zy}(\omega) & D_{zz}(\omega) \end{bmatrix} \tag{81}$$

Note that, for time scales much greater than the correlation times between the velocities, the velocity autocorrelation function reduces to

$$\langle \boldsymbol{v}(t_1)\boldsymbol{v}(t_2)\rangle = 2\boldsymbol{D}(0)\cdot\frac{1}{2\pi}\int_{-\infty}^{\infty} 1\cdot\mathrm{e}^{i\omega(t_2-t_1)}d\omega = 2\boldsymbol{D}(0)\cdot\delta(t_2-t_1) \tag{82}$$

where $\delta(\cdot)$ denotes the Dirac delta function. Equation 82 is also the result by Stepisnik [14]. For simplicity, and without loss of generality, all derivations presented in this section will be performed in one dimension.

It has been shown elsewhere [52, 53, 54, 55] that, when the particle velocities follow a Gaussian distribution, the fourth-order autocorrelation can be generalised as

$$\begin{aligned}\langle v(t_1)v(t_2)v(t_3)v(t_4)\rangle = \langle v(t_1)v(t_2)\rangle\cdot\langle v(t_3)v(t_4)\rangle + \langle v(t_1)v(t_3)\rangle\cdot\langle v(t_2)v(t_4)\rangle + \\ \langle v(t_1)v(t_4)\rangle\cdot\langle v(t_2)v(t_3)\rangle\end{aligned} \tag{83}$$

which is here approximated

$$\langle v(t_1)v(t_2)v(t_3)v(t_4)\rangle \approx 3\cdot\langle v(t_1)v(t_2)\rangle\cdot\langle v(t_3)v(t_4)\rangle \tag{84}$$

This approximation, while not necessary, immensely simplifies the algebra. It is an appropriate simplification in this context and its validity is discussed in Appendix B4. Particularly, the discussion demonstrates that the above approximation equates to the assumption that any two time-points in the set $\{t_1, t_2, t_3, t_4\}$ are approximately equal.

Consider a tissue model consisting of two compartments that may by convention be labelled intracellular and extracellular spaces. These will be associated with the subscripts *in* and *ex*, respectively. Following the work by Ning et al. [44], a particle at a given

time-point is associated with a vector describing the probability of being in either of the two compartments:

$$\boldsymbol{p}(t) = \begin{bmatrix} p_{in}(t) \\ p_{ex}(t) \end{bmatrix} \tag{85}$$

The exchange-driven time-evolution of the probability vector obeys the rate equation

$$\frac{d\boldsymbol{p}(t)}{dt} = K \cdot \boldsymbol{p}(t) \tag{86}$$

where the rate matrix is given by

$$K = \begin{bmatrix} -k_{in\to ex} & k_{ex\to in} \\ k_{in\to ex} & -k_{ex\to in} \end{bmatrix} \tag{87}$$

Equation 86 has the solution

$$\boldsymbol{p}(t) = \begin{bmatrix} p_{in\to in}(t) \\ p_{in\to ex}(t) \end{bmatrix} = \begin{bmatrix} f_{in} + f_{ex}e^{-kt} \\ f_{ex}(1 - e^{-kt}) \end{bmatrix} \tag{88}$$

for particles initially in the intracellular compartment, and

$$\boldsymbol{p}(t) = \begin{bmatrix} p_{ex\to in}(t) \\ p_{ex\to ex}(t) \end{bmatrix} = \begin{bmatrix} f_{in}(1 - e^{-kt}) \\ f_{ex} + f_{in}e^{-kt} \end{bmatrix} \tag{89}$$

for particles initially in the extracellular compartment. $f_Y$ denotes the signal fraction for compartment Y, which is the fraction of the total number of spins that will be present in this compartment at infinite times. $k = k_{in} + k_{ex}$ is the sum of the exchange rates between the two compartments. The parameters $f$ and $k$ are required to satisfy the equilibrium condition: $f_{in} \cdot k_{in\to ex} = f_{ex} \cdot k_{ex\to in}$. Further, all particles are assumed to only exist in either the intra- or extracellular compartment, which demands: $f_{in} + f_{ex} = 1$.

Confidence in the derivations presented in this section may be enhanced by showing consistence with the theory developed by Ning et al. under the assumption of Gaussian diffusion. To this end, both the intra- and extracellular diffusivities are set constant. That is, the velocity autocorrelation function is defined

$$\langle v(t_1)v(t_2)\rangle = \begin{cases} 2D_{in}\delta(t_2 - t_1) & ; \quad \text{if intracellular} \\ 2D_{ex}\delta(t_2 - t_1) & ; \quad \text{if extracellular} \end{cases} \tag{90}$$

The second-order moment in equation 78 is concerned with the events in the time intervals $[0 \quad t_1]$ and $(t_1 \quad t_2]$. Computing the velocity autocorrelation function thus demands

taking into account the possible states of a given spin in these time periods. Note that "state" here refers to the current behaviour of the particle: either moving within the same compartment or migrating to another. For a particle starting in the intracellular compartment (and either lingering or leaving), the velocity autocorrelation becomes

$$\begin{aligned}\langle v(t_1)v(t_2)\rangle_{in} = \big[&p_{in\to in}(t_1-0)\cdot p_{in\to in}(t_2-t_1)\cdot 2D_{in}\delta(t_2-t_1)+\\ &p_{in\to in}(t_1-0)\cdot p_{in\to ex}(t_2-t_1)\cdot 2D_{ex}\delta(t_2-t_1)+\\ &p_{in\to ex}(t_1-0)\cdot p_{ex\to in}(t_2-t_1)\cdot 2D_{in}\delta(t_2-t_1)+\\ &p_{in\to ex}(t_1-0)\cdot p_{ex\to ex}(t_2-t_1)\cdot 2D_{ex}\delta(t_2-t_1)\big]\end{aligned} \tag{91}$$

In words, equation 91 is a description of all possible states of a particle that is in the intracellular compartment at time $t = 0$. This particle could stay in the intracellular compartment in the time interval $[0 \quad t_1]$ and either stay in this compartment during $(t_1 \quad t_2]$ or transition to the extracellular compartment. Alternatively, the particle could migrate to the extracellular space during $[0 \quad t_1]$ and either stay in this state during $(t_1 \quad t_2]$ or return to the intracellular compartment. The transition probabilities $p_{in\to in}(t), p_{in\to ex}(t), p_{ex\to in}(t)$ and $p_{ex\to ex}(t)$ are provided by equations 88 and 89. Note that the argument $t$ in these definitions is substituted by the time differences $(t_1 - 0)$ and $(t_2 - t_1)$ in equation 91. For example, $p_{in\to in}(t_2 - t_1) = f_{in} + f_{ex}e^{-k(t_2-t_1)}$. Following this procedure for all the terms in equation 91, the velocity autocorrelation function for a particle initially in the intracellular space becomes:

$$\langle v(t_1)v(t_2)\rangle_{in} = 2\cdot\delta(t_2-t_1)\cdot(f_{ex}\cdot(D_{in}-D_{ex})e^{-kt_2} + f_{in}D_{in} + f_{ex}D_{ex}) \tag{92}$$

The equivalent of equation 91 for a particle starting in the extracellular compartment is

$$\begin{aligned}\langle v(t_1)v(t_2)\rangle_{ex} = \big[&p_{ex\to ex}(t_1-0)\cdot p_{ex\to ex}(t_2-t_1)\cdot 2D_{ex}\delta(t_2-t_1)+\\ &p_{ex\to ex}(t_1-0)\cdot p_{ex\to in}(t_2-t_1)\cdot 2D_{in}\delta(t_2-t_1)+\\ &p_{ex\to in}(t_1-0)\cdot p_{in\to ex}(t_2-t_1)\cdot 2D_{ex}\delta(t_2-t_1)+\\ &p_{ex\to in}(t_1-0)\cdot p_{in\to in}(t_2-t_1)\cdot 2D_{in}\delta(t_2-t_1)\big]\end{aligned} \tag{93}$$

which, after substituting the definitions of the transition probabilities in equations 88 and 89, evaluates to

$$\langle v(t_1)v(t_2)\rangle_{ex} = 2\cdot\delta(t_2-t_1)\cdot(f_{in}\cdot(D_{ex}-D_{in})e^{-kt_2} + f_{in}D_{in} + f_{ex}D_{ex}) \tag{94}$$

Having assumed that particles can only be in either of the two compartments above, the mean velocity autocorrelation function can be written

$$\langle v(t_1)v(t_2)\rangle = f_{in}\langle v(t_1)v(t_2)\rangle_{in} + f_{ex}\langle v(t_1)v(t_2)\rangle_{ex} = 2\delta(t_2 - t_1)(f_{in}D_{in} + f_{ex}D_{ex}) \quad (95)$$

That is

$$\langle v(t_1)v(t_2)\rangle = 2\delta(t_2 - t_1)\overline{D} \quad (96)$$

where $\overline{D}$ is the mean diffusivity defined here as $\overline{D} := f_{in}D_{in} + f_{ex}D_{ex}$. The second-order moment of the phase distribution can now be evaluated:

$$\begin{aligned}\langle \phi(T)^2\rangle &= \int_0^T \int_0^T q(t_1)q(t_2)\cdot 2\delta(t_2 - t_1)\overline{D}dt_1dt_2 \\ &= 2\overline{D}\cdot \int_0^T q(t_1)\int_{-\infty}^{\infty} q(t_2)\cdot\delta(t_2 - t_1)dt_1dt_2 \\ &= 2\overline{D}\cdot \int_0^T q(t_1)q(t_1)dt_1 \\ &= 2\overline{D}b \end{aligned} \quad (97)$$

where the equality $\int_0^T q(t)dt = \int_{-\infty}^{\infty} q(t)dt$ is motivated by the assumption that $q(t) = 0\ \forall\ t \notin [0 \quad T]$.

The fourth-order moment can be derived in a similar manner, with the key difference that the time intervals of interest are $[0 \quad t_1]$, $(t_1 \quad t_2]$, $(t_2 \quad t_3]$ and $(t_3 \quad t_4]$. To obtain the fourth-order velocity autocorrelation function, the factorisation into two second-order correlations given in equation 84 will be exploited. Since the two second-order correlations are functions of the time differences $(t_2 - t_1)$ and $(t_4 - t_3)$, the fourth-order correlation will be a combination of all possible particle events leading up to the time intervals $(t_1 \quad t_2]$ and $(t_3 \quad t_4]$. The full expressions equivalent to equations 91 and 93 for the fourth-order case can be found in Appendix B2, which, together with Appendix B1, contains the full derivation of the exchange theory presented in this section. The velocity autocorrelation functions for particles initially in the intra- and extracellular spaces are in this scenario given by

$$\begin{aligned}\langle v(t_1)v(t_2)v(t_3)v(t_4)\rangle_{in} = 3\cdot 4\cdot\delta(t_4 - t_3)\cdot(f_{in}f_{ex}(D_{in} - D_{ex})^2\cdot e^{-k(t_4 - t_2)} + \\ f_{ex}(D_{in} - D_{ex})(f_{in}D_{in} + f_{ex}D_{ex})\cdot e^{-kt_2} + f_{ex}(D_{in} - D_{ex})\cdot(f_{ex}D_{in} + f_{in}D_{ex})\cdot e^{-kt_4} + \\ (f_{in}D_{in} + f_{ex}D_{ex})^2\cdot\delta(t_2 - t_1))\end{aligned}$$

and

$$\langle v(t_1)v(t_2)v(t_3)v(t_4)\rangle_{ex} = 3\cdot 4\cdot \delta(t_4-t_3)\cdot(f_{in}f_{ex}(D_{in}-D_{ex})^2\cdot e^{-k(t_4-t_2)} - f_{in}(D_{in}-D_{ex})(f_{in}D_{in}+f_{ex}D_{ex})\cdot e^{-kt_2} - f_{in}(D_{in}-D_{ex})\cdot(f_{ex}D_{in}+f_{in}D_{ex})\cdot e^{-kt_4} + (f_{in}D_{in}+f_{ex}D_{ex})^2\cdot\delta(t_2-t_1))$$

respectively. Again, the assumption of all particles being in either of the two compartments allows the mean fourth-order velocity autocorrelation function to be expressed:

$$\begin{aligned}\langle v(t_1)v(t_2)v(t_3)v(t_4)\rangle &= f_{in}\langle v(t_1)v(t_2)v(t_3)v(t_4)\rangle_{in} + f_{ex}\langle v(t_1)v(t_2)v(t_3)v(t_4)\rangle_{ex}\\ &= 3\big[4\cdot f_{in}f_{ex}(D_{in}-D_{ex})^2\cdot\delta(t_2-t_1)\delta(t_4-t_3)e^{-k(t_4-t_2)} + \\ &\quad 4\cdot(f_{in}D_{in}+f_{ex}D_{ex})^2\cdot\delta(t_2-t_1)\delta(t_4-t_3)\big] \qquad (98)\end{aligned}$$

Defining the variance of the diffusivities in the two compartments as $\mathrm{Var}(D) := f_{in}f_{ex}(D_{in}-D_{ex})^2$ and recalling the definition of the mean diffusivity: $\overline{D} = f_{in}D_{in}+f_{ex}D_{ex}$, equation 99 becomes

$$\langle v(t_1)v(t_2)v(t_3)v(t_4)\rangle = 12\cdot\mathrm{Var}(D)\cdot\delta(t_2-t_1)\delta(t_4-t_3)e^{-k(t_4-t_2)} + 12\cdot\overline{D}^2\cdot\delta(t_2-t_1)\delta(t_4-t_3) \qquad (99)$$

Equation 99 allows the straightforward evaluation of the fourth-order moment of the phase distribution:

$$\begin{aligned}\langle\phi(T)^4\rangle &= \int_0^T\int_0^T\int_0^T\int_0^T q(t_1)q(t_2)q(t_3)q(t_4)[12\cdot\mathrm{Var}(D)\cdot\delta(t_2-t_1)\delta(t_4-t_3)e^{-k(t_4-t_2)} + \\ &\quad 12\cdot\overline{D}^2\cdot\delta(t_2-t_1)\delta(t_4-t_3)]dt_1dt_2dt_3dt_4\\ &= 12\cdot\mathrm{Var}(D)\int_0^T e^{-k(t_4-t_2)}\int_0^T q(t_2)^2q(t_4)^2dt_2dt_4 + 12\cdot\overline{D}^2b^2 \qquad (100)\end{aligned}$$

Defining $t := t_4 - t_2, t\in[-T,T]$, the above expression simplifies to

$$\begin{aligned}\langle\phi(T)^4\rangle &= 12\cdot\mathrm{Var}(D)\int_{-T}^T e^{-kt}\int_0^T q(t_2)^2q(t_2+t)^2dt_2dt + 12\cdot\overline{D}^2\cdot b^2\\ &= 12\cdot\mathrm{Var}(D)\int_{-T}^T e^{-kt}q_4(t)dt + 12\cdot\overline{D}^2\cdot b^2 \qquad (101)\end{aligned}$$

where $q_4(t) = \int_0^T q(t_2)^2q(t_2+t)^2dt_2$ is the fourth-order autocorrelation function of $q(t)$. Exchange-induced signal attenuation occurring in the time interval $[-T \quad 0)$ can be handled by imposing

$$\langle \phi(T)^4 \rangle = 12 \cdot \mathrm{Var}(D) \int_{-T}^{T} e^{-k|t|} q_4(|t|) dt + 12 \cdot \overline{D}^2 \cdot b^2$$
$$= 12 \cdot \mathrm{Var}(D) \cdot 2 \int_{0}^{T} e^{-kt} q_4(t) dt + 12 \cdot \overline{D}^2 \cdot b^2 \tag{102}$$

It is at this instance relevant to note that the expressions derived in this section are in complete agreement with the results of Ning et al. [44]. When inserted into equation 37, they yield the following second-order signal representation:

$$\ln(S) \approx -\frac{1}{2}\langle \phi^2 \rangle + \frac{1}{24}(\langle \phi^4 \rangle - 3\langle \phi^2 \rangle^2)$$
$$= -\overline{D}b + \frac{1}{24}\left[12 \cdot \mathrm{Var}(D) \cdot 2 \int_{0}^{T} e^{-kt} q_4(t) dt + 12 \cdot \overline{D}^2 \cdot b^2 - 3 \cdot (2\overline{D}b)^2\right]$$
$$= -\overline{D}b + \frac{1}{2}\mathrm{Var}(D) \cdot 2 \int_{0}^{T} e^{-kt} q_4(t) dt \tag{103}$$

That is

$$\ln(S) \approx -\overline{D}b + \frac{1}{2}\mathrm{Var}(D) h(\cdot) b^2 \tag{104}$$

where $h(\cdot) = \frac{2}{b^2} \int_0^T e^{-kt} q_4(t) dt$.

It is instructive to emphasise that equation 104 is the long-time-limit of the exchange-restriction theory to be elaborated in the following. The purpose of the work presented heretofore was to verify the veracity of the theoretical basis by demonstrating that it reduces to the results by Ning et al. in the long-time limit (where the velocity autocorrelation is defined by a Dirac delta function). What follows is the general derivation of the exchange-restriction theory that is expected to be valid at all time scales. The work adheres to the same methodology as applied to the long-time scenario, but entails substantially more involved arithmetic. In fact, for the sake of elegance and comprehensibility, progress is made by assuming Gaussian diffusion in the extracellular space. Henceforth, the velocity autocorrelation function will be given by

$$\langle v(t_1) v(t_2) \rangle = \begin{cases} \frac{1}{\pi} \int_{-\infty}^{\infty} D(\omega) \mathrm{e}^{i\omega(t_2 - t_1)} d\omega & ; \quad \text{if intracellular} \\ \\ 2D_{ex}\delta(t_2 - t_1) & ; \quad \text{if extracellular} \end{cases} \tag{105}$$

Note, however, that no aspect of the theory developed here demands the assumption above. The second-order velocity autocorrelation for particles starting in the intracellular

compartment is obtained by merging equation 105 with equations 91 and 93 to obtain

$$\begin{aligned}\langle v(t_1)v(t_2)\rangle_{in} = \big[&p_{in\to in}(t_1-0)\cdot p_{in\to in}(t_2-t_1)\cdot 2\cdot\frac{1}{2\pi}\int_{-\infty}^{\infty}D(\omega)\mathrm{e}^{i\omega(t_2-t_1)}d\omega+\\ &p_{in\to in}(t_1-0)\cdot p_{in\to ex}(t_2-t_1)\cdot 2D_{ex}\delta(t_2-t_1)+\\ &p_{in\to ex}(t_1-0)\cdot p_{ex\to in}(t_2-t_1)\cdot 2\cdot\frac{1}{2\pi}\int_{-\infty}^{\infty}D(\omega)\mathrm{e}^{i\omega(t_2-t_1)}d\omega+\\ &p_{in\to ex}(t_1-0)\cdot p_{ex\to ex}(t_2-t_1)\cdot 2D_{ex}\delta(t_2-t_1)\big]\end{aligned} \tag{106}$$

and similarly for particles initially in the extracellular space. Appendices B1 and B3 provide the full derivation of the restriction-exchange theory elaborated in this section. The second-order mean velocity autocorrelation function becomes

$$\begin{aligned}\langle v(t_1)v(t_2)\rangle &= f_{in}\langle v(t_1)v(t_2)\rangle_{in} + f_{ex}\langle v(t_1)v(t_2)\rangle_{ex}\\ &= 2\cdot\frac{f_{in}}{2\pi}\int_{-\infty}^{\infty}D(\omega)\mathrm{e}^{i\omega(t_2-t_1)}d\omega + 2\cdot f_{ex}D_{ex}\delta(t_2-t_1)\end{aligned} \tag{107}$$

The result above enables the derivation of the second-order moment:

$$\langle\phi(T)^2\rangle = \int_0^T\int_0^T q(t_1)q(t_2)\cdot\left[2\cdot\frac{f_{in}}{2\pi}\int_{-\infty}^{\infty}D(\omega)\mathrm{e}^{i\omega(t_2-t_1)}d\omega + 2\delta(t_2-t_1)D_{ex}\right]dt_1dt_2$$

That is

$$\langle\phi(T)^2\rangle = 2\cdot\frac{f_{in}}{2\pi}\left(\int_{-\infty}^{\infty}D(\omega)|Q(\omega)|^2d\omega\right) + 2\cdot f_{ex}D_{ex}b \tag{108}$$

It is worth noting that equation 108 comprises terms commonly used to describe the signal attenuation in diffusion MRI: one capturing time-dependent effects and the other describing stationary effects.

The fourth-order counterparts of equations 106 and 107 have been deemed too tedious to present here and can be found in Appendix B3. The fourth-order moment of the phase

distribution is in this case given by:

$$\begin{aligned}\langle\phi(T)^4\rangle = 12 f_{in} f_{ex} \int_{-\infty}^{\infty} e^{-kt} \Bigg[ \frac{1}{4\pi^2} \int_{-\infty}^{\infty}\int_{-\infty}^{\infty} D(\omega)D(\omega_1)Q(\omega)Q(\omega_1)Q_2(t,\omega,\omega_1)d\omega d\omega_1 \\ -2D_{ex}\frac{1}{2\pi}\int_{-\infty}^{\infty} D(\omega)Q(\omega)Q_3(t,\omega)d\omega + D_{ex}^2 Q_4(t)\Bigg]dt + \\ 12\Bigg[\frac{f_{in}f_{in}}{4\pi^2}\int_{-\infty}^{\infty} D(\omega)|Q(\omega)|^2 d\omega \int_{-\infty}^{\infty} D(\omega_1)|Q(\omega_1)|^2 d\omega_1 + \\ 2\frac{f_{in}f_{ex}}{2\pi}\cdot b \cdot \int_{-\infty}^{\infty} D(\omega)|Q(\omega)|^2 d\omega + f_{ex}f_{ex}D_{ex}^2 \cdot b^2\Bigg]\end{aligned} \tag{109}$$

where the correlation terms $Q_2, Q_3$ and $Q_4$ are given by

$$Q_2(t,\omega,\omega_1) = \int_{-\infty}^{\infty} q(t_2)e^{i\omega_1 t_2}\cdot q(t_2+t)e^{i\omega(t_2+t)}dt_2 \tag{110}$$

$$Q_3(t,\omega) = \int_{-\infty}^{\infty} q(t_2)^2\cdot q(t_2+t)e^{i\omega(t_2+t)}dt_2 \tag{111}$$

$$Q_4(t) = \int_{-\infty}^{\infty} q(t_2)^2 q(t_2+t)^2 dt_2 \tag{112}$$

The above equations mark the herald of a unified signal representation capturing exchange and restriction phenomena to second order:

$$\ln(S) \approx -\frac{1}{2}c_2 + \frac{1}{24}c_4 \tag{113}$$

where

$$c_2 = 2\cdot\frac{f_{in}}{2\pi}\Bigg(\int_{-\infty}^{\infty} D(\omega)|Q(\omega)|^2 d\omega\Bigg) + 2\cdot f_{ex}D_{ex}b \tag{114}$$

and

$$\begin{aligned}c_4 = 12 f_{in} f_{ex} \int_{-\infty}^{\infty} e^{-kt}\Bigg[\frac{1}{4\pi^2}\int_{-\infty}^{\infty}\int_{-\infty}^{\infty} D(\omega)D(\omega_1)Q(\omega)Q(\omega_1)Q_2(t,\omega,\omega_1)d\omega d\omega_1 \\ -2D_{ex}\frac{1}{2\pi}\int_{-\infty}^{\infty} D(\omega)Q(\omega)Q_3(t,\omega)d\omega + D_{ex}^2 Q_4(t)\Bigg]dt\end{aligned} \tag{115}$$

The theory presented in this section will be referred to as the VA (velocity-autocorrelations) model. Note that, despite the different paths taken in their derivation, the generalised model and the VA fundamentally describe the same physics. The VA model is to be perceived neither as a counterpart nor a replacement of the generalised model, but rather as its complement.

# 4 Methods

Numerical validation of all theory proposed in this thesis work was the goal of this section. The evaluation procedure aimed to investigate both accuracy and precision of parameter estimates when the developed theory is fitted to simulated data. With the intention of demonstrating the value of optimising gradient waveforms, a comparison of two distinct experimental protocols was performed. One set consisted of standard SDE waveforms with different exchange- and restriction weightings, adapted from Nilsson et al. [15]. The other protocol comprised a set of waveforms numerically optimised to minimise the variance in estimated parameters. This was done using the Cramer-Rao Lower Bound (CRLB) approach, described briefly in the following and extensively by Alexander [56].

A Monte-Carlo method was used to simulate random walkers in three distinct environments: single Gaussian pool, two exchanging Gaussian pools and a 2D substrate with restricted diffusion and exchange. All algorithms used were written during the course of this thesis work. The simulation framework - implemented in MATLAB© - is described in this section.

## 4.1 Gradient waveform optimisation

The goal of gradient waveform optimisation was to seek a set of waveforms that - when used to probe exchange and restriction - would yield the least variance in the estimated parameters. To this end, the CRLB and Fisher information matrix were employed. The optimisation was done in MATLAB© using the non-linear least squares solver *lsqnonlin*.

A set of nine SDE waveforms with different combinations of pulse durations ($\delta$) and time intervals ($\Delta$) was used to initialise the optimisation. These two parameters ($\delta$ and $\Delta$) were kept fixed for each waveform and the amplitude at each time-point was varied. Temporal resolution of the waveforms was kept at a fixed 1 ms. Following the work of Alexander [56], the objective function computed the sum of the coefficients of variation of the parameters of the model in question:

$$\tilde{F} = \sum_{i=1}^{M} \frac{\sigma_i^2}{\theta_i^2} \tag{116}$$

where $\theta_i$, $i = 1, 2, ...M$ denotes the model parameters and $\sigma_i$ is the standard deviation in $\theta_i$. In the case of exchange without restriction, the model in question refers to the generalised exchange model (equation 58). For exchange with restriction, the generalised model (equation 75) was used to evaluate the objective function. Note that this entails that the resulting optimised gradient waveforms are model-dependent. The parameters $\theta_i$ can assume different values, demanding the integration of $\tilde{F}$ over prior distributions

of all $\theta_i$. For simplicity, the parameters were assumed to come from $\delta$-function prior distributions centred at

$$\{D_1, D_2, f_1, f_2, k\} = \{0.1\ \mu\text{m}^2/\text{ms},\ 0.3\ \mu\text{m}^2/\text{ms},\ 0.7,\ 0.3,\ 10\ \text{s}^{-1}\}$$

for free diffusion with exchange and at

$$\{D_{in}, D_{ex}, f_{in}, f_{ex}, k, d\} = \{1.2\ \mu\text{m}^2/\text{ms},\ 1.2\ \mu\text{m}^2/\text{ms},\ 0.7,\ 0.3,\ 10\ \text{s}^{-1},\ 20\ \mu\text{m}\}$$

for restricted diffusion with exchange.

Waveform optimisation takes place prior to data acquisition, which implies that the parameter variances $\sigma_i^2$ are unknown. As is customary within the field of dMRI, the variances were represented by the corresponding CRLBs to obtain

$$F = \sum_{i=1}^{M} \frac{(J^{-1})_{ii}}{\theta_i^2} \tag{117}$$

where $(J^{-1})_{ii}$ is the CRLB for parameter $\theta_i$. This means that $(J^{-1})_{ii}$ is a lower bound on the variance of any unbiased estimator of the physical quantity represented by $\theta_i$. The terms $(J^{-1})_{ii}$ were extracted from the diagonal of the inverse of the Fisher information matrix defined generally by

$$J_{ij} = \left\langle \frac{\partial^2 \ln(p(x;\theta))}{\partial\theta_i \partial\theta_j} \right\rangle \tag{118}$$

where $p(x;\theta)$ is the likelihood of the data ($x$) given the model parameters ($\theta$). The Fisher information is thus dependent on the selected noise model. A Gaussian distribution was chosen following previous work [57, 58]. It must be emphasised, however, that a more robust optimisation procedure would have used the Rician noise distribution that is better suited to MRI measurements. That said, in a simulation context, the problem is circumvented by using a high SNR [59, 60]. The assumption of Gaussian noise allowed the Fisher information to be evaluated using

$$J_{ij} = \frac{1}{\sigma^2} \sum_{n=1}^{N} \frac{\partial S[n]}{\partial\theta_i} \frac{\partial S[n]}{\partial\theta_j} \tag{119}$$

where $n$ denotes the $n$-th combination of the parameters $\delta$ and $\Delta$ and $N = 9$. $S$ is the signal generated using the model and the gradient waveform with the $n$-th combination of $\delta$ and $\Delta$. $\sigma$ is the noise level in the measurements (that is, the standard deviation of the assumed Gaussian noise distribution). Closed-form expressions for the derivatives of the generalised model with respect to its input parameters are a challenge to derive. In the implementation used in this work, the derivatives were numerically approximated. The

resulting matrix in equation 119 was then inverted and its diagonal elements extracted to obtain the CRLBs, $(J^{-1})_{ii}$, required to evaluate the objective function in equation 117.

The solver sought the set of waveforms that minimised the parameter variances subject to the following constraints adapted from Middione et al. [61]:

$$g(t) \leq g_{max} \tag{120}$$

$$\left|\frac{dg(t)}{dt}\right| \leq s_{max} \tag{121}$$

$$\int_0^T g(t)dt = 0 \tag{122}$$

where $g_{max} = 80$ mT/m is the maximum gradient amplitude and $s_{max} = 70$ T/(m $\cdot$ s) is the maximum slew rate. These limits were chosen to reflect typical protocols on clinical scanners. Constraint 122 is the spin-echo condition which demands that the gradient waveform be balanced. The output from the optimiser was a set of nine waveforms designed for precision in estimates of exchange rate and compartment sizes. It is important to note that the problem of gradient waveform optimisation is riddled with multiple local minima. A more robust optimiser would employ a stochastic global solver such as SOMA (Self-Organising Migrating Algorithm) [56, 62].

## 4.2 One pool

A single pool of freely diffusing particles was simulated with the purpose of verifying the soundness of the simulation framework. One hundred thousand spins were allowed to make steps of fixed lengths but random directions in the Cartesian plane. That is, for a particle at position $\boldsymbol{r}(t)$ at time $t$, its new position at time $t + \Delta t$ was

$$\boldsymbol{r}(t + \Delta t) = \boldsymbol{r}(t) + \Delta r \cdot \boldsymbol{n} \tag{123}$$

where $\boldsymbol{n}$ is a unit vector in an arbitrary direction and $\Delta r$ is the step length given by

$$\Delta r = \sqrt{2 \cdot n \cdot D_0 \cdot \Delta t} \tag{124}$$

where $n = 2$ is the number of spatial dimensions and $D_0$ is the bulk diffusivity which was here set to 1.2 $\mu$m$^2$/ms. The time-step was set to $\Delta t = 10$ $\mu$s. Particle positions were recorded for a time $T = 160$ ms after which the net phase changes were computed using the discrete version of equation 14:

$$\phi_n(T) = \gamma \sum_{i=1}^{N} \boldsymbol{g}(i) \cdot \boldsymbol{r}_n(i) \cdot \Delta t \tag{125}$$

where $N = T/\Delta t$ and the subscript $n$ denotes the $n$-th particle ($n = 1, 2, 3, ..., 10^5$). The signal was calculated from the phases using equation 15 in its discrete form:

$$S = \frac{1}{N_p} \sum_{n=1}^{N_p} e^{-i\phi_n(T)} \tag{126}$$

where $N_p = 10^5$ is the total number of particles. This was done for different amplitudes of $g(t)$, resulting in different b-values in the range [0 2] ms/$\mu$m$^2$. Equation 20 was fitted to the resulting $S(b)$ data, allowing an estimation of the apparent diffusion coefficient. The fitting was done using the non-linear least squares solver *lsqnonlin* implemented in MATLAB©.

## 4.3 Two exchanging Gaussian pools

The one-pool environment was extended into two well-mixed exchanging pools of freely diffusing particles. The objective of this section was to validate the proposed generalisation of the Kärger model (equation 58).

Initial populations in the two pools (labelled 1 and 2 for convenience), were selected to match the equilibrium conditions:

$$N_1 = f_1 \cdot N_p \qquad ; \qquad N_2 = f_2 \cdot N_p \tag{127}$$

where $f_1$ and $f_2$ are the signal fractions and $N_p = 10^5$ is the total number of particles. Exchange rates between the two pools, $k_{12}$ and $k_{21}$, were varied to give the total exchange rates:

$$k = [0 \;\; 2 \;\; 4 \;\; 6 \;\; 8 \;\; 10] \;\; \text{s}^{-1}$$

ensuring that they invariably satisfied the equilibrium condition:

$$f_1 \cdot k_{12} = f_2 \cdot k_{21} \tag{128}$$

All other parameters were kept constant at the values $f_1 = 0.7$, $f_2 = 0.3$, $D_1 = 0.1$ $\mu$m$^2$/ms and $D_2 = 0.3$ $\mu$m$^2$/ms. The random walk mechanism was the same as described for the one-pool scenario. Exchange probabilities between the two pools were defined according to the work by Ning et al. [44]:

$$\begin{aligned} p_{12} &= f_2 \cdot (1 - e^{-k\Delta t}) \approx f_2 \cdot k \cdot \Delta t \\ p_{21} &= f_1 \cdot (1 - e^{-k\Delta t}) \approx f_1 \cdot k \cdot \Delta t \end{aligned} \tag{129}$$

The exchange mechanism was implemented by generating for each particle at every time-step a random number uniformly distributed between 0 and 1. Only those particles

for which this random number was less than the transition probability were allowed to complete the transition to the other pool. In pseudocode, this may be summarised:

$$\text{transition} = \begin{cases} \text{yes} & ; \quad \text{if } rand(0,1) < p \\ \text{no} & ; \quad \text{else} \end{cases}$$

Simulations were run for 240 ms at a resolution of 10 $\mu$s. Signal at different b-values was generated in the same way described by equations 125 and 126. An SDE protocol with pulse width fixed at $\delta = 3$ ms and varying total encoding times T = 120, 160, 200 and 240 ms was used. A maximum b-value of 10 ms/$\mu$m$^2$ arrived at in 6 steps yielded 24 signal samples for each simulated exchange rate. The Ning model and the generalised exchange model were fitted to the data using the same optimisation method as in the one-pool case. Both models had four free parameters: $f_1, D_1, D_2$ and $k$. A precision study was done by adding 100 realisations of Rice-distributed noise to the simulated signal at a fixed exchange rate of 10 s$^{-1}$ and an SNR of 200. The mean and standard deviation of the estimated exchange rates for both the Ning and generalised exchange models were extracted. At the same exchange rate and SNR, signal was generated using gradient waveforms numerically optimised for minimal variance in exchange rate. A fit of the generalised model was performed to allow comparison between the two experimental protocols. For proof of concept, the effect of using CRLB-optimised waveforms on the accuracy of exchange rates estimated with the generalised exchange model was also investigated.

## 4.4 Two compartments: restricted diffusion and exchange

This section presents the most important step in the validation process. Its purpose was to evaluate the generalised model as well as the velocity autocorrelation-based approach. The two-pool framework was extended to a more realistic tissue model consisting of an intracellular and extracellular compartment. The tissue model was a 2D substrate consisting of circular, uniformly arranged intracellular compartments representing the cross-section of a cylindrical geometry. A section of the substrate is shown in Figure 4.

Compartments were initialised with populations corresponding to equilibrium conditions, with a total particle count of $10^5$. Bulk diffusivities were set to $D_{in} = 1.2$ $\mu$m$^2$/ms and $D_{ex} = 1.2$ $\mu$m$^2$/ms for the intracellular and extracellular spaces, respectively. Signal fractions were $f_{in} = 0.7$ and $f_{ex} = 0.3$. Exchange rates and compartment diameter were varied as described in the following. The random walk mechanism mimicked the single-pool and two-pool cases (fixed steps in random directions). Particles incident on the cell membrane were allowed to cross it with a certain probability (discussed in detail below). Transmitted particle trajectories were rescaled to account for possibly changing diffusivity in the new medium. For instance, for transmission from the intracellular to the extracellular

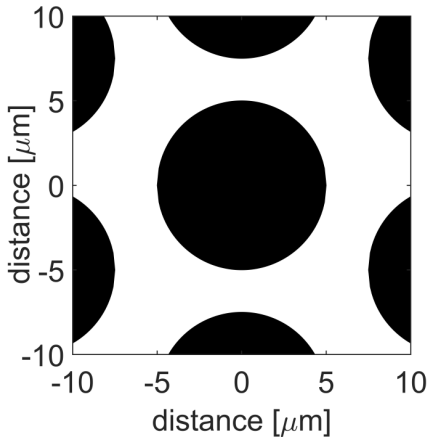


Figure 4: Part of the synthetic structure used in simulations of restricted diffusion with exchange. The substrate represents a cross-section through a cylindrical geometry shown here with a diameter of 10 $\mu$m. Black regions represent the intracellular compartment, while the extracellular space is shown in white.

compartment, the transmitted position was given by

$$\boldsymbol{r}_{transmitted}(t+\Delta t) = \boldsymbol{r}_{exit} + \frac{D_{ex}}{D_{in}} \cdot |\boldsymbol{r}(t+\Delta t) - \boldsymbol{r}_{exit}| \cdot \boldsymbol{n} \tag{130}$$

where $\boldsymbol{r}_{exit}$ is the position at which the particle crossed the membrane, $\boldsymbol{r}(t+\Delta t)$ is the position it would have been at had it continued in the same compartment and $\boldsymbol{n}$ is a unit vector along the direction of incidence. Reflected particle positions were calculated by determining the remaining section of the particle trajectory upon impact with the membrane, and reflecting this section back along the direction of incidence. To illustrate, the new position following reflection from the intracellular compartment was given by

$$\boldsymbol{r}_{reflected}(t+\Delta t) = \boldsymbol{r}_{exit} - |\boldsymbol{r}(t+\Delta t) - \boldsymbol{r}_{exit}| \cdot \boldsymbol{n} \tag{131}$$

The exchange probability was defined in terms of membrane permeability according to Szafer et al. [63]. For exchange from the intracellular to the extracellular compartment:

$$p_{in\rightarrow ex} = 4 \cdot \frac{\kappa}{v_{in}} \tag{132}$$

where $\kappa$ is the membrane permeability and $v_{in}$ is the particle velocity in the intracellular compartment, given by

$$v_{in} = \sqrt{\frac{2nD_{in}}{\Delta t}} \tag{133}$$

where $n = 2$ is the number of spatial dimensions. The corresponding probability of exchange from the extracellular to the intracellular compartment is obtained by interchanging the subscripts $in$ and $ex$. A relationship between the input permeability and

the simulated exchange rate was obtained by running a simulation with only intracellular particles and allowing transitions out of but not into this compartment. The exchange rate was obtained by fitting the following equation to the time-evolution of the intracellular population:

$$N_{in}(t) = N_{in}(0) \cdot e^{-k_{in \to ex} t} \tag{134}$$

This procedure was repeated for different values of the permeability, $\kappa$, and a general relationship between $\kappa$ and $k_{in \to ex}$ was obtained by fitting the following equation adapted from Tian X [43]:

$$k_{in \to ex} = \frac{X}{d} \cdot \left( \frac{1}{\kappa} + \frac{d}{Y \cdot D_{in}} \right)^{-1} \tag{135}$$

where $d$ is the cylinder diameter and $X$ and $Y$ were allowed to be free parameters. Figure 5 illustrates the fit for $d = 20$ $\mu$m.

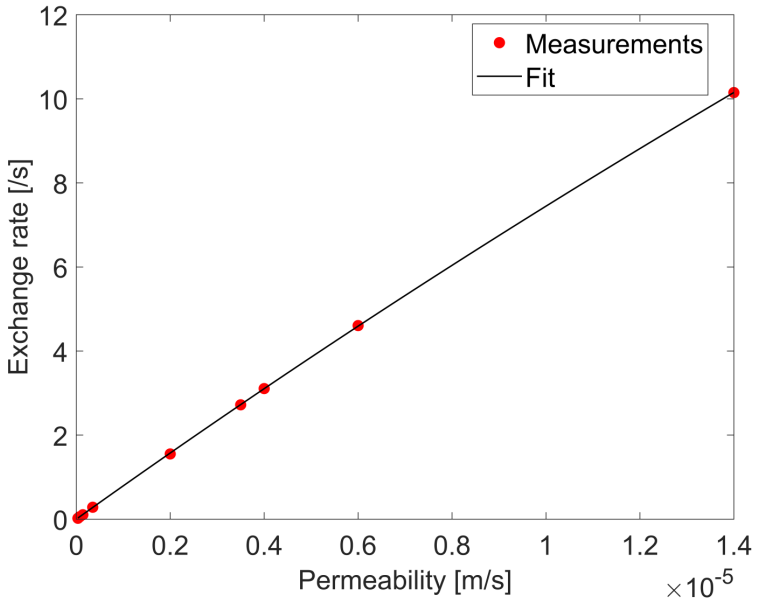


Figure 5: Fitting the input permeability to the observed exchange rate for a cylinder diameter of 20 $\mu$m. The measurements were done by recording the time-evolution of the intracellular population $N_{in}$ for different permeabilities, $k_{in \to ex} \neq 0$ and $k_{ex \to in} = 0$ and fitting equation 134. The intrinsic diffusivity was fixed at 1.2 $\mu$m$^2$/ms. The fitted curve corresponds to equation 135 with $X$ and $Y$ as free parameters.

Simulations were run for a total time $T = 160$ ms at a resolution of $\Delta t = 10$ $\mu$s, with mean particle positions being saved every 1 ms. The coarser time-grid was chosen to minimise computational expense and to match the temporal resolution used for gradient waveform

optimisation. Signals were determined using equation 126. With a fixed compartment diameter of 20 $\mu$m, the permeability was varied to yield the exchange rates

$$k = [1\ \ 3.3\ \ 5\ \ 8.3\ \ 10]\ \mathrm{s}^{-1}$$

While keeping the exchange rate fixed at $k = 10\ \mathrm{s}^{-1}$, the compartment diameter was varied to the values

$$d = [4\ \ 8\ \ 12\ \ 16\ \ 20]\ \ \mu\mathrm{m}$$

There were five free parameters to optimise: $f_{in}$, $D_{in}$, $D_{ex}$, $k$ and $d$. Both of the forward models used for estimating these parameters (generalised and VA) do not explicitly contain the diameter $d$ in their closed-form expressions. Rather, the diameter is embedded in the diffusion spectrum, $D(\omega)$, as defined in equation 9 for cylinders. For clarity, the full expression for $D(\omega)$ showing the relation to the cylinder diameter is given by

$$D(\omega) = \sum_n \frac{2(R/\mu_n)^2}{\mu_n^2 - 1} \cdot \frac{\left(\frac{\mu_n}{R}\right)^2 D_0 \omega^2}{\left(\frac{\mu_n}{R}\right)^4 D_0^2 + \omega^2} \tag{136}$$

which, after inserting $d = 2R$, simplifies to

$$D(\omega) = \sum_{n=1}^{\infty} \frac{2}{(\mu_n^2 - 1)} \cdot \frac{D_{in}\omega^2 d^4}{(16\mu_n^4 D_{in}^2 + \omega^2 d^4)} \tag{137}$$

Recall that $\mu_n$ is the $n$-th zero of the Bessel function of the first order and kind. The summation in equation 137 was truncated at $n = 200$, a limit that is sufficient to provide an accurate representation of $D(\omega)$. The dependence of $D(\omega)$ on $d$ for the values of $d$ used in the simulations is depicted in Figure 6. To obtain the diameter from the diffusion spectrum, the fitting algorithm accepted an initial guess for the parameter $d$ and used it to evaluate $D(\omega)$ according to equation 137. The resulting spectrum was then used together with the initial guesses for the other parameters ($f_{in}$, $D_{in}$, $D_{ex}$ and $k$) to calculate predicted signals using equations 75 (generalised model) and 113 (VA). A comparison between the predicted and simulated signals was performed by the fitting algorithm, followed by an iterative adjustment of all five parameters. The solution to the problem was the set $\{f_{in}, D_{in}, D_{ex}, k, d\}$ that gave the best agreement between model prediction and simulated data.

The above simulations were done at an infinite SNR to evaluate accuracy of fit. Signals were generated using a set of pulsed gradient waveforms adapted from Nilsson et al. [15]. Nine waveforms and a maximum b-value of 10 ms/$\mu$m$^2$ achieved in 10 steps resulted in 90 signal samples for each simulated diameter and exchange rate. The generalised model was fitted to the data using *lsqnonlin*. A similar procedure but with a maximum b-value of 5 ms/$\mu$m$^2$ was followed for the velocity-autocorrelation (VA) approach.

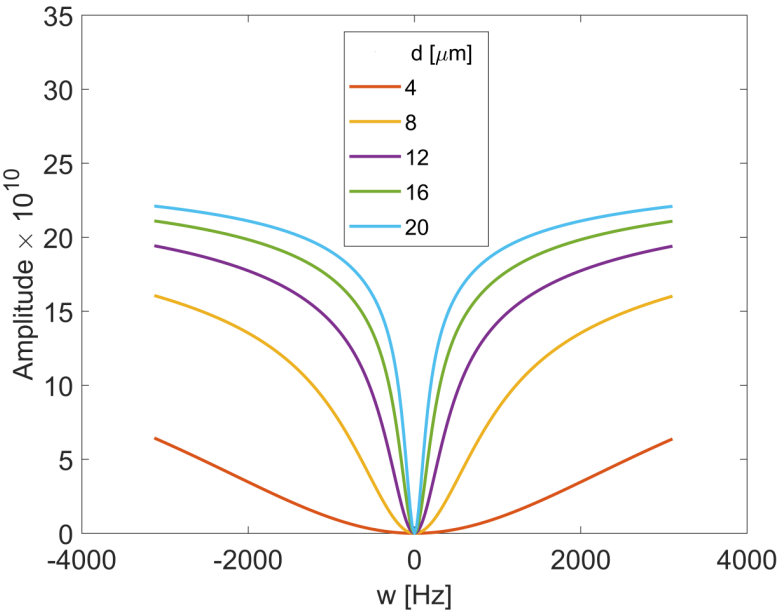


Figure 6: Diffusion spectra for different radii of a cylindrical geometry. These curves were generated using equation 137 with $D_{in} = 1$ $\mu$m$^2$/ms and an upper limit $n = 200$ for $\mu_n$.

Rice-distributed noise at a generous SNR of 200 was then added to signals generated at $k = 10$ s$^{-1}$ and $d = 20$ $\mu$m, giving 100 samples. Both the generalised and VA models were fitted to the resulting data, with the aim of studying the precision of parameter estimates. Noise was also added to signals generated with gradient waveforms optimised for precision in the estimated diameter and exchange rate. The generalised model was fitted to the resulting data for comparison with the SDE protocol.

# 5 Results and Discussion

Results from the numerical validation of the theory developed in this thesis work are presented in this section. The findings pertain to the three simulation environments explored: a single pool, two exchanging pools and a two-compartment system.

## 5.1 One pool

The simulated signal from a single pool of freely diffusing particles is shown in Figure 7a, together with the mono-exponential fit. Excellent agreement is evident between simulation and theory, as was also demonstrated by the correctly estimated mean diffusivity of 1.2001 $\mu$m$^2$/ms. The SDE waveform used to generate the signal is shown in Figure 7b. These results provide a confirmation that the simulation framework used in this thesis work was sound.

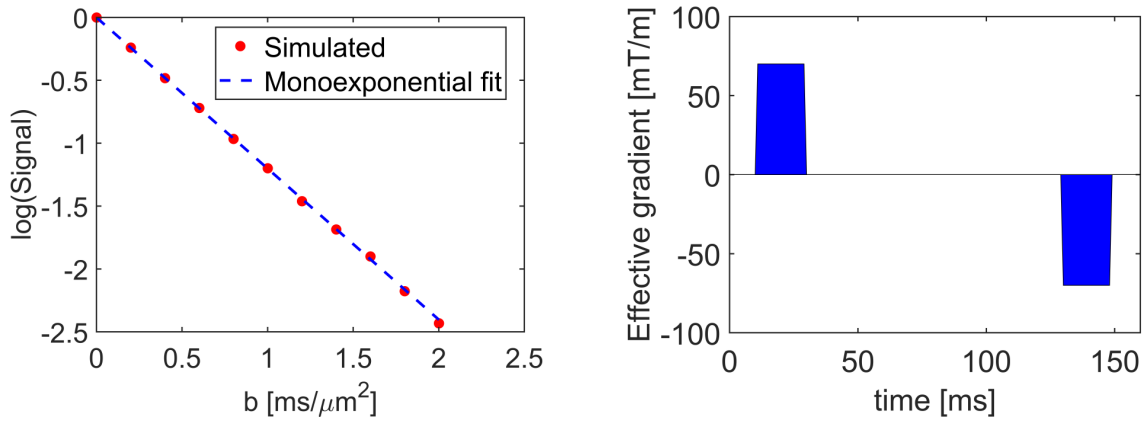


(a) (b)

Figure 7: (a): Mono-exponential fit to signal from one Gaussian pool with an intrinsic diffusivity of 1.2 $\mu$m$^2$/s (b): Gradient waveform used to generate the signal in (a). The different b-values were obtained by scaling this waveform while maintaining its timing fixed.

## 5.2 Two exchanging Gaussian pools

SDE waveforms used to measure exchange in the two-pool setting are shown in Figure 8a. Signal differences due to exchange as induced by these waveforms are shown in Figure 8b.

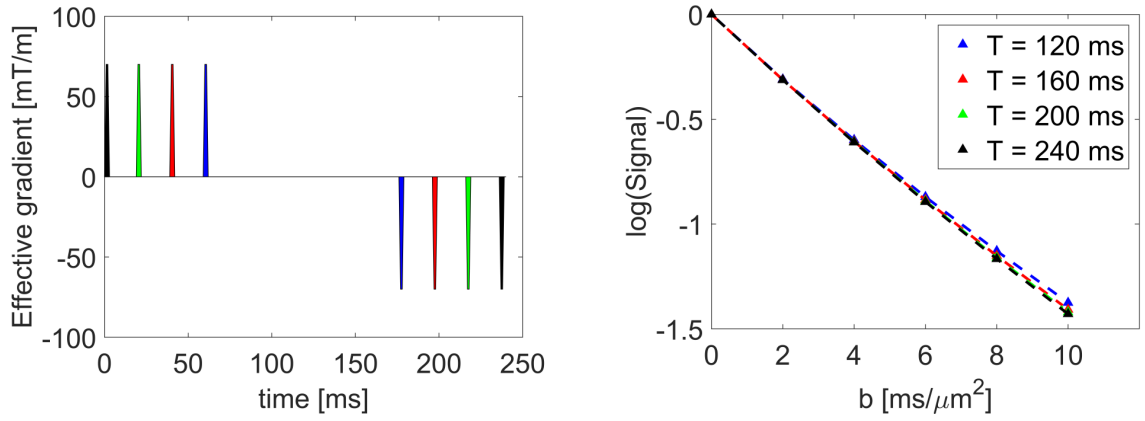


(a) (b)

Figure 8: (a): The set of gradient waveforms used to measure exchange between two well-mixed pools. All four waveforms have a fixed width of $\delta = 3$ ms and different total encoding times of $T = 120, 160, 200$ and 240 ms. (b): Signals generated using the gradient waveforms in (a). Each curve is shown in the same colour as its corresponding gradient waveform. The exchange rate was 10 s$^{-1}$ and the pool diffusivities were 0.1 $\mu$m$^2$/ms and 0.3 $\mu$m$^2$/ms. The divergence in the curves seen at high b-values is due to exchange.

The curves in Figure 8b were plotted for a fixed exchange rate of 10 $s^{-1}$. High b-values were required to probe exchange in this experiment due to the low intrinsic diffusivities assigned to the particle pools.

Fits of the Ning model and the generalised exchange model are shown in Figure 9 for a maximum b-value of 10 ms/$\mu m^2$ (9a) and 40 ms/$\mu m^2$ (9b). The Ning model shows fitting error at high b-values due to its truncation of high order terms in $b$. Excellent agreement is apparent between the generalised exchange model and simulated data at all b-values. This is an expected result since one of the motivations behind the derivation of this model was to eliminate the restriction on b-value.

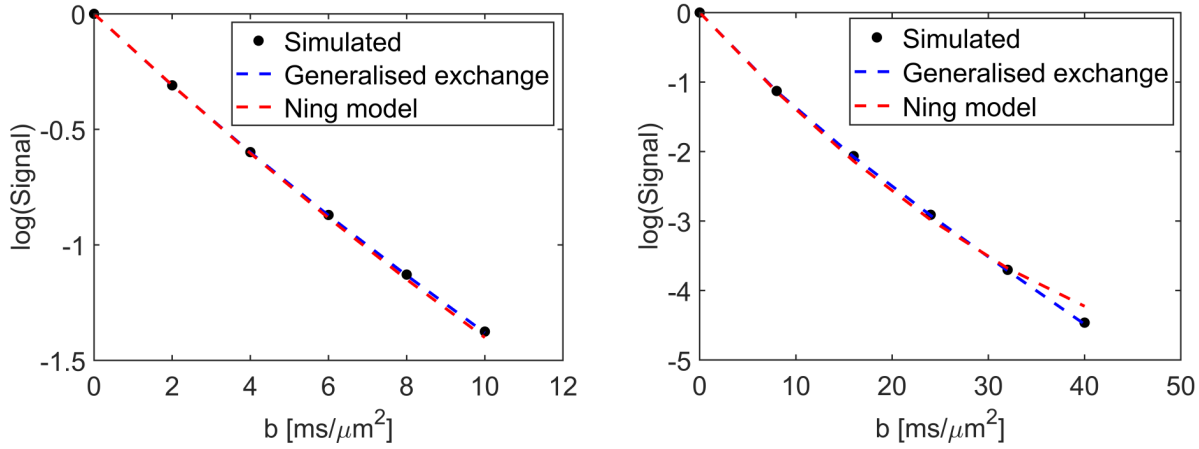


Figure 9: (a): Fit of the Ning model and the generalised exchange model to signals from two pools, for a maximum b-value of 10 ms/$\mu m^2$. The simulated data shown was generated using the waveform with $T = 240$ ms, an exchange rate of 10 $s^{-1}$ and pool diffusivities of 0.1 $\mu m^2$/ms and 0.3 $\mu m^2$/ms. (b): Same fit as described in (a) but with a maximum b-value of 40 ms/$\mu m^2$.

The trends shown in Figure 9 are also reflected in the accuracy of parameter estimates. Figure 10 presents the accuracy of the Ning model versus the generalised exchange model in estimating the exchange rate. Note the superb coherence between simulated and estimated exchange rates observed with the generalised exchange model. The Ning model tends to underestimate high exchange rates and overestimate low rates. This is a manifestation of the combined effects of high b-values and long total encoding times, both of which void the assumptions of this model. Consider Figure 11 which shows the estimated exchange rates at different b-values and encoding times. Exchange rates measured with the Ning model decrease with the encoding time and increase with b-value. The generalised exchange model provides stable estimates at the longest simulated encoding time and all b-values. This result is in harmony with theoretical expectations: the generalised exchange model places no restrictions on either b-value or total encoding time.

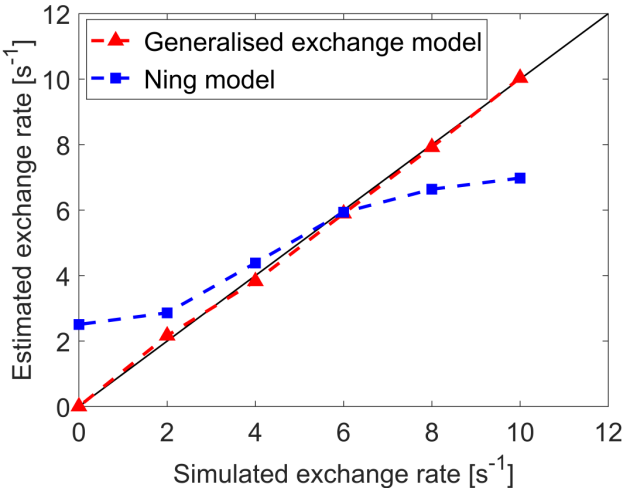


Figure 10: Comparison between the Ning and the generalised exchange models in accuracy of estimated exchange rates between two Gaussian pools. The diagonal shown in black is the line of equality representing complete agreement between estimated and simulated exchange rate. A maximum b-value of 10 ms/$\mu$m$^2$ was used in the simulations. The generalised exchange model gives accurate exchange rates at all simulated values, while the Ning model overestimates low rates and underestimates high ones.

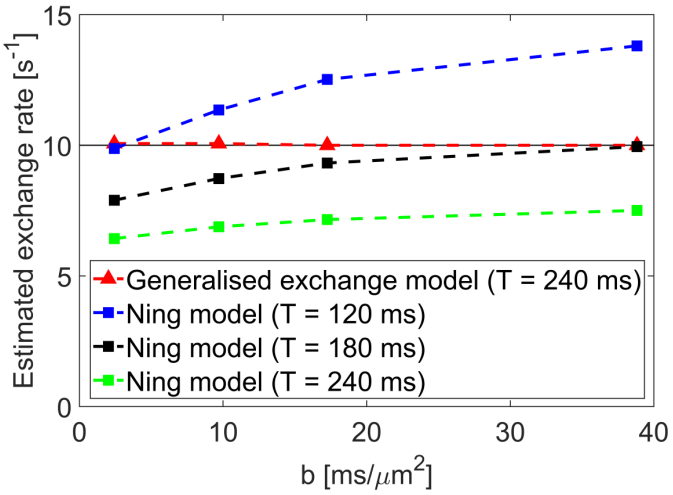


Figure 11: Dependence of exchange rates estimated by the Ning model on maximum b-value and total encoding time in an SDE experiment. For comparison, estimates by the generalised exchange model are shown for the longest simulated encoding time (240 ms). Simulations were performed in a two-pool environment with free diffusion and exchange. The true exchange rate was 10 s$^{-1}$. The acquisition protocol was a set of SDE waveforms with fixed width $\delta = 3$ ms (as shown in Figure 8a) and different total encoding times ($T = 120$, 180 and 240 ms). Exchange estimates by the Ning model vary with both b-value and $T$, which is not seen with the generalised exchange model even at the longest simulated encoding time.

Figure 12 shows a comparison of the precision in estimated exchange rates between the Ning and the generalised exchange models. A more accurate but less precise result is obtained with the generalised exchange model (mean 10.1 $s^{-1}$ and standard deviation 1.3 $s^{-1}$). The Ning model provides a more precise but less accurate result (mean 6.4 $s^{-1}$ and standard deviation 0.5 $s^{-1}$).

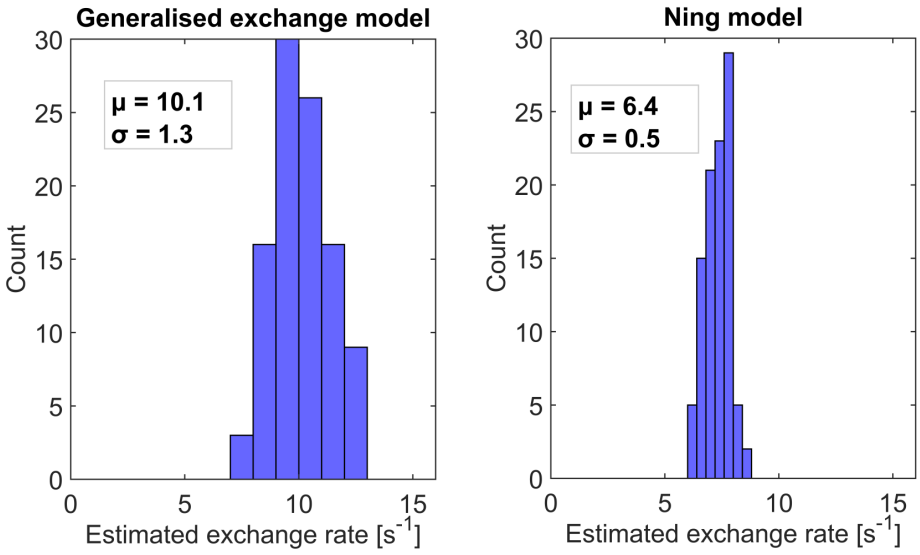


Figure 12: Comparison of precision in estimated exchange rate between the generalised exchange model and the Ning model. Simulations were performed in a two-pool setting modelling free diffusion and exchange. The true exchange rate was 10 $s^{-1}$. Signals were generated using the gradient waveforms shown in Figure 8a with a maximum b-value of 10 ms/$\mu$m$^2$. The histograms show results from fits to 100 signal curves obtained by adding Rician noise at an SNR of 200. The symbols $\mu$ and $\sigma$ denote mean and standard deviation, respectively. Estimates by the generalised exchange model are more accurate but less precise than estimates by the Ning model.

Gradient waveforms optimised for precision in estimates of the exchange rate are shown in Figure 13. The waveforms are non-trivial functions of time, but do share some characteristics. In particular, there is a common tendency to switch sign more than once during the first half of the total encoding time. All four waveforms exhibit a few relatively sharp peaks. However, these seemingly rapid switches need not pose a challenge, provided all hardware and physiological constraints are met. The impact of the optimised waveforms on accuracy and precision is shown in Figure 14. As anticipated, the waveforms have no effect on accuracy - a result which demonstrates the compatibility of the generalised exchange model with arbitrary gradient waveforms. Precision is, however, notably improved (mean 9.6 $s^{-1}$, standard deviation 0.7 $s^{-1}$, precision increase 200%).

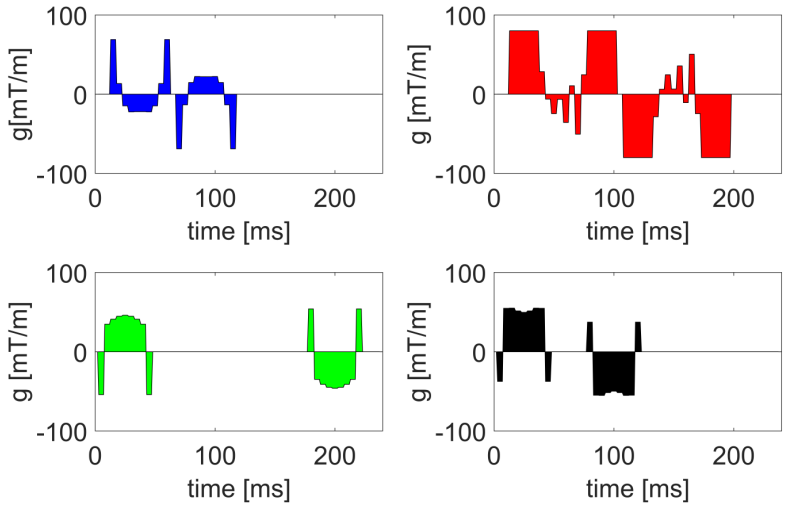


Figure 13: Gradient waveforms optimised for minimum variance in exchange rates between two Gaussian pools, estimated using the generalised exchange model. The waveforms were obtained using the Cramer-Rao Lower Bound (CRLB)-approach, initialised with different SDE waveforms at a temporal resolution of 1 ms. Timing parameters (pulse width, $\delta$ and time interval, $\Delta$) were kept fixed and the gradient amplitude at every time-point was allowed to vary.

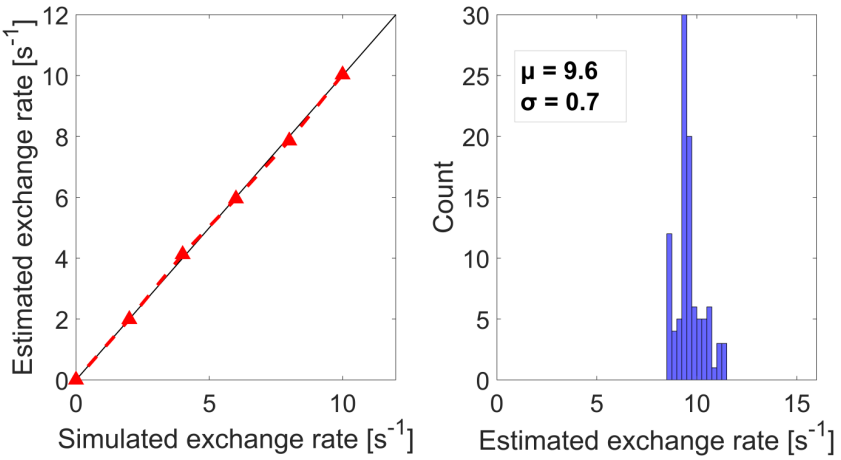


Figure 14: Left: accuracy in exchange rates estimated with the generalised exchange model. The black diagonal is the line of equality indicating complete agreement between estimated and simulated exchange rates. Simulations modelled exchange between two Gaussian pools, and signals were generated using the optimised waveforms in Figure 13 with a maximum b-value of 10 ms/$\mu$m$^2$. There is good agreement between estimated and simulated exchange rates. Right: precision in estimated exchange rates with the generalised exchange model and the optimised waveforms in Figure 13. The true exchange rate was 10 s$^{-1}$. One hundred signal curves were generated by adding Rice-distributed noise at an SNR of 200. The standard deviation in the figure is about half the value reported for the generalised exchange model in Figure12.

## 5.3 Two compartments: restricted diffusion and exchange

Figure 15 shows the set of SDE waveforms used for measuring compartment diameters and exchange rates in a two-compartment substrate. Waveforms in the same column have equal pulse width ($\delta$) and those in the same row have equal time intervals ($\Delta$). The blend of different values of these timing parameters is meant to yield different exchange and restriction weightings at different time scales.

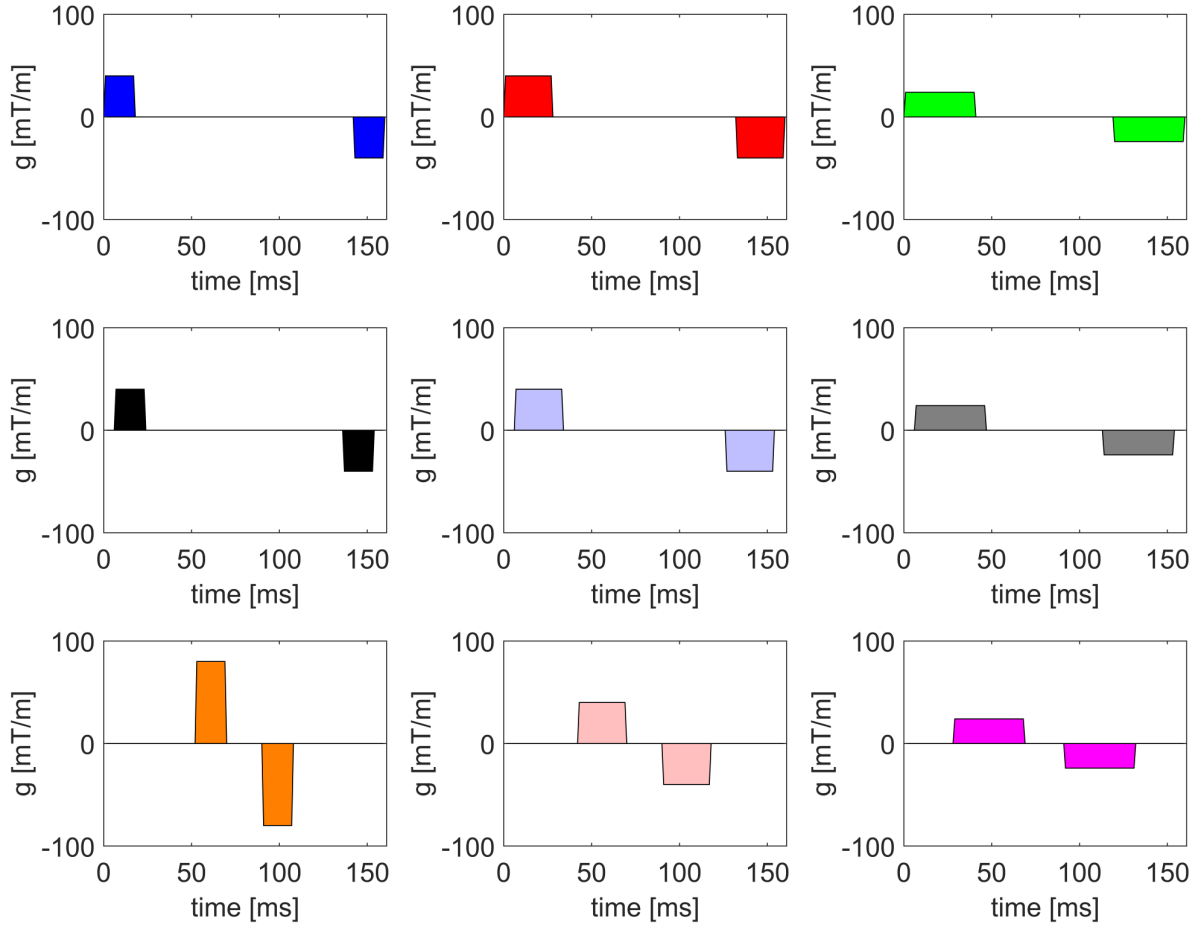


Figure 15: Pulsed-gradient waveforms used to probe restricted diffusion and exchange. Waveforms in each column have the same duration ($\delta$) while those in the same row have equal time intervals ($\Delta$). Different combinations of $\delta$ and $\Delta$ are used to obtain different exchange and restriction weightings. The waveforms in this protocol have a maximum amplitude of 80 mT/m and a maximum slew rate of 70 T/(m·s).

The signal differences due to exchange and restriction under the influence of these waveforms are shown in Figure 16a. Every signal curve is plotted in the same colour as the gradient waveform that generated it. Contrary to the two-pool scenario, a relatively low

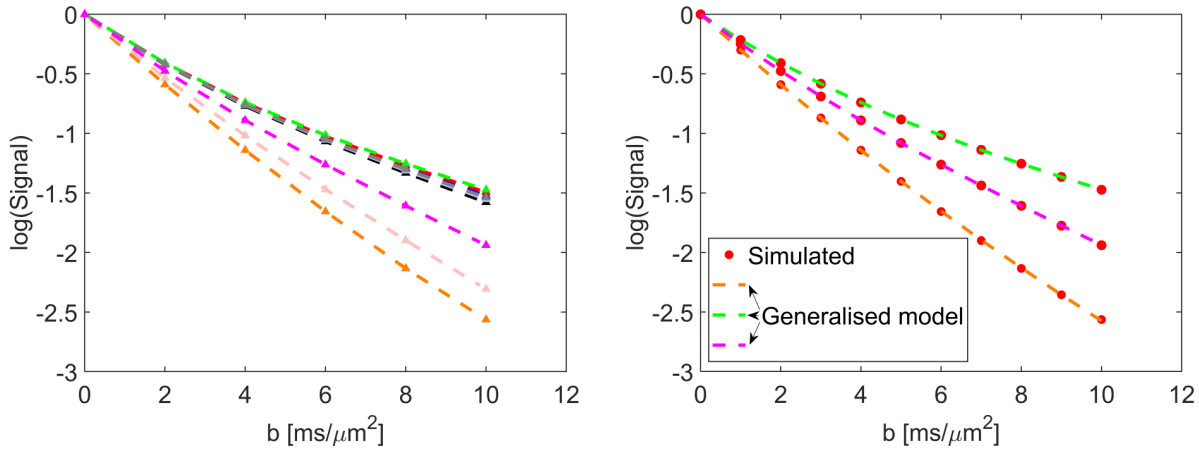


(a) (b)

Figure 16: (a): Signals generated using the SDE waveforms in Figure 15 in a two-compartment setup modelling restricted diffusion and exchange. The signal curves are plotted in the same colour as the gradient waveform that generated them. An exchange rate of 10 $s^{-1}$ and a compartment diameter of 20 $\mu$m were used to obtain the data shown. The divergence of the signal curves with growing b-value is a result of restricted diffusion and exchange. (b): Fit of the generalised model to the simulated signal curves. For clarity, the fit is shown for only the three curves with least, intermediate and most attenuation (green, violet and orange, respectively). The generalised model fits the simulated data well.

b-value of 2 ms/$\mu$m$^2$ would enable probing of restriction and exchange in this experiment. Regardless, considerably higher b-values were simulated to demonstrate the versatility of the developed theory. Note the uneven separation of the signal curves in Figure 16a: three distinct curves and six in a group. Figure 16b shows that the generalised model fits the simulated data well up to the maximum b-value of 10 ms/$\mu$m$^2$. For clarity, the fit is depicted only for the signal curves with most, intermediate and least attenuation. This corresponds to the curves plotted in orange, violet and green, respectively.

As is evident in Figure 17, the generalised model provides accurate estimates of exchange rate and compartment diameter over a wide range of values of these parameters. Some degree of bias can be noted for diameters around 4 $\mu$m and an exchange rate of 1 $s^{-1}$. Since no aspect of the generalised model can be used to explain the observed bias, it can be attributed to the simulation framework. It is likely that the discrepancy may be eliminated by increasing the number of random walkers in the simulations.

Results of the study of precision in the estimated diameter and exchange rate with SDE waveforms are presented in Figure 18. There is a slight tendency of the generalised model to overestimate exchange (mean 10.7 $s^{-1}$, standard deviation 1.3 $s^{-1}$) and underestimate

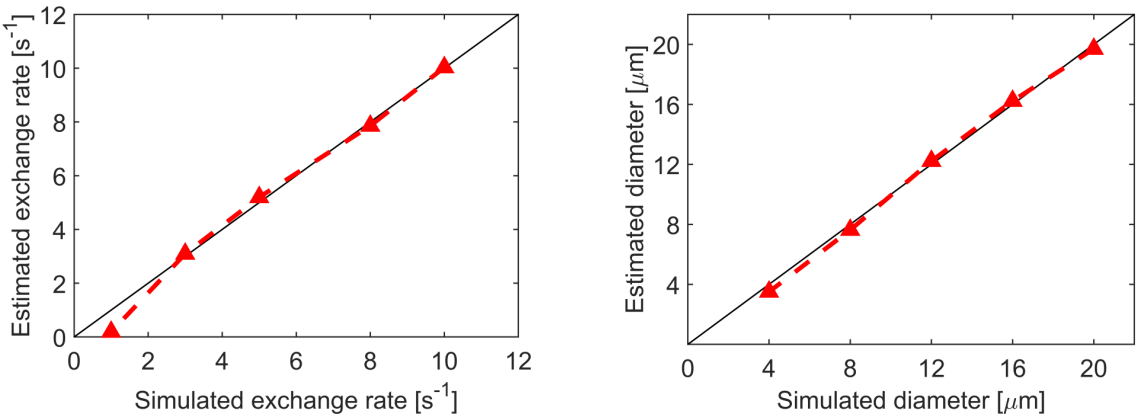


(a) (b)

Figure 17: (a): Accuracy of the generalised model in estimating the exchange rate between two compartments in a cylindrical geometry. The diagonal on the correlation plot represents complete coherence between model and simulation. Exchange rates shown in the figure were estimated from signals generated using the SDE gradient waveforms in Figure 15 with a maximum b-value of 10 ms/$\mu$m$^2$. The compartment diameter was fixed at 20 $\mu$m. (b): Accuracy of estimated compartment diameter with the generalised model. The same acquisition protocol as described in (a) was used, with the exchange rate being kept fixed at 10 s$^{-1}$.

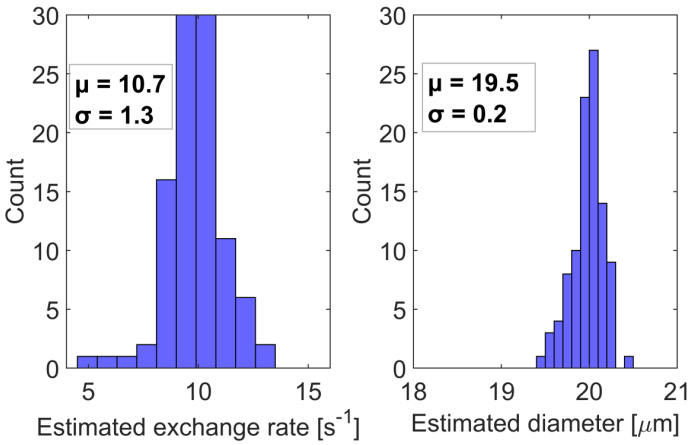


Figure 18: Precision of the generalised model in estimating the exchange rate between two compartments (left) and the compartment diameter (right) in a cylindrical substrate. The true exchange rate and diameter were 10 s$^{-1}$ and 20 $\mu$m, respectively. Signals from which the exchange rate and diameter were estimated were generated using the SDE protocol in Figure 15 with a maximum b-value of 10 ms/$\mu$m$^2$. Rice-distributed noise was added to obtain 100 signal curves at an SNR of 200. The mean and standard deviation of the distributions are denoted by $\mu$ and $\sigma$, respectively.

the diameter (mean 19.5 $\mu$m, standard deviation 0.2 $\mu$m). However, the estimated parameters are in remarkable agreement with the underlying values.

Free waveforms optimised for precision in diameter and exchange rate estimates are shown in Figure 19. The resulting shape of each waveform is determined by the time settings of the initial SDE guess (pulse width and spacing). Note that "pulse spacing" in the discussion below is referring to the time interval between the end of the first pulse and the start of the second one. This is to be distinguished from the waveform parameter $\Delta$, which is the difference between the start times of the two pulses. It is apparent from Figure 19 that the pulse spacing is more influential than pulse width in deciding the output shape. Waveforms with short spacings (blue, red, light red and magenta) have a characteristic

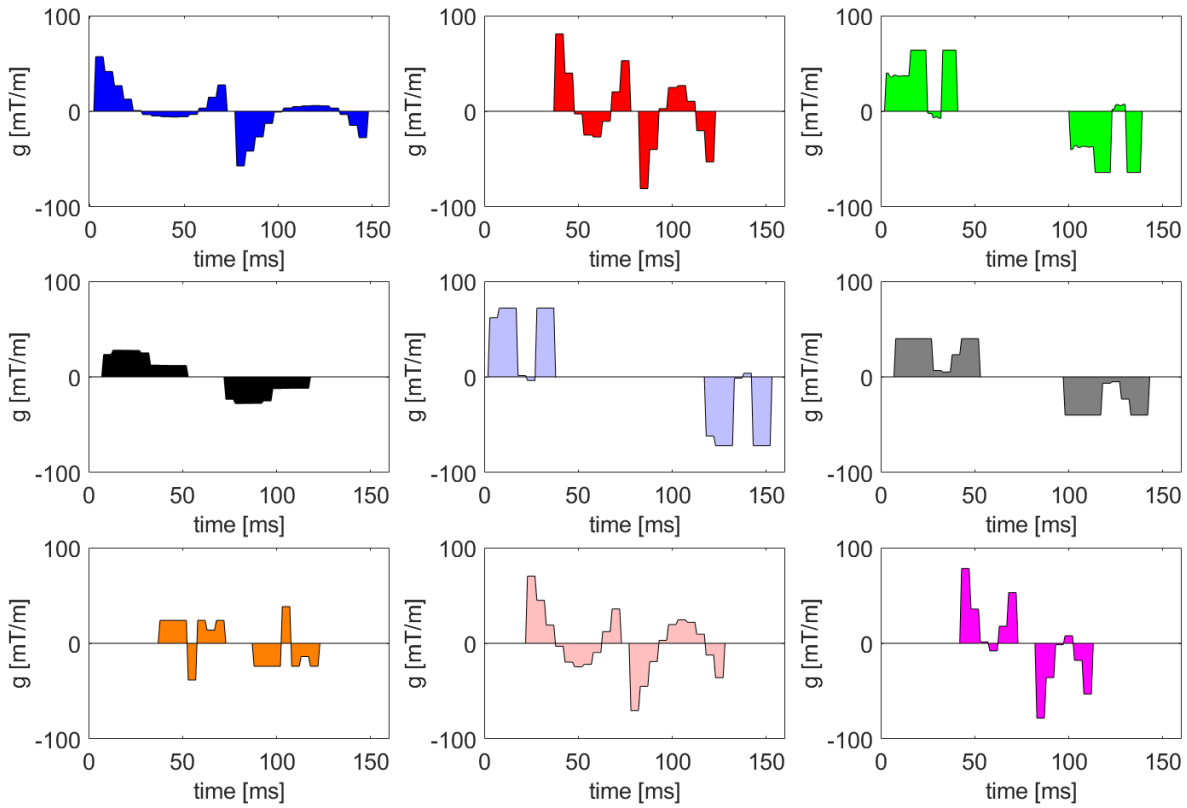


Figure 19: A set of gradient waveforms optimised for precision in exchange rate and compartment diameter estimated with the generalised model. Optimisation was done using the Cramer-Rao Lower Bound (CRLB) method at a temporal resolution of 1 ms. SDE waveforms with different combinations of durations ($\delta$) and time intervals ($\Delta$) were used as initial guesses. The optimiser kept these timing parameters fixed and varied the amplitude of the waveform in every time-point. Maximum amplitude and slew rate were constrained to 80 mT/m and 70 T/(m·s), respectively.

shape and so do waveforms with long spacings (green, light blue and grey). Shapes of waveforms with intermediate spacings (black and orange) are not as easily characterised.

Signal differences driven by restriction and exchange as determined by the optimised waveforms are shown in Figure 20a. The signals are plotted in the same colours as the gradient waveform that generated them. Note that nearly all the waveforms in the optimised protocol produce distinct signal curves, which is in contrast to Figure 16a for the SDE protocol. The fit of the generalised model to the signals generated by the optimised waveforms is shown in Figure 20b for the gray, orange and light red signal curves (corresponding to least, intermediate and most attenuation, respectively). It is worth highlighting that the result in Figure 20b illustrates the versatility of the generalised model in terms of gradient waveform design.

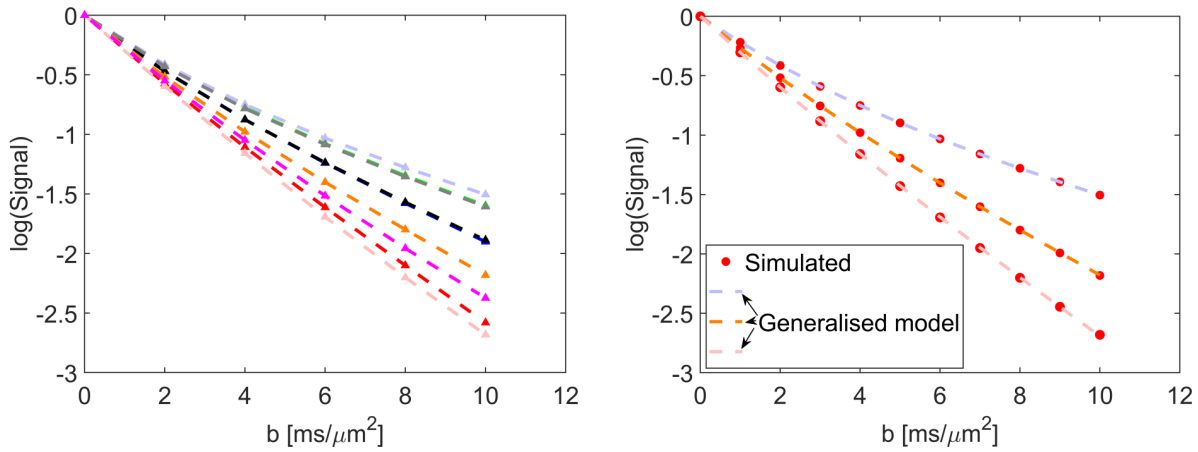


(a) (b)

Figure 20: (a): Signals acquired from a two-compartment substrate simulating restricted diffusion and exchange. The exchange rate and compartment diameter were 10 $s^{-1}$ and 20 $\mu$m, respectively. Gradient waveforms shown in Figure 19 were used to generate the signal curves. Each curve is plotted in the same colour as its corresponding gradient waveform. Restricted diffusion and exchange induce the separation of the curves with increasing b-value. (b): Fit of the generalised model to the simulated signals, shown for signal curves with least, intermediate and most attenuation (gray, orange and light red, respectively). There is good agreement between the simulated data and the generalised model.

The impact of the optimised waveforms on parameter estimates is displayed in Figure 21. The effect on precision in exchange rate is negligible (mean 11 $s^{-1}$, standard deviation 1.2 $s^{-1}$, precision increase 8%), while the improvement in diameter estimates is notable (mean 20.5 $\mu$m, standard deviation 0.1 $\mu$m, precision increase 200 %). These results may be improved by addressing the shortcomings of the waveform optimisation as outlined in Section 4.1.

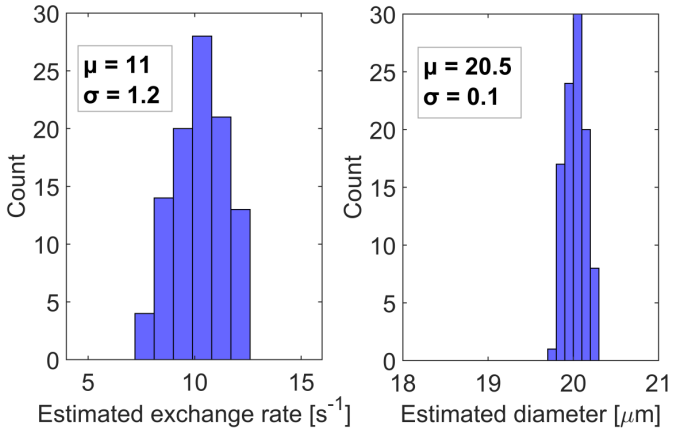


Figure 21: Effect of numerically optimised waveforms on the precision of estimated exchange rate (left) and compartment diameter (right) in a cylindrical confinement. The true exchange rate and diameter were 10 s$^{-1}$ and 20 $\mu$m, respectively. Signals used to estimate the parameters were generated using the optimised gradient waveforms in Figure 19 with a maximum b-value of 10 ms/$\mu$m$^2$. Rice-distributed noise was added to obtain 100 signal curves at an SNR of 200. The standard deviation in the diameter is half the value provided in Figure 18.

Results of fitting the VA signal representation are shown in Figure 22. Note that these

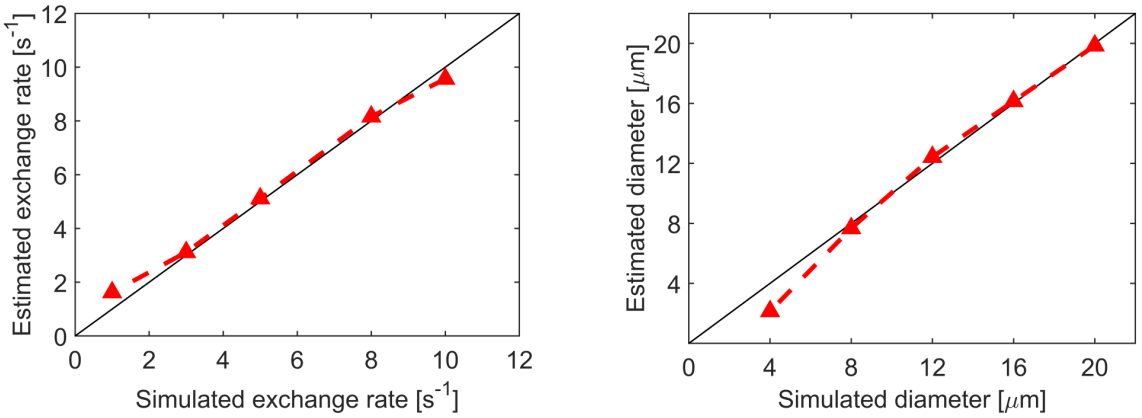


(a) (b)

Figure 22: (a): Accuracy of the VA model in estimating the exchange rate between two compartments on a cylindrical substrate. The diagonal in black represents full agreement between estimated and simulated exchange rates. Simulated data from which the exchange rates were estimated was obtained using the SDE gradient waveforms in Figure 15 with a maximum b-value of 5 ms/$\mu$m$^2$. A fixed compartment diameter of 20 $\mu$m was used while the exchange rate was varied. (b): Accuracy of estimated compartment diameter with the VA model. Simulated data was obtained in the same way as described in (a), except with varying diameters and a fixed exchange rate of 10 s$^{-1}$.

results correspond to simulations with SDE waveforms. The VA model gives accurate estimates of moderate exchange rates. Low rates are slightly overestimated while high rates are somewhat underestimated. This behaviour is reminiscent of the Ning model at high b-values and long encoding times. In the case of the VA model, this bias can be attributed to its truncation of higher order terms in $b$. A possible solution is to use an acquisition protocol with a maximum b-value that is lower than 5 ms/$\mu$m$^2$. The VA underestimates the smallest simulated diameter (4 $\mu$m). Good agreement with simulations is evident for larger diameters. The underestimation of small compartment sizes was also observed, albeit to a lesser degree, with the generalised model. As noted for the generalised model, increasing the number of random walkers may alleviate this weakness.

Figure 23 shows estimated exchange rates and diameters from SDE signals using the VA model. The parameter estimates are close to the ground truth: mean exchange rate of 9.7 s$^{-1}$ with a standard deviation of 0.9 s$^{-1}$ and mean diameter of 20 $\mu$m with a standard deviation of 0.2 $\mu$m. These results indicate that the precision of the VA at an SNR of 200 parallels that of the generalised model.

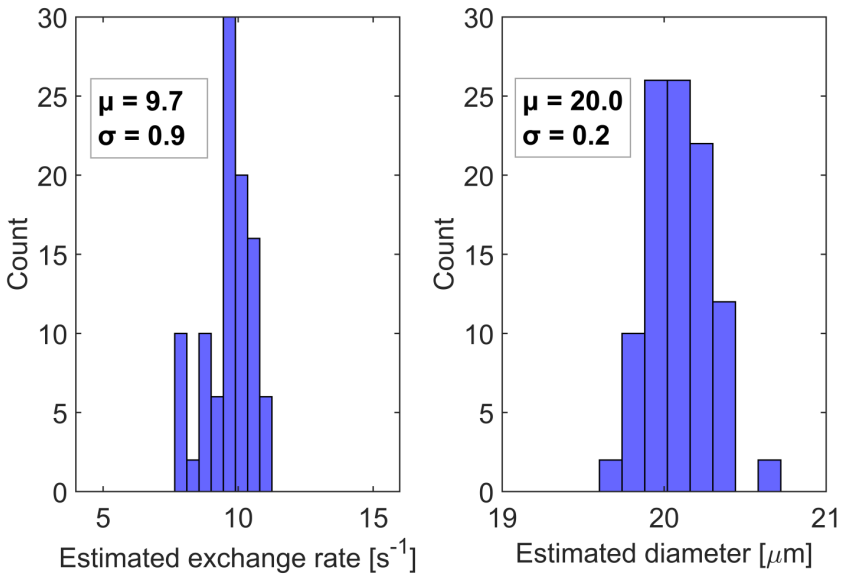


Figure 23: Precision of the VA model in estimating the exchange rate (left) and compartment diameter (right) in a two-compartment substrate modelling restricted diffusion and exchange. The true exchange rate and diameter were 10 s$^{-1}$ and 20 $\mu$m, respectively. Signals used to estimate exchange rate and diameter were generated using the SDE protocol shown in Figure 15 with a maximum b-value of 5 ms/$\mu$m$^2$. One hundred signals were generated as a result of adding Rician noise at an SNR of 200.

# 6 Outlook

This thesis work has developed a robust generalisation of the exchange theory in diffusion MRI that accommodates arbitrary gradient waveforms and is valid for all b-values and all time scales. A second-order expansion of the developed theory was shown to concur with the signal representation derived by Ning et al. [44]. Monte Carlo simulations saw the generalised theory developed here providing superior exchange estimates when compared with the Ning model. Numerically optimised waveforms with the generalised exchange model improved precision in exchange rates by a factor of 2 compared to SDE waveforms. This highlights the benefit of choosing free waveforms over standard sequences.

The present work has also demonstrated that the generalised exchange model can be successfully combined with restriction theory, yielding a unified framework describing the effects of restricted diffusion and exchange at all time scales. Excellent coherence with simulations was observed. A drastic improvement in precision of the estimated compartment diameter was obtained with optimised gradient waveforms (200% relative to SDE sequences). Precision in exchange rate was largely unaffected and a possible remedy is an optimisation technique that varies the timing of the waveforms in addition to their amplitude. There is ample room for improvement of the waveform optimisation framework by using a more appropriate noise model together with a global solver.

With the objective of deriving a restriction-exchange signal equation easier to interpret than the generalised model, an alternative angle was also explored. The relationship between the particle velocity autocorrelation function and restricted diffusion was exploited to derive a second-order signal representation valid for moderate b-values, all time scales and arbitrary gradient waveforms. Numerical validation of this approach gave promising results. That said, this theory is to be perceived as an instrument for gaining insights about the generalised model and providing conceptual understanding towards the design of experiments to probe exchange and restriction. For forward modelling and parameter estimation, the generalised model is the more appropriate choice.

The outcome of this work serves as a stepping stone for future research towards optimising experiments to provide reliable parameter estimates while minimising scan times. Such research will be central to the ultimate clinical implementation of the approach presented in this thesis work.

# References


[1] World Health Organisation. The top 10 causes of death [Internet]. Who.int. 2020 [cited 29 May 2020]. Available from: https://www.who.int/news-room/fact-sheets/detail/the-top-10-causes-of-death

[2] Sanak D, Horak D, Herzig R. Hlustik P. Kanovsky P. The role of magnetic resonance imaging for acute ischemic stroke. Biomed Pap Med Fac Univ Palacky Olomouc Czech Repub. 2009 Sep;153(3):181-7

[3] Drake-Pérez M, Boto J, Fitsiori A, Lovblad K, Vargas MI. Clinical applications of diffusion weighted imaging in neuroradiology. Insights Imaging. 2018 May;9(4):535-547

[4] Chilla GS, Tan CH, Xu C, Poh CL. Diffusion weighted magnetic resonance imaging and its recent trend-a survey. Quant Imaging Med Surg. 2015 Jun;5(3):407-22

[5] Mabray MC, Cha S. Advanced MR Imaging Techniques in Daily Practice. Neuroimaging Clin N Am. 2016 Nov;26(4):647-666

[6] Baliyan V, Das CJ, Sharma R, Gupta AK. Diffusion weighted imaging: Technique and applications. World J Radiol. 2016 Sep;8(9):785-798

[7] Okorie CK, Ogbole GI, Owolabi MO, Ogun O, Adeyinka A, Ogunniyi A. Role of Diffusion-weighted Imaging in Acute Stroke Management using Low-field Magnetic Resonance Imaging in Resource-limited Settings. West Afr J Radiol. 2015 Jul-Dec;22(2):61-66

[8] Bourne R, Panagiotaki E. Limitations and Prospects for Diffusion-Weighted MRI of the Prostate. Diagnostics. 2016 May;6(2):21.

[9] Lampinen B, Szczepankiewicz F, van Westen D, Englund E, C Sundgren P, Lätt J, Ståhlberg F, Nilsson M. Optimal experimental design for filter exchange imaging: Apparent exchange rate measurements in the healthy brain and in intracranial tumors. Magn Reson Med. 2017 Mar;77(3):1104-1114

[10] Baserga R. Is cell size important?. Cell Cycle. 2007 Apr;6(7):814-6

[11] Jiang X, Li H, Xie J, McKinley ET, Zhao P, Gore JC, Xu J. In vivo imaging of cancer cell size and cellularity using temporal diffusion spectroscopy. Magn Reson Med. 2017 Jul;78(1):156-164

[12] Reynaud O. Time-Dependent Diffusion MRI in Cancer: Tissue Modeling and Applications. Front Phys. 2017 Nov;5

[13] Lee HS, Papaioannou A, Novikov DS, Fieremans E. In vivo observation and biophysical interpretation of time-dependent diffusion in human cortical gray matter [Preprint] 2020. Available from https://doi.org/10.1016/j.neuroimage.2020.117054

[14] Stepišnik J. Time-dependent self-diffusion by NMR spin-echo. Physica B: Condensed Matter. 1993 May;183(4):343-350.

[15] Nilsson M, Westin CF, Brabec J, Lasic S, Szczepankiewicz F. A unified framework for analysis of time-dependent diffusion: numerical validation of a restriction-exchange correlation experiment. Proceedings of ISMRM. Montreal, QC, Canada. 2019

[16] Edelman RR. The history of MR imaging as seen through the pages of radiology. Radiology. 2014 Nov;273(2 Suppl):S181-200

[17] Grover VP, Tognarelli JM, Crossey MM, Cox IJ, Taylor-Robinson SD, McPhail MJ. Magnetic Resonance Imaging: Principles and Techniques: Lessons for Clinicians. J Clin Exp Hepatol. 2015 Sep;5(3):246-55

[18] Bloch F, Hansen WW, Packard ME. Nuclear induction. Phys Rev. 1946 Oct; 69(127)

[19] Purcell EM, Torrey HC, Pound RV. Resonance absorption by nuclear magnetic moments in a solid. Phys Rev.1946 Jan; 69:37-38

[20] Damadian R. Tumor detection by nuclear magnetic resonance. Science. 1971 Mar;171(3976):1151-1153

[21] Lauterbur PC. Image formation by induced local interactions. Examples employing nuclear magnetic resonance. Clin Orthop Relat Res. 1973 Mar ;242(5394):190-191

[22] Westbrook C, Roth CK, Talbot J.MRI in Practice. 4th ed. London: John Wiley & Sons, Inc.; 2011.

[23] Hanson L. Is quantum mechanics necessary for understanding magnetic resonance?. Concepts Magn. Reson. 2008 Sep;32A(5):329-340.

[24] Brown R. F.R.S. Hon. M.R.S.E. & R.I. Acad. V.P.L.S. (1828) XXVII. A brief account of microscopical observations made in the months of June, July and August 1827, on the particles contained in the pollen of plants; and on the general existence of active molecules in organic and inorganic bodies. The Philosophical Magazine. 4(21): 161-173

[25] Fick, A. Ueber Diffusion. Ann. Phys.1855; 170:59-86

[26] Kingsley PB. Introduction to diffusion tensor imaging mathematics: Part III. Tensor calculation, noise, simulations, and optimization. Concepts Magn Reson. 2006 Mar; 28A(2):155-179

[27] Einstein A. Investiations on the theory of the Brownian movement. Dover Publications Inc. 1956

[28] Kiselev VG. Fundamentals of diffusion MRI physics. NMR Biomed. 2017 Mar;30(3):e3602

[29] Johansen-Berg H. Behren TEJ. Diffusion MRI. 1st Edition. Academic Press. 2009

[30] Brabec J et al. Time-dependent diffusion in undulating structures: Impact on axon diameter estimation. NMR Biomed. 2020 Mar;33(3):e4187

[31] Hall MG. Continuity, the Bloch-Torrey equation, and Diffusion MRI. arXiv: Medical Physics. 2016

[32] Torrey HC. Bloch Equations with Diffusion Terms. Physical Review. 1956 Nov; 104(3):563-565

[33] Kuchel P, Pagès G, Nagashima K, Velan S, Vijayaragavan V, Nagarajan V et al. Stejskal-tanner equation derived in full. Concepts Magn Reson. 2012 Sep;40A(5):205-214.

[34] Stejskal EO, Tanner JE. Spin diffusion measurements: spin echoes in the presence of a time-de- pendent field gradient. J Chem Phys. 1965 Jan; 42:288–292.

[35] Callaghan PT. Principles of Nuclear Magnetic Resonance Microscopy. New York: Oxford University Press; 1991.

[36] Razumas V, Lindman B, Nylander T. Surface and Colloid Science. Berlin Heidelber: Springer Verlag; 2001

[37] Tycko R. Nuclear magnetic resonance probes of molecular dynamics. Dordrecht: Kluwer Academic; 1995.

[38] Rutledge D. Signal Treatment and Signal Analysis in NMR. Burlington: Elsevier Science; 1996.

[39] Zheng Q. Computing Relations between Moments and Cumulants. Computational Statistics. 2002 Dec;17(4):507-515.

[40] Rodriguez A. Tsallis C. A generalisation of the cumulant expansion. Application to a scale-invariant probabilitic model. J Math Phys. 2010 Jul;51(7)

[41] Kärger J. NMR self-diffusion studies in heterogeneous systems. Adv Colloid Interfac. 1985 Aug;23:129–148.

[42] Fieremans E, Novikov D, Jensen J, Helpern J. Monte Carlo study of a two-compartment exchange model of diffusion. NMR Biomed. 2010 Aug;23(7):711-724.

[43] Tian X, Li H, Jiang X, Xie J, Gore J, Xu J. Evaluation and comparison of diffusion MR methods for measuring apparent transcytolemmal water exchange rate constant. J Magn Reson. 2017 Feb;275:29-37.

[44] Ning L, Nilsson M, Lasič S, Westin C, Rathi Y. Cumulant expansions for measuring water exchange using diffusion MRI. J Chem Phys. 2018 Feb;148(7):074109.

[45] Yablonskiy D, Sukstanskii A. Theoretical models of the diffusion weighted MR signal. NMR Biomed. 2010 Aug;23(7):661-681.

[46] Nilsson M, Lasič S, Drobnjak I, Topgaard D, Westin C. Resolution limit of cylinder diameter estimation by diffusion MRI: The impact of gradient waveform and orientation dispersion. NMR Biomed. 2017 Jul;30(7):e3711.

[47] deSwiet TM, Sen PN. Time dependent diffusion coefficient in a disordered medium. J Chem Phys. 1998 Aug;104(1):206–209

[48] Latour LL, Svoboda K, Mitra PP, Sotak CH. Time-dependent diffusion of water in a biological model system. Proc Natl Acad Sci USA. 1994 Feb;91(4):1229–1233

[49] Novikov DS, Fieremans E, Jensen JH, Helpern JA. Random walk with barriers. Nat Phys. 2011 Mar; 7:508–514

[50] Maple (2018). Maplesoft, a division of Waterloo Maple Inc., Waterloo, Ontario

[51] Parsons EC Jr, Does MD, Gore JC. Temporal diffusion spectroscopy: theory and implementation in restricted systems using oscillating gradients. Magn Reson Med. 2006 Jan;55(1):75-84

[52] Chandrasekhar S. The Relation Between the Fourth and Second Order Correlations When the Velocity Follows a Gaussian Distribution. In: Spiegel E. The Theory of Turbulence. Lecture Notes in Physics, vol 810. Dordrecht: Springer; 2011.p.61-69

[53] Perina J. Quantum statistics of linear and nonlinear optical phenomena. Netherlands: Springer; 1984.

[54] Wang MC, Uhlenbeck GE. On the theory the Brownian motion II. Rev Mod Phys. 1945 Apr; 17(2-3):323-342

[55] Balkovsky E, Chertkov M, Kolokolov I, Lebedev V. The fourth-order correlation function of a randomly advected passive scalar. arXiv: chao-dyn. 1995

[56] Alexander DC. A general framework for experiment design in diffusion MRI and its application in measuring direct tissue-microstructure features. Magn Reson Med. 2008 Aug;60(2):439-48

[57] Mohammad A, Maier SE, Yu-Hua Gu I, Mehnert A, Kahl F. Optimal Experiment Design for Monoexponential Model Fitting: Application to Apparent Diffusion Coefficient Imaging. Biomed Res Int. 2015 Dec;2015:138060

[58] Brihuega-Moreno O, Heese FP, Hall LD. Optimization of Diffusion Measurements Using Cramer-Rao Lower Bound Theory and Its Application to Articular Cartilage. Magn Reson Med. 2003 Nov;50(5):1069-76

[59] Gudbjartsson H, Patz S. The Rician Distribution of Noisy MRI Data. Magn Reson Med. 1995 Dec;34(6):910–914

[60] Bouhrara M, Spencer RG. Fisher Information and Cramér-Rao Lower Bound for Experimental Design in Parallel Imaging. Magn Reson Med. 2018 Jun;79(6):3249–3255

[61] Middione MJ, Loecher M, Moulin K, Ennis DB. Optimization methods for magnetic resonance imaging gradient waveform design [Preprint] 2020. Availbale from https://doi.org/10.1002/nbm.4308

[62] Onwubolu G, Babu B. New optimization techniques in engineering. Berlin: Springer; 2004.

[63] Szafer A, Zhong J, Gore J. Theoretical Model for Water Diffusion in Tissues. Magn Reson Med. 1995 May;33(5):697-712

# A Appendix: Generalising the Kärger model

## Appendix A1

GENERALISING THE KÄRGER MODEL:

**This is a Maple script that generates terms of the second-order series expansion of the generalised Kärger model, in both exact (S9) and approximate (S12) forms.**

```
> restart
> K := [ -k12   k21 ]
       [  k12  -k21 ] :   Exchange rates
> ADC := [ D1   0  ]
         [ 0    D2 ] :   Diffusivities
> ones := [ 1  1 ] :
> F := [ f1 ]
       [ f2 ] :          Signal fractions
> M(q) := (K·d_t − ADC·q^2·d_t) :
```

**We will begin with a few values of N and then generalise to any N**

```
> S := ones • LinearAlgebra[MatrixExponential](M(q1))
       • LinearAlgebra[MatrixExponential](M(q2)) • F :
> #S:=ones.LinearAlgebra[MatrixExponential](M(q1))
       • LinearAlgebra[MatrixExponential](M(q2))
       • LinearAlgebra[MatrixExponential](M(q3))
       • LinearAlgebra[MatrixExponential](M(q4))
       • LinearAlgebra[MatrixExponential](M(q5)) • F :
```

**Take multivariate Taylor expansion of ln(S) around q_i = 0**

```
> S1 := mtaylor(ln(S), [q1 = 0, q2 = 0, q3 = 0, q4 = 0, q5 = 0, q6 = 0, q7 = 0], 5) :
```

**Simplify the results by making some substitutions**

```
> S1 := simplify(S1, sqrt) assuming (k12 + k21 > 0, T > 0) :   Exchange rates are positive
> S1 := simplify(subs(f1 + f2 = 1, S1)) :                      Signal fractions must add up to 1
> S1 := simplify(subs(f1 k12 − f2 k21 = 0, S1)) :              Condition of equilibrium
> S1 := simplify(subs(k21 = f1·k, k12 = f2·k, S1)) :           Condition of equilibrium
> S1 := simplify(subs(f1 + f2 = 1, S1)) :
```

```
> S3 := subs( (D2-D1)^2 = VarD/(f1*f2), S1 ) :          Definition of variance
> S4 := collect(S3, VarD) :
> S5 := collect(S4, D2^2) :
> S6 := collect(S5, D1^2) :
> S7 := ( (collect(S6, D1)) ) :
> S8 := ( algsubs( (D1 - D2)^2 = VarD/(f1*f2), S7 ) ) :
> S9 := collect( (S8), VarD)
```

$$S9 := \mathrm{D}_1 \left( -d\_t\,(q1^2+q2^2)\,f_1\,(f_1+f_2) - \frac{1}{k^2}\left(2 f_1 f_2\,(d\_t\,k\,q1^4 + d\_t\,k\,q2^4 + \mathrm{e}^{-d\_t\,k}\,q1^4 \right.\right. \tag{1}$$

$$\left.\left. - 2\,\mathrm{e}^{-d\_t\,k}\,q1^2\,q2^2 + \mathrm{e}^{-d\_t\,k}\,q2^4 + q1^2\,q2^2\,\mathrm{e}^{-2\,d\_t\,k} - q1^4 + q2^2\,q1^2 - q2^4)\,\mathrm{D}_2\right)\right)$$

$$+ \frac{1}{k^2}\left(2 f_1 f_2\,(d\_t\,k\,q1^4 + d\_t\,k\,q2^4 + \mathrm{e}^{-d\_t\,k}\,q1^4 - 2\,\mathrm{e}^{-d\_t\,k}\,q1^2\,q2^2 + \mathrm{e}^{-d\_t\,k}\,q2^4\right.$$

$$\left. + q1^2\,q2^2\,\mathrm{e}^{-2\,d\_t\,k} - q1^4 + q2^2\,q1^2 - q2^4)\,\mathrm{D}_2\,\mathrm{D}_1\right) - d\_t\,(q1^2+q2^2)\,f_2\,(f_1+f_2)\,\mathrm{D}_2$$

$$+ \frac{1}{k^2}\left((d\_t\,k\,q1^4 + d\_t\,k\,q2^4 + \mathrm{e}^{-d\_t\,k}\,q1^4 - 2\,\mathrm{e}^{-d\_t\,k}\,q1^2\,q2^2 + \mathrm{e}^{-d\_t\,k}\,q2^4 + q1^2\,q2^2\,\mathrm{e}^{-2\,d\_t\,k}\right.$$

$$\left. - q1^4 + q2^2\,q1^2 - q2^4)\,VarD\right)$$

**Now expand the exponentials in S9 to third order**

```
> S10 := simplify( subs( e^(-d_t*k) = 1 - k*d_t + k^2*d_t^2/2 - k^3*d_t^3/6, e^(-2*d_t*k) = 1 - 2*k*d_t
      + 4*k^2*d_t^2/2 - 8*k^3*d_t^3/6, e^(-3*d_t*k) = 1 - 3*k*d_t + 9*k^2*d_t^2/2 - 27*k^3*d_t^3/6, e^(-4*d_t*k) = 1
      - 4*k*d_t + 16*k^2*d_t^2/2 - 4^3*k^3*d_t^3/6 , e^(-5*d_t*k) = 1 - 5*k*d_t + 25*k^2*d_t^2/2
      - 5^3*k^3*d_t^3/6, e^(-6*d_t*k) = 1 - 6*k*d_t + 36*k^2*d_t^2/2 - 6^3*k^3*d_t^3/6, e^(-7*d_t*k) = 1 - 7*k*d_t
      + 49*k^2*d_t^2/2 - 7^3*k^3*d_t^3/6, S9 ) ) :
> S11 := ( subs( (D1-D2)^2 = VarD/(f1*f2), S10 ) ) :
> S12 := collect(simplify(S11), VarD)
```

$$S12 := -\frac{d\_t\,(d\_t\,(d\_t\,k-3)\,q1^4 + 6\,d\_t\,(d\_t\,k-1)\,q2^2\,q1^2 + q2^4\,d\_t\,(d\_t\,k-3))\,VarD}{6} \tag{2}$$

$$- \frac{d\_t\left(6\,(f_1+f_2)\,(\mathrm{D}_1 f_1 + \mathrm{D}_2 f_2)\,q1^2 + 6\,q2^2\,(f_1+f_2)\,(\mathrm{D}_1 f_1 + \mathrm{D}_2 f_2)\right)}{6}$$

# Appendix A2

DERIVING THE SECOND-ORDER EXPANSION OF THE GENERALISED KÄRGER MODEL: EXACT FORM

**Now we will gather the results for a few values of N:**
**We start with the full expression where the exponential terms are not approximated with polynomials**
**We will gather the expressions for S9 above for N = 1 up to N = 7**

***N* = 1 :**

$$S9\_1 := -\frac{q1^2\left(d\_t\,k^2 f_1^3 + 2\,d\_t\,k^2 f_1^2 f_2 + d\_t\,k^2 f_1 f_2^2\right)\mathrm{D}_1}{k^2} - \frac{q1^2\left(d\_t\,k^2 f_1^2 f_2 + 2\,d\_t\,k^2 f_1 f_2^2 + d\_t\,k^2 f_2^3\right)\mathrm{D}_2}{k^2} - \frac{q1^2\left(-q1^2\,\mathrm{e}^{-d\_t\,k} + f_1\,q1^2 + \left(\frac{q1^2}{f_1} - \frac{k\,q1^2\,d\_t}{f_1 f_2}\right) f_2 f_1\right) VarD}{k^2}$$

***N* = 2 :**

$$S9\_2 := -\frac{f_2\left(\left(-d\_t\,k+1\right)q1^4 - q1^2\,q2^2 - q2^4\left(d\_t\,k-1\right)\right) f_1\,\mathrm{D}_1^2}{k^2} + \left(-\frac{f_2\left(\left(2\,d\_t\,k-2\right)q1^4 + 2\,q1^2\,q2^2 + 2\,q2^4\left(d\_t\,k-1\right)\right) f_1\,\mathrm{D}_2}{k^2} + \frac{-d\_t\left(q1^2+q2^2\right) f_1^2\,k^2 - f_2\,k^2\,d\_t\left(q1^2+q2^2\right) f_1}{k^2}\right)\mathrm{D}_1 - \frac{f_2\left(\left(-d\_t\,k+1\right)q1^4 - q1^2\,q2^2 - q2^4\left(d\_t\,k-1\right)\right) f_1\,\mathrm{D}_2^2}{k^2} + \frac{\left(-f_2\,k^2\,d\_t\left(q1^2+q2^2\right) f_1 - k^2\,d\_t\,f_2^2\left(q1^2+q2^2\right)\right)\mathrm{D}_2}{k^2} + \frac{\left(\left(q1-q2\right)^2\left(q1+q2\right)^2\mathrm{e}^{-d\_t\,k} + q1^2\,q2^2\,\mathrm{e}^{-2\,d\_t\,k}\right) VarD}{k^2}$$

***N* = 3 :**

$$S9\_3 := -\frac{f_2\left(\left(-d\_t\,k+1\right)q1^4 - q2^2\,q1^2 + \left(-d\_t\,k+1\right)q2^4 - q3^2\,q2^2 - q3^4\left(d\_t\,k-1\right)\right) f_1\,\mathrm{D}_1^2}{k^2} + \left(-\frac{f_2\left(\left(2\,d\_t\,k-2\right)q1^4 + 2\,q2^2\,q1^2 + \left(2\,d\_t\,k-2\right)q2^4 + 2\,q3^2\,q2^2 + 2\,q3^4\left(d\_t\,k-1\right)\right) f_1\,\mathrm{D}_2}{k^2} + \frac{-d\_t\left(q1^2+q2^2+q3^2\right) f_1^2\,k^2 - f_2\,k^2\,d\_t\left(q1^2+q2^2+q3^2\right) f_1}{k^2}\right)\mathrm{D}_1$$

$$- \frac{f_2 \left( \left( -d\_t\, k + 1 \right) q1^4 - q2^2\, q1^2 + \left( -d\_t\, k + 1 \right) q2^4 - q3^2\, q2^2 - q3^4 \left( d\_t\, k - 1 \right) \right) f_1\, \mathrm{D}_2^2}{k^2}$$

$$+ \frac{\left( -f_2\, k^2\, d\_t \left( q1^2 + q2^2 + q3^2 \right) f_1 - k^2\, d\_t\, f_2^2 \left( q1^2 + q2^2 + q3^2 \right) \right) \mathrm{D}_2}{k^2} + \frac{1}{k^2} \left( \left( \left( q1^2 + q1\, q3 \right.\right.\right.$$

$$\left.\left.\left. - q2^2 + q3^2 \right) \left( q1^2 - q1\, q3 - q2^2 + q3^2 \right) \mathrm{e}^{-d\_t\, k} + \left( \left( q2^2 - 2\, q3^2 \right) q1^2 + q3^2\, q2^2 \right) \mathrm{e}^{-2\, d\_t\, k} \right.\right.$$

$$\left. + q1^2\, q3^2\, \mathrm{e}^{-3\, d\_t\, k} \right)\, VarD \Big)$$

**$N = 4$ :**

$$S9\_4 := -\frac{1}{k^2} \left( f_2 \left( \left( -d\_t\, k + 1 \right) q1^4 - q1^2\, q2^2 + \left( -d\_t\, k + 1 \right) q2^4 - q2^2\, q3^2 + \left( -d\_t\, k + 1 \right) q3^4 \right.\right.$$

$$\left.\left. - q3^2\, q4^2 - q4^4 \left( d\_t\, k - 1 \right) \right) f_1\, \mathrm{D}_1^2 \right) + \left( -\frac{1}{k^2} \left( f_2 \left( \left( 2\, d\_t\, k - 2 \right) q1^4 + 2\, q1^2\, q2^2 + \left( 2\, d\_t\, k \right.\right.\right.\right.$$

$$\left.\left.\left.\left. - 2 \right) q2^4 + 2\, q2^2\, q3^2 + \left( 2\, d\_t\, k - 2 \right) q3^4 + 2\, q3^2\, q4^2 + 2\, q4^4 \left( d\_t\, k - 1 \right) \right) f_1\, \mathrm{D}_2 \right) \right.$$

$$\left. + \frac{-d\_t \left( q1^2 + q2^2 + q3^2 + q4^2 \right) f_1^2\, k^2 - f_2\, k^2\, d\_t \left( q1^2 + q2^2 + q3^2 + q4^2 \right) f_1}{k^2} \right) \mathrm{D}_1$$

$$- \frac{1}{k^2} \left( f_2 \left( \left( -d\_t\, k + 1 \right) q1^4 - q1^2\, q2^2 + \left( -d\_t\, k + 1 \right) q2^4 - q2^2\, q3^2 + \left( -d\_t\, k + 1 \right) q3^4 \right.\right.$$

$$\left.\left. - q3^2\, q4^2 - q4^4 \left( d\_t\, k - 1 \right) \right) f_1\, \mathrm{D}_2^2 \right)$$

$$+ \frac{\left( -f_2\, k^2\, d\_t \left( q1^2 + q2^2 + q3^2 + q4^2 \right) f_1 - k^2\, f_2^2\, d\_t \left( q1^2 + q2^2 + q3^2 + q4^2 \right) \right) \mathrm{D}_2}{k^2}$$

$$+ \frac{1}{k^2} \left( \left( \left( q1^4 + \left( -2\, q2^2 + q3^2 \right) q1^2 + q2^4 + \left( -2\, q3^2 + q4^2 \right) q2^2 + \left( q3 - q4 \right)^2 \left( q3 \right.\right.\right.\right.$$

$$\left.\left.\left.\left. + q4 \right)^2 \right) \mathrm{e}^{-d\_t\, k} + \left( \left( q2^2 - 2\, q3^2 + q4^2 \right) q1^2 + \left( q3^2 - 2\, q4^2 \right) q2^2 + q3^2\, q4^2 \right) \mathrm{e}^{-2\, d\_t\, k} + \left( \left( q3^2 \right.\right.\right.$$

$$\left.\left.\left. - 2\, q4^2 \right) q1^2 + q2^2\, q4^2 \right) \mathrm{e}^{-3\, d\_t\, k} + q1^2\, q4^2\, \mathrm{e}^{-4\, d\_t\, k} \right)\, VarD \Big)$$

**$N = 5$ :**

$$S9\_5 := -\frac{1}{k^2} \left( \left( \left( -d\_t\, k + 1 \right) q1^4 - q1^2\, q2^2 + \left( -d\_t\, k + 1 \right) q2^4 - q2^2\, q3^2 + \left( -d\_t\, k + 1 \right) q3^4 \right.\right.$$

$$\left.\left. - q3^2\, q4^2 + \left( -d\_t\, k + 1 \right) q4^4 - q4^2\, q5^2 - q5^4 \left( d\_t\, k - 1 \right) \right) f_2 f_1\, \mathrm{D}_1^2 \right) + \left( -\frac{1}{k^2} \left( \left( \left( 2\, d\_t\, k \right.\right.\right.\right.$$

$$\left.\left.\left.\left. - 2 \right) q1^4 + 2\, q1^2\, q2^2 + \left( 2\, d\_t\, k - 2 \right) q2^4 + 2\, q2^2\, q3^2 + \left( 2\, d\_t\, k - 2 \right) q3^4 + 2\, q3^2\, q4^2 + \left( 2\, d\_t\, k \right.\right.\right.\right.$$

$$\left.\left.\left.\left. - 2 \right) q4^4 + 2\, q4^2\, q5^2 + 2\, q5^4 \left( d\_t\, k - 1 \right) \right) f_2 f_1\, \mathrm{D}_2 \right) \right.$$

$$\left. + \frac{-d\_t \left( q1^2 + q2^2 + q3^2 + q4^2 + q5^2 \right) f_1^2\, k^2 - k^2\, d\_t \left( q1^2 + q2^2 + q3^2 + q4^2 + q5^2 \right) f_2 f_1}{k^2} \right)$$

$$D_1 - \frac{1}{k^2}\left(\left(\left(-d\_t\,k+1\right)q1^4 - q1^2\,q2^2 + \left(-d\_t\,k+1\right)q2^4 - q2^2\,q3^2 + \left(-d\_t\,k+1\right)q3^4 - q3^2\,q4^2 + \left(-d\_t\,k+1\right)q4^4 - q4^2\,q5^2 - q5^4\left(d\_t\,k-1\right)\right)f_2 f_1\,D_2^2\right) + \frac{\left(-k^2\,d\_t\left(q1^2+q2^2+q3^2+q4^2+q5^2\right)f_2 f_1 - k^2 f_2^2\,d\_t\left(q1^2+q2^2+q3^2+q4^2+q5^2\right)\right)D_2}{k^2} + \frac{1}{k^2}\left(\left(\left(q1^4+\left(-2\,q2^2+q3^2\right)q1^2+q2^4+\left(-2\,q3^2+q4^2\right)q2^2+q3^4+\left(-2\,q4^2+q5^2\right)q3^2+\left(q4-q5\right)^2\left(q4+q5\right)^2\right)e^{-d\_t\,k} + \left(\left(q2^2-2\,q3^2+q4^2\right)q1^2+\left(q3^2-2\,q4^2+q5^2\right)q2^2+\left(q4^2-2\,q5^2\right)q3^2+q4^2\,q5^2\right)e^{-2\,d\_t\,k} + \left(\left(q3^2-2\,q4^2+q5^2\right)q1^2+\left(q4^2-2\,q5^2\right)q2^2+q3^2\,q5^2\right)e^{-3\,d\_t\,k} + \left(\left(q4^2-2\,q5^2\right)q1^2+q2^2\,q5^2\right)e^{-4\,d\_t\,k} + q1^2\,q5^2\,e^{-5\,d\_t\,k}\right)VarD\right)$$

**$N = 6$ :**

$$S9\_6 := -\frac{1}{k^2}\left(\left(\left(-d\_t\,k+1\right)q1^4 - q1^2\,q2^2 + \left(-d\_t\,k+1\right)q2^4 - q2^2\,q3^2 + \left(-d\_t\,k+1\right)q3^4 - q3^2\,q4^2 + \left(-d\_t\,k+1\right)q4^4 - q4^2\,q5^2 + \left(-d\_t\,k+1\right)q5^4 - q5^2\,q6^2 - q6^4\left(d\_t\,k-1\right)\right)f_2 f_1\,D_1^2\right) + \left(-\frac{1}{k^2}\left(\left(\left(2\,d\_t\,k-2\right)q1^4 + 2\,q1^2\,q2^2 + \left(2\,d\_t\,k-2\right)q2^4 + 2\,q2^2\,q3^2 + \left(2\,d\_t\,k-2\right)q3^4 + 2\,q3^2\,q4^2 + \left(2\,d\_t\,k-2\right)q4^4 + 2\,q4^2\,q5^2 + \left(2\,d\_t\,k-2\right)q5^4 + 2\,q5^2\,q6^2 + 2\,q6^4\left(d\_t\,k-1\right)\right)f_2 f_1\,D_2\right) + \frac{1}{k^2}\left(-d\_t\left(q1^2+q2^2+q3^2+q4^2+q5^2+q6^2\right)f_1^2\,k^2 - k^2\,d\_t\left(q1^2+q2^2+q3^2+q4^2+q5^2+q6^2\right)f_2 f_1\right)\right)D_1 - \frac{1}{k^2}\left(\left(\left(-d\_t\,k+1\right)q1^4 - q1^2\,q2^2 + \left(-d\_t\,k+1\right)q2^4 - q2^2\,q3^2 + \left(-d\_t\,k+1\right)q3^4 - q3^2\,q4^2 + \left(-d\_t\,k+1\right)q4^4 - q4^2\,q5^2 + \left(-d\_t\,k+1\right)q5^4 - q5^2\,q6^2 - q6^4\left(d\_t\,k-1\right)\right)f_2 f_1\,D_2^2\right) + \frac{1}{k^2}\left(\left(-k^2\,d\_t\left(q1^2+q2^2+q3^2+q4^2+q5^2+q6^2\right)f_2 f_1 - k^2 f_2^2\,d\_t\left(q1^2+q2^2+q3^2+q4^2+q5^2+q6^2\right)\right)D_2\right) + \frac{1}{k^2}\left(\left(\left(q1^4+\left(-2\,q2^2+q3^2\right)q1^2+q2^4+\left(-2\,q3^2+q4^2\right)q2^2+q3^4+\left(-2\,q4^2+q5^2\right)q3^2+\left(-2\,q5^2+q6^2\right)q4^2+\left(q5-q6\right)^2\left(q5+q6\right)^2\right)e^{-d\_t\,k} + \left(\left(q2^2-2\,q3^2+q4^2\right)q1^2+\left(q3^2-2\,q4^2+q5^2\right)q2^2+\left(q4^2-2\,q5^2+q6^2\right)q3^2+\left(q5^2-2\,q6^2\right)q4^2+q5^2\,q6^2\right)e^{-2\,d\_t\,k} + \left(\left(q3^2-2\,q4^2+q5^2\right)q1^2+\left(q4^2-2\,q5^2+q6^2\right)q2^2+\left(q5^2-2\,q6^2\right)q3^2+q4^2\,q6^2\right)e^{-3\,d\_t\,k} + \left(\left(q4^2-2\,q5^2+q6^2\right)q1^2+\left(q5^2-2\,q6^2\right)q2^2+q3^2\,q6^2\right)e^{-4\,d\_t\,k} + \left(\left(q5^2-2\,q6^2\right)q1^2+q2^2\,q6^2\right)e^{-5\,d\_t\,k} + e^{-6\,d\_t\,k}\,q1^2\,q6^2\right)VarD\right)$$

**N = 7 :**

$$S9\_7 := -\frac{1}{k^2}\Big(\big((-d\_t\,k+1)\,q1^4 - q1^2\,q2^2 + (-d\_t\,k+1)\,q2^4 - q2^2\,q3^2 + (-d\_t\,k+1)\,q3^4 - q3^2\,q4^2 + (-d\_t\,k+1)\,q4^4 - q4^2\,q5^2 + (-d\_t\,k+1)\,q5^4 - q5^2\,q6^2 + (-d\_t\,k+1)\,q6^4 - q6^2\,q7^2 - q7^4\,(d\_t\,k-1)\big)\,f_2 f_1\,D_1^2\Big) + \left(-\frac{1}{k^2}\Big(\big((2\,d\_t\,k-2)\,q1^4 + 2\,q1^2\,q2^2 + (2\,d\_t\,k-2)\,q2^4 + 2\,q2^2\,q3^2 + (2\,d\_t\,k-2)\,q3^4 + 2\,q3^2\,q4^2 + (2\,d\_t\,k-2)\,q4^4 + 2\,q4^2\,q5^2 + (2\,d\_t\,k-2)\,q5^4 + 2\,q5^2\,q6^2 + (2\,d\_t\,k-2)\,q6^4 + 2\,q6^2\,q7^2 + 2\,q7^4\,(d\_t\,k-1)\big)\,f_2 f_1\,D_2\Big) + \frac{1}{k^2}\Big(-d\_t\,\big(q1^2+q2^2+q3^2+q4^2+q5^2+q6^2+q7^2\big)\,f_1^2\,k^2 - k^2\,d\_t\,\big(q1^2+q2^2+q3^2+q4^2+q5^2+q6^2+q7^2\big)\,f_2 f_1\Big)\Big)\,D_1 - \frac{1}{k^2}\Big(\big((-d\_t\,k+1)\,q1^4 - q1^2\,q2^2 + (-d\_t\,k+1)\,q2^4 - q2^2\,q3^2 + (-d\_t\,k+1)\,q3^4 - q3^2\,q4^2 + (-d\_t\,k+1)\,q4^4 - q4^2\,q5^2 + (-d\_t\,k+1)\,q5^4 - q5^2\,q6^2 + (-d\_t\,k+1)\,q6^4 - q6^2\,q7^2 - q7^4\,(d\_t\,k-1)\big)\,f_2 f_1\,D_2^2\Big) + \frac{1}{k^2}\Big(\Big(-k^2\,d\_t\,\big(q1^2+q2^2+q3^2+q4^2+q5^2+q6^2+q7^2\big)\,f_2 f_1 - k^2 f_2^2\,d\_t\,\big(q1^2+q2^2+q3^2+q4^2+q5^2+q6^2+q7^2\big)\Big)\,D_2\Big) + \frac{1}{k^2}\Big(\big(\big(q1^4 + \big(-2\,q2^2+q3^2\big)\,q1^2 + q2^4 + \big(-2\,q3^2+q4^2\big)\,q2^2 + q3^4 + \big(-2\,q4^2+q5^2\big)\,q3^2 + q4^4 + \big(-2\,q5^2+q6^2\big)\,q4^2 + q5^4 + \big(-2\,q6^2+q7^2\big)\,q5^2 + (q6-q7)^2\,(q6+q7)^2\big)\,e^{-d\_t\,k} + \big(\big(q2^2-2\,q3^2+q4^2\big)\,q1^2 + \big(q3^2-2\,q4^2+q5^2\big)\,q2^2 + \big(q4^2-2\,q5^2+q6^2\big)\,q3^2 + \big(q5^2-2\,q6^2+q7^2\big)\,q4^2 + \big(q6^2-2\,q7^2\big)\,q5^2 + q6^2\,q7^2\big)\,e^{-2\,d\_t\,k} + \big(\big(q3^2-2\,q4^2+q5^2\big)\,q1^2 + \big(q4^2-2\,q5^2+q6^2\big)\,q2^2 + \big(q5^2-2\,q6^2+q7^2\big)\,q3^2 + \big(q6^2-2\,q7^2\big)\,q4^2 + q5^2\,q7^2\big)\,e^{-3\,d\_t\,k} + \big(\big(q4^2-2\,q5^2+q6^2\big)\,q1^2 + \big(q5^2-2\,q6^2+q7^2\big)\,q2^2 + \big(q6^2-2\,q7^2\big)\,q3^2 + q4^2\,q7^2\big)\,e^{-4\,d\_t\,k} + \big(\big(q5^2-2\,q6^2+q7^2\big)\,q1^2 + \big(q6^2-2\,q7^2\big)\,q2^2 + q3^2\,q7^2\big)\,e^{-5\,d\_t\,k} + \big(\big(q6^2-2\,q7^2\big)\,q1^2 + q2^2\,q7^2\big)\,e^{-6\,d\_t\,k} + e^{-7\,d\_t\,k}\,q1^2\,q7^2\big)\,VarD\Big)$$

**When we have an expression for S9_N, we are done.**
**We will do the generalisation of the above expressions in chunks.**

We start with the coefficient of $D_1^2$. We group the terms below to make pattern identification easier: There is a $1/k^2$ in front of every term, but we temporarily omit it in the steps below.

$$Coeff\_D1D1\_N\_2 := \big((-d\_t\,k+1)\,q1^4 - q1^2\,q2^2 - q2^4\,(d\_t\,k-1)\big)$$

$$Coeff\_D1D1\_N\_3 := \big((-d\_t\,k+1)\,q1^4 - q2^2\,q1^2 + (-d\_t\,k+1)\,q2^4 - q3^2\,q2^2 - q3^4\,(d\_t\,k-1)\big)$$

$$Coeff\_D1D1\_N\_4 := \big((-d\_t\,k+1)\,q1^4 - q1^2\,q2^2 + (-d\_t\,k+1)\,q2^4 - q2^2\,q3^2 + (-d\_t\,k+1)\,q3^4 - q3^2\,q4^2 - q4^4\,(d\_t\,k-1)\big)$$

$$Coeff\_D1D1\_N\_5 := \big((-d\_t\,k+1)\,q1^4 - q1^2\,q2^2 + (-d\_t\,k+1)\,q2^4 - q2^2\,q3^2 + (-d\_t\,k+1)\,q3^4 - q3^2\,q4^2 + (-d\_t\,k+1)\,q4^4 - q4^2\,q5^2 - q5^4\,(d\_t\,k-1)\big)$$

We can see that the coefficient of $D_1^2$ for any N is given by

$$Coeff\_D1D1\_N\_N := (1 - k \cdot d\_t) \cdot \sum_{i=1}^{N} q_i^4 - \sum_{i=1}^{N-1} q_i^2 \cdot q_{i+1}^2$$

Now we will generalise the coefficient of VarD:
We group the coefficients below for N = 2, .., 5:

$$Coeff\_VarD\_N\_2 := \left( (q1 - q2)^2 (q1 + q2)^2 e^{-d\_t k} + q1^2 q2^2 e^{-2 d\_t k} \right)$$

$$Coeff\_VarD\_N\_3 := \left( \left( q1^2 + q1\, q3 - q2^2 + q3^2 \right) \left( q1^2 - q1\, q3 - q2^2 + q3^2 \right) e^{-d\_t k} + \left( \left( q2^2 - 2\, q3^2 \right) q1^2 + q3^2\, q2^2 \right) e^{-2 d\_t k} + q1^2\, q3^2\, e^{-3 d\_t k} \right)$$

$$Coeff\_VarD\_N\_4 := \left( \left( q1^4 + \left( -2\, q2^2 + q3^2 \right) q1^2 + q2^4 + \left( -2\, q3^2 + q4^2 \right) q2^2 + (q3 - q4)^2 (q3 + q4)^2 \right) e^{-d\_t k} + \left( \left( q2^2 - 2\, q3^2 + q4^2 \right) q1^2 + \left( q3^2 - 2\, q4^2 \right) q2^2 + q3^2\, q4^2 \right) e^{-2 d\_t k} + \left( \left( q3^2 - 2\, q4^2 \right) q1^2 + q2^2\, q4^2 \right) e^{-3 d\_t k} + q1^2\, q4^2\, e^{-4 d\_t k} \right)$$

$$Coeff\_VarD\_N\_5 := \left( \left( q1^4 + \left( -2 \cdot q2^2 + q3^2 \right) \cdot q1^2 + q2^4 + \left( -2 \cdot q3^2 + q4^2 \right) \cdot q2^2 + q3^4 + \left( -2 \cdot q4^2 + q5^2 \right) \cdot q3^2 + (q4 - q5)^2 \cdot (q4 + q5)^2 \right) \cdot e^{-d\_t \cdot k} + \left( \left( q2^2 - 2 \cdot q3^2 + q4^2 \right) \cdot q1^2 + \left( q3^2 - 2 \cdot q4^2 + q5^2 \right) \cdot q2^2 + \left( q4^2 - 2 \cdot q5^2 \right) \cdot q3^2 + q4^2 \cdot q5^2 \right) \cdot e^{-2 \cdot d\_t \cdot k} + \left( \left( q3^2 - 2 \cdot q4^2 + q5^2 \right) \cdot q1^2 + \left( q4^2 - 2 \cdot q5^2 \right) \cdot q2^2 + q3^2 \cdot q5^2 \right) \cdot e^{-3 \cdot d\_t \cdot k} + \left( \left( q4^2 - 2 \cdot q5^2 \right) \cdot q1^2 + q2^2 \cdot q5^2 \right) \cdot e^{-4 \cdot d\_t \cdot k} + q1^2 \cdot q5^2 \cdot e^{-5 \cdot d\_t \cdot k} \right)$$

The terms above can all be written as sums of the terms:

$$Coeff\_expN\_N\_2 := \left( \sum_{i=1}^{N-1} q_i^2 \cdot q_{i+1}^2 - 2 \cdot \sum_{i=1}^{N-2} q_i^2 \cdot q_{i+2}^2 + \sum_{i=1}^{N-3} q_i^2 \cdot q_{i+3}^2 \right) \cdot e^{-2 \cdot k \cdot \Delta t}$$

$$Coeff\_expN\_N\_3 := \left( \sum_{i=1}^{N-2} q_i^2 \cdot q_{i+2}^2 - 2 \cdot \sum_{i=1}^{N-3} q_i^2 \cdot q_{i+3}^2 + \sum_{i=1}^{N-4} q_i^2 \cdot q_{i+4}^2 \right) \cdot e^{-3 \cdot k \cdot \Delta t}$$

$$Coeff\_expN\_N\_4 := \left( \sum_{i=1}^{N-3} q_i^2 \cdot q_{i+3}^2 - 2 \cdot \sum_{i=1}^{N-4} q_i^2 \cdot q_{i+4}^2 + \sum_{i=1}^{N-5} q_i^2 \cdot q_{i+5}^2 \right) \cdot e^{-4 \cdot k \cdot \Delta t}$$

which we easily generalise to:

$$Coeff\_expN\_N\_N := \sum_{j=1}^{N} \left( \left( \sum_{i=1}^{N-(j-1)} q_i^2 \cdot q_{i+(j-1)}^2 - 2 \cdot \sum_{i=1}^{N-j} q_i^2 \cdot q_{i+j}^2 + \sum_{i=1}^{N-(j+1)} q_i^2 \cdot q_{i+(j+1)}^2 \right) \cdot e^{-j \cdot k \cdot \Delta t} \right)$$

Now we can generalise the entire expansion (S9) as:

$$S = -Y \cdot f_1 \cdot f_2 \cdot D_1^2 + 2 \cdot Y \cdot f_1 \cdot f_2 \cdot D_1 \cdot D_2 - b \cdot f_1 \cdot D_1 - Y \cdot f_1 \cdot f_2 \cdot D_2^2 - b \cdot f_2 \cdot D_2 + Z \cdot f_1 \cdot f_2 \cdot \left(D_1 - D_2\right)^2$$

Where

$$b := \sum_{i=1}^{N} q_i^2 \cdot \Delta t$$

$$Z := \frac{1}{k^2} \cdot \sum_{j=1}^{N} \left( \left( \sum_{i=1}^{N-(j-1)} q_i^2 \cdot q_{i+(j-1)}^2 - 2 \cdot \sum_{i=1}^{N-j} q_i^2 \cdot q_{i+j}^2 + \sum_{i=1}^{N-(j+1)} q_i^2 \cdot q_{i+(j+1)}^2 \right) \cdot e^{-j \cdot k \cdot \Delta t} \right)$$

$$Y := \frac{1}{k^2} \left( (1 - k \cdot \Delta t) \cdot \sum_{i=1}^{N} q_i^4 - \sum_{i=1}^{N-1} q_i^2 \cdot q_{i+1}^2 \right)$$

We have written $f_1 \cdot f_2 \cdot \left(D_1 - D_2\right)^2$ instead of just VarD to allow the simplifications below:

$$S = -Y \cdot f_1 \cdot f_2 \cdot \left(D_1^2 - 2 \cdot D_1 \cdot D_2 + D_2^2\right) - b \cdot \left(f_1 \cdot D_1 + f_2 \cdot D_2\right) + Z \cdot f_1 \cdot f_2 \cdot \left(D_1 - D_2\right)^2$$

$$S = -Y \cdot f_1 \cdot f_2 \cdot \left(D_1 - D_2\right)^2 - b \cdot \left(f_1 \cdot D_1 + f_2 \cdot D_2\right) + Z \cdot f_1 \cdot f_2 \cdot \left(D_1 - D_2\right)^2$$

$$S = -b \cdot \left(f_1 \cdot D_1 + f_2 \cdot D_2\right) + f_1 \cdot f_2 \cdot \left(D_1 - D_2\right)^2 \cdot (Z - Y)$$

That is

$$S = -b \cdot \overline{D} + Var(D) \cdot (Z - Y); \qquad \text{with} \qquad \overline{D} = f_1 \cdot D_1 + f_2 \cdot D_2 \quad ; \quad Var(D) = f_1 \cdot f_2 \cdot \left(D_1 - D_2\right)^2$$

That is

$$S = -b \cdot \overline{D} + \frac{Var(D)}{k^2} \cdot \left( \sum_{j=1}^{N} \left( \left( \sum_{i=1}^{N-(j-1)} q_i^2 \cdot q_{i+(j-1)}^2 - 2 \cdot \sum_{i=1}^{N-j} q_i^2 \cdot q_{i+j}^2 + \sum_{i=1}^{N-(j+1)} q_i^2 \cdot q_{i+(j+1)}^2 \right) \cdot e^{-j \cdot k \cdot \Delta t} \right) - (1 - k \cdot \Delta t) \cdot \sum_{i=1}^{N} q_i^4 + \sum_{i=1}^{N-1} q_i^2 \cdot q_{i+1}^2 \right)$$

**This is the second-order expansion of the generalised Kärger model. Done.**

# Appendix A3

DERIVING THE SECOND-ORDER EXPANSION OF THE GENERALISED KÄRGER MODEL: APPROXIMATE FORM

**Now we will also generalise the approximate form of the expansion:**
**We start by gathering the signal expressions (S12) for a few values of N:**

**N=2** :

$$S12\_2 := -\frac{d\_t\left(d\_t\left(d\_t\,k-3\right)q1^4+6\,d\_t\left(d\_t\,k-1\right)q2^2\,q1^2+d\_t\left(d\_t\,k-3\right)q2^4\right)\,VarD}{6}$$
$$-\frac{d\_t\left(6\left(f_1+f_2\right)\left(\mathrm{D}_1 f_1+\mathrm{D}_2 f_2\right)q1^2+6\left(f_1+f_2\right)\left(\mathrm{D}_1 f_1+\mathrm{D}_2 f_2\right)q2^2\right)}{6}$$

:

**N=3:**

$$S12\_3 := -\frac{1}{6}\left(d\_t\left(\left(q1^4+\left(6\,q2^2+12\,q3^2\right)q1^2+q2^4+6\,q3^2\,q2^2+q3^4\right)k\,d\_t^2-3\left(q1^2+q2^2+q3^2\right)^2 d\_t\right)VarD\right)-d\_t\left(q1^2+q2^2+q3^2\right)\left(f_1+f_2\right)\left(\mathrm{D}_1 f_1+\mathrm{D}_2 f_2\right):$$

**N = 4:**

$$S12\_4 := -\frac{1}{6}\left(d\_t\left(k\left(q1^4+\left(6\,q2^2+12\,q3^2+18\,q4^2\right)q1^2+q2^4+\left(6\,q3^2+12\,q4^2\right)q2^2+q3^4+6\,q3^2\,q4^2+q4^4\right)d\_t^2-3\left(q1^2+q2^2+q3^2+q4^2\right)^2 d\_t\right)VarD\right)-d\_t\left(q1^2+q2^2+q3^2+q4^2\right)\left(f_1+f_2\right)\left(\mathrm{D}_1 f_1+\mathrm{D}_2 f_2\right):$$

**N = 5:**

$$S12\_5 := -\frac{1}{6}\left(d\_t\left(\left(q1^4+\left(6\,q2^2+12\,q3^2+18\,q4^2+24\,q5^2\right)q1^2+q2^4+\left(6\,q3^2+12\,q4^2+18\,q5^2\right)q2^2+q3^4+\left(6\,q4^2+12\,q5^2\right)q3^2+q4^4+6\,q4^2\,q5^2+q5^4\right)k\,d\_t^2-3\left(q1^2+q2^2+q3^2+q4^2+q5^2\right)^2 d\_t\right)VarD\right)-\left(q1^2+q2^2+q3^2+q4^2+q5^2\right)d\_t\left(f_1+f_2\right)\left(f_1\,\mathrm{D}_1+f_2\,\mathrm{D}_2\right):$$

**N = 6:**

$$S12\_6 := -\frac{1}{6}\left(\left(k\left(q1^4+\left(6\,q2^2+12\,q3^2+18\,q4^2+24\,q5^2+30\,q6^2\right)q1^2+q2^4+\left(6\,q3^2+12\,q4^2+18\,q5^2+24\,q6^2\right)q2^2+q3^4+\left(6\,q4^2+12\,q5^2+18\,q6^2\right)q3^2+q4^4+\left(6\,q5^2+12\,q6^2\right)q4^2+q5^4+6\,q5^2\,q6^2+q6^4\right)d\_t^2-3\left(q1^2+q2^2+q3^2+q4^2+q5^2+q6^2\right)^2 d\_t\right)d\_t\,VarD\right)-\left(q1^2+q2^2+q3^2+q4^2+q5^2+q6^2\right)\left(f_1+f_2\right)\left(f_1\,\mathrm{D}_1+f_2\,\mathrm{D}_2\right)d\_t:$$

**N = 7:**

$$S12\_7 := -\frac{1}{6}\left(d\_t\left(\left(q1^4 + \left(6\,q2^2 + 12\,q3^2 + 18\,q4^2 + 24\,q5^2 + 30\,q6^2 + 36\,q7^2\right)q1^2 + q2^4 + \left(6\,q3^2 + 12\,q4^2 + 18\,q5^2 + 24\,q6^2 + 30\,q7^2\right)q2^2 + q3^4 + \left(6\,q4^2 + 12\,q5^2 + 18\,q6^2 + 24\,q7^2\right)q3^2 + q4^4 + \left(6\,q5^2 + 12\,q6^2 + 18\,q7^2\right)q4^2 + q5^4 + \left(6\,q6^2 + 12\,q7^2\right)q5^2 + q6^4 + 6\,q6^2\,q7^2 + q7^4\right)k\,d\_t^2 - 3\left(q1^2 + q2^2 + q3^2 + q4^2 + q5^2 + q6^2 + q7^2\right)^2 d\_t\right)VarD\right) - \left(f_1 + f_2\right)\left(f_1\,\mathrm{D}_1 + f_2\,\mathrm{D}_2\right)d\_t\left(q1^2 + q2^2 + q3^2 + q4^2 + q5^2 + q6^2 + q7^2\right):$$

Here, we can immediately see that all the expressions above can be written:

$$S = -b\cdot\overline{\mathrm{D}} - \frac{1}{6}\cdot X\cdot Var(\mathrm{D})$$

Where

$$b := \sum_{i=1}^{N} q_i^2\cdot\Delta t \;;\qquad \overline{\mathrm{D}} = f_1\cdot\mathrm{D}_1 + f_2\cdot\mathrm{D}_2 \;;\qquad Var(\mathrm{D}) = f_1\cdot f_2\cdot\left(\mathrm{D}_1 - \mathrm{D}_2\right)^2$$

$$X := \sum_{i=1}^{N}\left(q_i^4\cdot\Delta t^3\cdot k\right) + \sum_{j=1}^{N-1}\left(6\cdot j\cdot\sum_{i=1}^{N-j}\left(q_i^2\cdot q_{i+j}^2\right)\right)\cdot\Delta t^3\cdot k - 3\cdot\left(\sum_{i=1}^{N} q_1^2\right)^2\cdot\Delta t^2$$

Now if we define: $\Delta$

$$Q4 := \sum_{i=1}^{N}\left(q_i^4\cdot\Delta t^2\right)\cdot\Delta t + \sum_{j=1}^{N-1}\left(6\cdot j\cdot\sum_{i=1}^{N-j}\left(q_i^2\cdot q_{i+j}^2\right)\right)\cdot\Delta t^2\cdot\Delta t$$

We have:

$$S = -b\cdot\overline{\mathrm{D}} - \frac{1}{6}\cdot Var(\mathrm{D})\cdot\left(-3\cdot b^2 + k\cdot Q4\right)$$

Equivalently:

$$S = -b\cdot\overline{\mathrm{D}} - \frac{1}{6}\cdot Var(\mathrm{D})\cdot\left(-3\cdot b^2 + k\cdot Q4\right)$$

$$S = -b\cdot\overline{\mathrm{D}} + \frac{3}{6}\cdot Var(\mathrm{D})\cdot\left(b^2 - k\cdot\frac{Q4}{3}\right)$$

$$S = -b\cdot\overline{\mathrm{D}} + \frac{1}{2}\cdot Var(\mathrm{D})\cdot\left(1 - k\cdot\frac{Q4}{3\,b^2}\right)\cdot b^2$$

**This last equation is the approximate form of the second-order series expansion of the generalised Kärger model.**

# Appendix A4

DERIVING THE EXCHANGE TERM FOR THE GENERALISED KÄRGER MODEL WITH CONSTANT q

The exchange term is given by

$$h(\cdot) = \frac{2}{b^2 \cdot k^2} \cdot \left[ \sum_{j=1}^{N} \left( \left( \sum_{i=1}^{N-(j-1)} q_i^2 \cdot q_{i+(j-1)}^2 - 2 \cdot \sum_{i=1}^{N-j} q_i^2 \cdot q_{i+j}^2 + \sum_{i=1}^{N-(j+1)} q_i^2 \cdot q_{i+(j+1)}^2 \right) \cdot e^{-j \cdot k \cdot \Delta t} \right) - (1 - k \cdot \Delta t) \cdot \sum_{i=1}^{N} q_i^4 + \sum_{i=1}^{N-1} q_i^2 \cdot q_{i+1}^2 \right]$$

which we can express:

$$h(\cdot) = \frac{2}{b^2 \cdot k^2} \cdot \left[ \sum_{j=1}^{N-2} \left( e^{-j \cdot k \cdot \Delta t} \cdot \left( \sum_{i=1}^{N-(j-1)} q_i^2 \cdot q_{i+(j-1)}^2 - 2 \cdot \sum_{i=1}^{N-j} q_i^2 \cdot q_{i+j}^2 + \sum_{i=1}^{N-(j+1)} q_i^2 \cdot q_{i+(j+1)}^2 \right) \right) + e^{-(N-1) \cdot k \cdot \Delta t} \cdot \left( \sum_{i=1}^{2} q_i^2 \cdot q_{i+(N-2)}^2 - 2 \cdot \sum_{i=1}^{1} q_i^2 \cdot q_{i+(N-1)}^2 \right) + e^{-N \cdot k \cdot \Delta t} \cdot \left( q_1^2 \cdot q_N^2 \right) - (1 - k \cdot \Delta t) \cdot \sum_{i=1}^{N} q_i^4 + \sum_{i=1}^{N-1} q_i^2 \cdot q_{i+1}^2 \right]$$

For a constant q, we have

$$b = \sum_{i=1}^{N} q_i^2 \Delta t = N \cdot q^2 \cdot \Delta t \Rightarrow q^2 = \frac{b}{N \cdot \Delta t} = \frac{b}{T}$$

where $q$ is the constant q-value. Insertion in $h(\cdot)$ gives:

$$h(\cdot) = \frac{2}{b^2 \cdot k^2} \cdot \left[ \sum_{j=1}^{N-2} \left( e^{-j \cdot k \cdot \Delta t} \cdot \left( \sum_{i=1}^{N-(j-1)} q^4 - 2 \cdot \sum_{i=1}^{N-j} q^4 + \sum_{i=1}^{N-(j+1)} q^4 \right) \right) + e^{-(N-1) \cdot k \cdot \Delta t} \cdot \left( \sum_{i=1}^{2} q^4 - 2 \cdot \sum_{i=1}^{1} q^4 \right) + e^{-N \cdot k \cdot \Delta t} \cdot q^4 - (1 - k \cdot \Delta t) \cdot \sum_{i=1}^{N} q^4 + \sum_{i=1}^{N-1} q^4 \right]$$

Since the terms under summation are independent of the summation index, we can write:

$$h(\cdot) = \frac{2}{b^2 \cdot k^2} \cdot q^4 \left[ \sum_{j=1}^{N-2} \left( e^{-j \cdot k \cdot \Delta t} \cdot \left( \sum_{i=1}^{N-(j-1)} 1 - 2 \cdot \sum_{i=1}^{N-j} 1 + \sum_{i=1}^{N-(j+1)} 1 \right) \right) + e^{-(N-1) \cdot k \cdot \Delta t} \cdot \left( \sum_{i=1}^{2} 1 - 2 \cdot \sum_{i=1}^{1} 1 \right) + e^{-N \cdot k \cdot \Delta t} \cdot 1 - (1 - k \cdot \Delta t) \cdot \sum_{i=1}^{N} 1 + \sum_{i=1}^{N-1} 1 \right]$$

$$h(\cdot) = \frac{2}{b^2 \cdot k^2} \cdot q^4 \left[ \sum_{j=1}^{N-2} \left( e^{-j \cdot k \cdot \Delta t} \cdot (0) \right) + e^{-(N-1) \cdot k \cdot \Delta t} \cdot (0) + e^{-N \cdot k \cdot \Delta t} - (1 - k \cdot \Delta t) \cdot N + (N-1) \right]$$

$$h(\cdot) = \frac{2}{b^2 \cdot k^2} \cdot q^4 \cdot \left[ e^{-N \cdot k \cdot \Delta t} - (1 - k \cdot N \cdot \Delta t) \right] = \frac{2}{b^2 \cdot k^2} \cdot q^4 \cdot \left[ e^{-kT} - (1 - kT) \right]$$

Inserting $q^2 = \frac{b}{T}$ provides

$$h(\cdot) = \frac{2}{b^2 \cdot k^2} \cdot \left( \frac{b}{T} \right)^2 \cdot \left[ e^{-kT} - (1 - kT) \right]$$

That is

$$h(\cdot) = \frac{2}{(kT)^2} \cdot \left[ e^{-kT} - (1 - kT) \right]$$

Done.

# Appendix A5

DERIVING THE EXCHANGE-WEIGHTING TIME FOR THE GENERALISED KÄRGER MODEL WITH CONSTANT q

The exchange-weighting time, Γ, is given by

$$\Gamma = \frac{Q4}{3\,b^2} = \frac{1}{3\,b^2}\left[\sum_{i=1}^{N}\left(q_i^4\cdot\Delta t^2\right)\cdot\Delta t + \sum_{j=1}^{N-1}\left(6\cdot j\cdot\sum_{i=1}^{N-j}\left(q_i^2\cdot q_{i+j}^2\right)\right)\cdot\Delta t^2\cdot\Delta t\right]$$

For a constant q, we have

$$b = \sum_{i=1}^{N} q_i^2\Delta t = N\cdot q^2\cdot\Delta t \Rightarrow q^2 = \frac{b}{N\cdot\Delta t} = \frac{b}{T}$$

where $q$ is the constant q-value. Insertion in Γ gives:

$$\Gamma = \frac{1}{3\,b^2}\cdot q^4\cdot\left[\sum_{i=1}^{N}\Delta t^2\cdot\Delta t + \sum_{j=1}^{N-1}\left(6\cdot j\cdot\sum_{i=1}^{N-j}(1)\right)\cdot\Delta t^2\cdot\Delta t\right]$$

$$\Gamma = \frac{1}{3\,b^2}\cdot q^4\cdot\left[N\cdot\Delta t^3 + \sum_{j=1}^{N-1}(6\cdot j\cdot(N-j))\cdot\Delta t^3\right]$$

$$\Gamma = \frac{1}{3\,b^2}\cdot q^4\cdot\left[N\cdot\Delta t^3 + N\cdot\Delta t^3\cdot\sum_{j=1}^{N-1}6\,j - \Delta t^3\cdot\sum_{j=1}^{N-1}6\,j^2\right]$$

$$\Gamma = \frac{1}{3\,b^2}\cdot q^4\cdot\Delta t^3\left[N + N\cdot\sum_{j=1}^{N-1}6\,j - \sum_{j=1}^{N-1}6\,j^2\right]$$

Using the relations: $\sum_{n=1}^{N} n = \frac{1}{2}N(N+1)$ and $\sum_{n=1}^{N} n^2 = \frac{1}{6}N(N+1)(2N+1)$, we have

$$\Gamma = \frac{1}{3\,b^2}\cdot q^4\cdot\Delta t^3\left[N + 6\cdot N\cdot\frac{1}{2}\cdot(N-1)\cdot N - 6\cdot\frac{1}{6}\cdot(N-1)\cdot N\cdot(2N-1)\right]$$

$$\Gamma = \frac{1}{3\,b^2}\cdot q^4\cdot\Delta t^3\left[N + 3N^3 - 3N^2 - 2N^3 + 3N^2 - N\right] = \frac{1}{3\,b^2}\cdot q^4\cdot N\cdot\Delta t^3\left[N^3\right]$$

Substituting $q^2$ with $\frac{b}{N\cdot\Delta t}$ gives

$$\Gamma = \frac{1}{3\,b^2}\cdot\left(\frac{b^2}{N^2\Delta t^2}\right)\cdot\Delta t^3 N^3 = \frac{1}{3}\cdot N\cdot\Delta t$$

That is, $\Gamma = \frac{T}{3}$

# B Appendix: Deriving the VA model

## Appendix B1

**Maple script for evaluating the mean second- and fourth-order velocity autocorrelation functions**

```
> restart
```

Define transition probabilities between compartments
1 denotes intracellular
2 denotes extracellular

```
> p11(t) := f1 + f2·exp(-k·t):
> p12(t) := f2·(1 - exp(-k·t)):
> p21(t) := f1·(1 - exp(-k·t)):
> p22(t) := f2 + f1·exp(-k·t):
```

Define velocity autocorrelation function

```
> v_v1(t1, t2) := 2·D_1·Dirac(t2 - t1):        Intracellular under Gaussian assumption
> #v_v1(t1, t2) := (2·1)/(2·π) ∫_{-∞}^{∞} D(w)·exp(1 I·w·(t2 - t1)) dw:  Intracellular non-Gaussian
> v_v2(t1, t2) := 2· D_2·Dirac(t2 - t1):    Extracellular, Gaussian diffusion
```

Evaluate mean second-order velocity autocorrelation function

```
> VV(t1, t2) := f1·(p11(t1)·p11(t2 - t1)·v_v1(t1, t2) + p12(t1)·p21(t2 - t1)·v_v1(t1, t2)
      + p11(t1)·p12(t2 - t1)·v_v2(t1, t2) + p12(t1)·p22(t2 - t1)·v_v2(t1, t2)) + f2·(p21(t1)
      ·p11(t2 - t1)·v_v1(t1, t2) + p22(t1)·p21(t2 - t1)·v_v1(t1, t2) + p21(t1)·p12(t2 - t1)
      ·v_v2(t1, t2) + p22(t1)·p22(t2 - t1)·v_v2(t1, t2)):
> V2 := simplify(subs(VV(t1, t2, t3, t4)))
```

$$V2 := 2\,\mathrm{Dirac}(t2 - t1)\,(f1 + f2)^2\,(f1\,D\_1 + f2\,D\_2) \qquad \textbf{(1)}$$

Evaluate mean fourth-order velocity autocorrelation function

```
> VVVV(t1, t2, t3, t4) := f1·(p11(t1)·p11(t2 - t1)·v_v1(t1, t2)·p11(t3 - t2)·p11(t4 - t3)
      ·v_v1(t3, t4) + p11(t1)·p11(t2 - t1)·v_v1(t1, t2)·p11(t3 - t2)·p12(t4 - t3)·v_v2(t3, t4)
      + p11(t1)·p11(t2 - t1)·v_v1(t1, t2)·p12(t3 - t2)·p21(t4 - t3)·v_v1(t3, t4) + p11(t1)
      ·p11(t2 - t1)·v_v1(t1, t2)·p12(t3 - t2)·p22(t4 - t3)·v_v2(t3, t4) + p11(t1)·p12(t2
      - t1)·v_v2(t1, t2)·p21(t3 - t2)·p11(t4 - t3)·v_v1(t3, t4) + p11(t1)·p12(t2 - t1)
      ·v_v2(t1, t2)·p21(t3 - t2)·p12(t4 - t3)·v_v2(t3, t4) + p11(t1)·p12(t2 - t1)·v_v2(t1, t2)
      ·p22(t3 - t2)·p21(t4 - t3)·v_v1(t3, t4) + p11(t1)·p12(t2 - t1)·v_v2(t1, t2)·p22(t3
      - t2)·p22(t4 - t3)·v_v2(t3, t4) + p12(t1)·p21(t2 - t1)·v_v1(t1, t2)·p11(t3 - t2)
      ·p11(t4 - t3)·v_v1(t3, t4) + p12(t1)·p21(t2 - t1)·v_v1(t1, t2)·p11(t3 - t2)·p12(t4
      - t3)·v_v2(t3, t4) + p12(t1)·p21(t2 - t1)·v_v1(t1, t2)·p12(t3 - t2)·p21(t4 - t3)
      ·v_v1(t3, t4) + p12(t1)·p21(t2 - t1)·v_v1(t1, t2)·p12(t3 - t2)·p22(t4 - t3)·v_v2(t3, t4)
      + p12(t1)·p22(t2 - t1)·v_v2(t1, t2)·p21(t3 - t2)·p11(t4 - t3)·v_v1(t3, t4) + p12(t1)
      ·p22(t2 - t1)·v_v2(t1, t2)·p21(t3 - t2)·p12(t4 - t3)·v_v2(t3, t4) + p12(t1)·p22(t2
```

$$-t1)\cdot v\_v2(t1,t2)\cdot p22(t3-t2)\cdot p21(t4-t3)\cdot v\_v1(t3,t4)+p12(t1)\cdot p22(t2-t1)\cdot v\_v2(t1,t2)\cdot p22(t3-t2)\cdot p22(t4-t3)\cdot v\_v2(t3,t4))+$$

$$+f2\cdot(p21(t1)\cdot p11(t2-t1)\cdot v\_v1(t1,t2)\cdot p11(t3-t2)\cdot p11(t4-t3)\cdot v\_v1(t3,t4)+p21(t1)\cdot p11(t2-t1)\cdot v\_v1(t1,t2)\cdot p11(t3-t2)\cdot p12(t4-t3)\cdot v\_v2(t3,t4)+p21(t1)\cdot p11(t2-t1)\cdot v\_v1(t1,t2)\cdot p12(t3-t2)\cdot p21(t4-t3)\cdot v\_v1(t3,t4)+p21(t1)\cdot p11(t2-t1)\cdot v\_v1(t1,t2)\cdot p12(t3-t2)\cdot p22(t4-t3)\cdot v\_v2(t3,t4)+p21(t1)\cdot p12(t2-t1)\cdot v\_v2(t1,t2)\cdot p21(t3-t2)\cdot p11(t4-t3)\cdot v\_v1(t3,t4)+p21(t1)\cdot p12(t2-t1)\cdot v\_v2(t1,t2)\cdot p21(t3-t2)\cdot p12(t4-t3)\cdot v\_v2(t3,t4)+p21(t1)\cdot p12(t2-t1)\cdot v\_v2(t1,t2)\cdot p22(t3-t2)\cdot p21(t4-t3)\cdot v\_v1(t3,t4)+p21(t1)\cdot p12(t2-t1)\cdot v\_v2(t1,t2)\cdot p22(t3-t2)\cdot p22(t4-t3)\cdot v\_v2(t3,t4)+p22(t1)\cdot p21(t2-t1)\cdot v\_v1(t1,t2)\cdot p11(t3-t2)\cdot p11(t4-t3)\cdot v\_v1(t3,t4)+p22(t1)\cdot p21(t2-t1)\cdot v\_v1(t1,t2)\cdot p11(t3-t2)\cdot p12(t4-t3)\cdot v\_v2(t3,t4)+p22(t1)\cdot p21(t2-t1)\cdot v\_v1(t1,t2)\cdot p12(t3-t2)\cdot p21(t4-t3)\cdot v\_v1(t3,t4)+p22(t1)\cdot p21(t2-t1)\cdot v\_v1(t1,t2)\cdot p12(t3-t2)\cdot p22(t4-t3)\cdot v\_v2(t3,t4)+p22(t1)\cdot p22(t2-t1)\cdot v\_v2(t1,t2)\cdot p21(t3-t2)\cdot p11(t4-t3)\cdot v\_v1(t3,t4)+p22(t1)\cdot p22(t2-t1)\cdot v\_v2(t1,t2)\cdot p21(t3-t2)\cdot p12(t4-t3)\cdot v\_v2(t3,t4)+p22(t1)\cdot p22(t2-t1)\cdot v\_v2(t1,t2)\cdot p22(t3-t2)\cdot p21(t4-t3)\cdot v\_v1(t3,t4)+p22(t1)\cdot p22(t2-t1)\cdot v\_v2(t1,t2)\cdot p22(t3-t2)\cdot p22(t4-t3)\cdot v\_v2(t3,t4)):$$

> $V4 := simplify(collect(VVVV(t1,t2,t3,t4), e^{k(-t4+t2)}))$

$$V4 := 4\,\mathrm{Dirac}(t4-t3)\,(f1\,f2\,(D\_1-D\_2)^2\,e^{k(-t4+t2)}+(D\_1\,f1+D\_2\,f2)^2)\,\mathrm{Dirac}(t2-t1)\,(f1+f2)^3 \quad (2)$$

## Appendix B2: Long-time limit of the VA model

This appendix presents the derivation of the VA model in the case of free diffusion with exchange.

The dMRI signal attenuation equation can be expressed:

$$S/S_0 = \langle \mathrm{e}^{-i\phi} \rangle \tag{B.1}$$

where $\phi$ is the spin phase defined by

$$\phi(T) = \gamma \int_0^T g(t) r(t) dt \tag{B.2}$$

The signal attenuation can be approximated with its cumulant expansion:

$$\ln(S/S_0) \approx -\frac{1}{2}\langle \phi^2 \rangle + \frac{1}{24}(\langle \phi^4 \rangle - 3\langle \phi^2 \rangle^2) \tag{B.3}$$

The second- and fourth-order moments of the phase distribution can be obtained by expressing the phase in terms of particle velocities. Integration by parts gives

$$\phi(T) = -\int_0^T q(t) v(t) dt \tag{B.4}$$

The moments are then given by

$$\langle \phi(T)^2 \rangle = \int_0^T \int_0^T q(t_1) q(t_2) \langle v(t_1) v(t_2) \rangle dt_1 dt_2 \tag{B.5}$$

and

$$\langle \phi(T)^4 \rangle = \int_0^T \int_0^T \int_0^T \int_0^T q(t_1) q(t_2) q(t_3) q(t_4) \langle v(t_1) v(t_2) v(t_3) v(t_4) \rangle dt_1 dt_2 dt_3 dt_4 \tag{B.6}$$

The velocity-autocorrelation function is defined as the inverse Fourier transform of the diffusion spectrum:

$$\langle v(t_1) v(t_2) \rangle = \frac{1}{\pi} \int_{-\infty}^{\infty} D(\omega) \mathrm{e}^{i\omega(t_2 - t_1)} d\omega \tag{B.7}$$

For measurement times much larger than the correlation times between the velocities:

$$\langle v(t_1) v(t_2) \rangle = 2D(0) \cdot \delta(t_2 - t_1) \tag{B.8}$$

**Two-compartment formalism**

Consider a two-compartment system consisting of intracellular and extracellular spaces, denoted by the subscripts $in$ and $ex$, respectively. Associate each particle with a probability vector given by

$$\boldsymbol{p}(t) = \begin{bmatrix} p_{in}(t) \\ p_{ex}(t) \end{bmatrix} \tag{B.9}$$

that has a time-dependence obeying:

$$\frac{d\boldsymbol{p}(t)}{dt} = K \cdot \boldsymbol{p}(t) \tag{B.10}$$

where $K$ is the rate matrix:

$$K = \begin{bmatrix} -k_{in\to ex} & k_{ex\to in} \\ k_{in\to ex} & -k_{ex\to in} \end{bmatrix} \tag{B.11}$$

which has the solution

$$\boldsymbol{p}(t) = \begin{cases} \begin{bmatrix} p_{in\to in}(t) \\ p_{in\to ex}(t) \end{bmatrix} = \begin{bmatrix} f_{in} + f_{ex}e^{-kt} \\ f_{ex}(1-e^{-kt}) \end{bmatrix} & ;\ \text{if} \quad \begin{bmatrix} p_{in}(t) \\ p_{ex}(t) \end{bmatrix} = \begin{bmatrix} 1 \\ 0 \end{bmatrix} \\ \begin{bmatrix} p_{ex\to in}(t) \\ p_{ex\to ex}(t) \end{bmatrix} = \begin{bmatrix} f_{in}(1-e^{-kt}) \\ f_{ex} + f_{in}e^{-kt} \end{bmatrix} & ;\ \text{if} \quad \begin{bmatrix} p_{in}(t) \\ p_{ex}(t) \end{bmatrix} = \begin{bmatrix} 0 \\ 1 \end{bmatrix} \end{cases} \tag{B.12}$$

where $k = k_{in} + k_{ex}$ and the signal fractions $f_{in}$ and $f_{ex}$ satisfy $f_{in} + f_{ex} = 1$. Further, equilibrium demands $f_{in} \cdot k_{in\to ex} = f_{ex} \cdot k_{ex\to in}$.

**Evaluating the mean second-order velocity autocorrelation function**

The second-order velocity autocorrelation (VA) function is given by

$$\langle v(t_1)v(t_2)\rangle = \begin{cases} 2D_{in}\delta(t_2-t_1) & ; \quad \text{if intracellular} \\ 2D_{ex}\delta(t_2-t_1) & ; \quad \text{if extracellular} \end{cases} \tag{B.13}$$

Evaluating the mean VA requires considering all possible particle states in $\begin{bmatrix} 0 & t_1 \end{bmatrix}$ and $(t_1 \quad t_2]$:
For $\begin{bmatrix} p_{in}(0) & p_{ex}(0) \end{bmatrix} = \begin{bmatrix} 1 & 0 \end{bmatrix}$ (particles initially intracellular):

$$\begin{aligned}\langle v(t_1)v(t_2)\rangle_{in} = \big[&p_{in\to in}(t_1-0)\cdot p_{in\to in}(t_2-t_1)\cdot 2D_{in}\delta(t_2-t_1)+\\ &p_{in\to in}(t_1-0)\cdot p_{in\to ex}(t_2-t_1)\cdot 2D_{ex}\delta(t_2-t_1)+\\ &p_{in\to ex}(t_1-0)\cdot p_{ex\to in}(t_2-t_1)\cdot 2D_{in}\delta(t_2-t_1)+\\ &p_{in\to ex}(t_1-0)\cdot p_{ex\to ex}(t_2-t_1)\cdot 2D_{ex}\delta(t_2-t_1)\big]\end{aligned} \tag{B.14}$$

Inserting

$$\begin{aligned}p_{in\to in}(t) &= f_{in} + f_{ex}e^{-kt}\\ p_{in\to ex}(t) &= f_{ex}(1-e^{-kt})\\ p_{ex\to in}(t) &= f_{in}(1-e^{-kt})\\ p_{ex\to ex}(t) &= f_{ex} + f_{in}e^{-kt}\end{aligned} \tag{B.15}$$

gives:

$$\langle v(t_1)v(t_2)\rangle_{in} = 2\cdot\delta(t_2-t_1)\cdot(f_{ex}\cdot(D_{in}-D_{ex})e^{-kt_2} + f_{in}D_{in} + f_{ex}D_{ex}) \tag{B.16}$$

For $\begin{bmatrix}p_{in}(0) & p_{ex}(0)\end{bmatrix} = \begin{bmatrix}0 & 1\end{bmatrix}$ (particles initially extracellular):

$$\begin{aligned}\langle v(t_1)v(t_2)\rangle_{ex} = \big[&p_{ex\to ex}(t_1-0)\cdot p_{ex\to ex}(t_2-t_1)\cdot 2D_{ex}\delta(t_2-t_1)+\\ &p_{ex\to ex}(t_1-0)\cdot p_{ex\to in}(t_2-t_1)\cdot 2D_{in}\delta(t_2-t_1)+\\ &p_{ex\to in}(t_1-0)\cdot p_{in\to ex}(t_2-t_1)\cdot 2D_{ex}\delta(t_2-t_1)+\\ &p_{ex\to in}(t_1-0)\cdot p_{in\to in}(t_2-t_1)\cdot 2D_{in}\delta(t_2-t_1)\big]\end{aligned} \tag{B.17}$$

Inserting the probability definitions in equation B.15 gives:

$$\langle v(t_1)v(t_2)\rangle_{ex} = 2\cdot\delta(t_2-t_1)\cdot(f_{in}\cdot(D_{in}-D_{ex})e^{-kt_2} + f_{in}D_{in} + f_{ex}D_{ex}) \tag{B.18}$$

The mean second-order VA function becomes:

$$\begin{aligned}\langle v(t_1)v(t_2)\rangle &= f_{in}\langle v(t_1)v(t_2)\rangle_{in} + f_{ex}\langle v(t_1)v(t_2)\rangle_{ex}\\ &= f_{in}\cdot 2\cdot\delta(t_2-t_1)\cdot(f_{ex}\cdot(D_{in}-D_{ex})e^{-kt_2}+\\ &f_{in}D_{in} + f_{ex}D_{ex}) + f_{ex}\cdot 2\cdot\delta(t_2-t_1)\cdot(f_{in}\cdot(D_{in}-D_{ex})e^{-kt_2} + f_{in}D_{in} + f_{ex}D_{ex})\end{aligned}$$

$$= 2\delta(t_2 - t_1)(f_{in}D_{in} + f_{ex}D_{ex}) \tag{B.19}$$

Defining the mean diffusivity as: $\overline{D} := f_{in}D_{in} + f_{ex}D_{ex}$ yields:

$$\langle v(t_1)v(t_2)\rangle = 2\delta(t_2 - t_1)\overline{D} \tag{B.20}$$

**Evaluating the second-order moment of the phase distribution**

$$\begin{aligned}
\langle \phi(T)^2 \rangle &= \int_0^T \int_0^T q(t_1)q(t_2)\langle v(t_1)v(t_2)\rangle dt_1 dt_2 \\
&= \int_0^T \int_0^T q(t_1)q(t_2) \cdot 2\delta(t_2 - t_1)\overline{D} dt_1 dt_2 \\
&= 2\overline{D} \cdot \int_0^T q(t_1) \int_{-\infty}^{\infty} q(t_2) \cdot \delta(t_2 - t_1) dt_1 dt_2 \\
&= 2\overline{D} \cdot \int_0^T q(t_1)q(t_1) dt_1 \\
&= 2\overline{D} \cdot \int_0^T q^2(t_1) dt_1 \\
&= 2\overline{D}b
\end{aligned} \tag{B.21}$$

where $\int_0^T q(t)dt = \int_{-\infty}^{\infty} q(t)dt$ because $q(t) = 0 \ \forall \ t \notin [0 \quad T]$.

**Evaluating the mean fourth-order velocity autocorrelation function**

The fourth-order VA function is here generalised:

$$\begin{aligned}
\langle v(t_1)v(t_2)v(t_3)v(t_4)\rangle &= \langle v(t_1)v(t_2)\rangle \cdot \langle v(t_3)v(t_4)\rangle + \langle v(t_1)v(t_3)\rangle \cdot \langle v(t_2)v(t_4)\rangle + \\
&\quad \langle v(t_1)v(t_4)\rangle \cdot \langle v(t_2)v(t_3)\rangle \\
&\approx 3 \cdot \langle v(t_1)v(t_2)\rangle \cdot \langle v(t_3)v(t_4)\rangle
\end{aligned} \tag{B.22}$$

The second-order component $\langle v(t_1)v(t_2)\rangle$ is as defined earlier and $\langle v(t_3)v(t_4)\rangle$ is similarly defined:

$$\langle v(t_3)v(t_4)\rangle = \begin{cases} 2D_{in}\delta(t_4 - t_3) & ; \quad \text{if intracellular} \\ 2D_{ex}\delta(t_4 - t_3) & ; \quad \text{if extracellular} \end{cases} \tag{B.23}$$

To evaluate the mean fourth-order VA, all possible particle states in $[0 \quad t_1]$, $(t_1 \quad t_2]$, $(t_2 \quad t_3]$ and $(t_3 \quad t_4]$ must be considered.
For $\begin{bmatrix} p_{in}(0) & p_{ex}(0) \end{bmatrix} = \begin{bmatrix} 1 & 0 \end{bmatrix}$ (particles initially intracellular):

$$\langle v(t_1)v(t_2)v(t_3)v(t_4)\rangle_{in} = 3\cdot$$
$$\begin{aligned}
&\big[p_{in\to in}(t_1-0)\cdot p_{in\to in}(t_2-t_1)\cdot 2D_{in}\delta(t_2-t_1)\cdot p_{in\to in}(t_3-t_2)\cdot p_{in\to in}(t_4-t_3)\cdot 2D_{in}\delta(t_4-t_3)+\\
&p_{in\to in}(t_1-0)\cdot p_{in\to in}(t_2-t_1)\cdot 2D_{in}\delta(t_2-t_1)\cdot p_{in\to in}(t_3-t_2)\cdot p_{in\to ex}(t_4-t_3)\cdot 2D_{ex}\delta(t_4-t_3)+\\
&p_{in\to in}(t_1-0)\cdot p_{in\to in}(t_2-t_1)\cdot 2D_{in}\delta(t_2-t_1)\cdot p_{in\to ex}(t_3-t_2)\cdot p_{ex\to in}(t_4-t_3)\cdot 2D_{in}\delta(t_4-t_3)+\\
&p_{in\to in}(t_1-0)\cdot p_{in\to in}(t_2-t_1)\cdot 2D_{in}\delta(t_2-t_1)\cdot p_{in\to ex}(t_3-t_2)\cdot p_{ex\to ex}(t_4-t_3)\cdot 2D_{ex}\delta(t_4-t_3)+\\
&p_{in\to in}(t_1-0)\cdot p_{in\to ex}(t_2-t_1)\cdot 2D_{ex}\delta(t_2-t_1)\cdot p_{ex\to in}(t_3-t_2)\cdot p_{in\to in}(t_4-t_3)\cdot 2D_{in}\delta(t_4-t_3)+\\
&p_{in\to in}(t_1-0)\cdot p_{in\to ex}(t_2-t_1)\cdot 2D_{ex}\delta(t_2-t_1)\cdot p_{ex\to in}(t_3-t_2)\cdot p_{in\to ex}(t_4-t_3)\cdot 2D_{ex}\delta(t_4-t_3)+\\
&p_{in\to in}(t_1-0)\cdot p_{in\to ex}(t_2-t_1)\cdot 2D_{ex}\delta(t_2-t_1)\cdot p_{ex\to ex}(t_3-t_2)\cdot p_{ex\to in}(t_4-t_3)\cdot 2D_{in}\delta(t_4-t_3)+\\
&p_{in\to in}(t_1-0)\cdot p_{in\to ex}(t_2-t_1)\cdot 2D_{ex}\delta(t_2-t_1)\cdot p_{ex\to ex}(t_3-t_2)\cdot p_{ex\to ex}(t_4-t_3)\cdot 2D_{ex}\delta(t_4-t_3)+\\
&p_{in\to ex}(t_1-0)\cdot p_{ex\to in}(t_2-t_1)\cdot 2D_{in}\delta(t_2-t_1)\cdot p_{in\to in}(t_3-t_2)\cdot p_{in\to in}(t_4-t_3)\cdot 2D_{in}\delta(t_4-t_3)+\\
&p_{in\to ex}(t_1-0)\cdot p_{ex\to in}(t_2-t_1)\cdot 2D_{in}\delta(t_2-t_1)\cdot p_{in\to in}(t_3-t_2)\cdot p_{in\to ex}(t_4-t_3)\cdot 2D_{ex}\delta(t_4-t_3)+\\
&p_{in\to ex}(t_1-0)\cdot p_{ex\to in}(t_2-t_1)\cdot 2D_{in}\delta(t_2-t_1)\cdot p_{in\to ex}(t_3-t_2)\cdot p_{ex\to in}(t_4-t_3)\cdot 2D_{in}\delta(t_4-t_3)+\\
&p_{in\to ex}(t_1-0)\cdot p_{ex\to in}(t_2-t_1)\cdot 2D_{in}\delta(t_2-t_1)\cdot p_{in\to ex}(t_3-t_2)\cdot p_{ex\to ex}(t_4-t_3)\cdot 2D_{ex}\delta(t_4-t_3)+\\
&p_{in\to ex}(t_1-0)\cdot p_{ex\to ex}(t_2-t_1)\cdot 2D_{ex}\delta(t_2-t_1)\cdot p_{ex\to in}(t_3-t_2)\cdot p_{in\to in}(t_4-t_3)\cdot 2D_{in}\delta(t_4-t_3)+\\
&p_{in\to ex}(t_1-0)\cdot p_{ex\to ex}(t_2-t_1)\cdot 2D_{ex}\delta(t_2-t_1)\cdot p_{ex\to in}(t_3-t_2)\cdot p_{in\to ex}(t_4-t_3)\cdot 2D_{ex}\delta(t_4-t_3)+\\
&p_{in\to ex}(t_1-0)\cdot p_{ex\to ex}(t_2-t_1)\cdot 2D_{ex}\delta(t_2-t_1)\cdot p_{ex\to ex}(t_3-t_2)\cdot p_{ex\to in}(t_4-t_3)\cdot 2D_{in}\delta(t_4-t_3)+\\
&p_{in\to ex}(t_1-0)\cdot p_{ex\to ex}(t_2-t_1)\cdot 2D_{ex}\delta(t_2-t_1)\cdot p_{ex\to ex}(t_3-t_2)\cdot p_{ex\to ex}(t_4-t_3)\cdot 2D_{ex}\delta(t_4-t_3)\big]
\end{aligned} \tag{B.24}$$

The right-hand-side of equation B.24 is the probabilistic representation of the product $3\cdot\langle v(t_1)v(t_2)\rangle\cdot\langle v(t_3)v(t_4)\rangle = 3\cdot 2D\delta(t_2-t_1)\cdot 2D\delta(t_4-t_3)$ where $D$ is either $D_{in}$ or $D_{ex}$ depending on the state of the particle in the time intervals $(t_1 \quad t_2]$ and $(t_3 \quad t_4]$.

Inserting the definitions of transition probabilities in equation B.15 yields:

$$\begin{aligned}
\langle v(t_1)v(t_2)v(t_3)v(t_4)\rangle_{in} = 3\cdot 4\cdot\delta(t_4-t_3)\cdot(f_{in}f_{ex}(D_{in}-D_{ex})^2\cdot e^{-k(t_4-t_2)}+\\
f_{ex}(D_{in}-D_{ex})(f_{in}D_{in}+f_{ex}D_{ex})\cdot e^{-kt_2}+f_{ex}(D_{in}-D_{ex})\cdot(f_{ex}D_{in}+f_{in}D_{ex})\cdot e^{-kt_4}+\\
(f_{in}D_{in}+f_{ex}D_{ex})^2\cdot\delta(t_2-t_1))
\end{aligned}$$

For $\begin{bmatrix} p_{in}(0) & p_{ex}(0) \end{bmatrix} = \begin{bmatrix} 0 & 1 \end{bmatrix}$ (particles initially extracellular):

$$\langle v(t_1)v(t_2)v(t_3)v(t_4)\rangle_{ex} = 3\cdot$$
$$\begin{aligned}
&\big[p_{ex\to in}(t_1-0)\cdot p_{in\to in}(t_2-t_1)\cdot 2D_{in}\delta(t_2-t_1)\cdot p_{in\to in}(t_3-t_2)\cdot p_{in\to in}(t_4-t_3)\cdot 2D_{in}\delta(t_4-t_3)+\\
&p_{ex\to in}(t_1-0)\cdot p_{in\to in}(t_2-t_1)\cdot 2D_{in}\delta(t_2-t_1)\cdot p_{in\to in}(t_3-t_2)\cdot p_{in\to ex}(t_4-t_3)\cdot 2D_{ex}\delta(t_4-t_3)+\\
&p_{ex\to in}(t_1-0)\cdot p_{in\to in}(t_2-t_1)\cdot 2D_{in}\delta(t_2-t_1)\cdot p_{in\to ex}(t_3-t_2)\cdot p_{ex\to in}(t_4-t_3)\cdot 2D_{in}\delta(t_4-t_3)+\\
&p_{ex\to in}(t_1-0)\cdot p_{in\to in}(t_2-t_1)\cdot 2D_{in}\delta(t_2-t_1)\cdot p_{in\to ex}(t_3-t_2)\cdot p_{ex\to ex}(t_4-t_3)\cdot 2D_{ex}\delta(t_4-t_3)+\\
&p_{ex\to in}(t_1-0)\cdot p_{in\to ex}(t_2-t_1)\cdot 2D_{ex}\delta(t_2-t_1)\cdot p_{ex\to in}(t_3-t_2)\cdot p_{in\to in}(t_4-t_3)\cdot 2D_{in}\delta(t_4-t_3)+\\
&p_{ex\to in}(t_1-0)\cdot p_{in\to ex}(t_2-t_1)\cdot 2D_{ex}\delta(t_2-t_1)\cdot p_{ex\to in}(t_3-t_2)\cdot p_{in\to ex}(t_4-t_3)\cdot 2D_{ex}\delta(t_4-t_3)+\\
&p_{ex\to in}(t_1-0)\cdot p_{in\to ex}(t_2-t_1)\cdot 2D_{ex}\delta(t_2-t_1)\cdot p_{ex\to ex}(t_3-t_2)\cdot p_{ex\to in}(t_4-t_3)\cdot 2D_{in}\delta(t_4-t_3)+\\
&p_{ex\to in}(t_1-0)\cdot p_{in\to ex}(t_2-t_1)\cdot 2D_{ex}\delta(t_2-t_1)\cdot p_{ex\to ex}(t_3-t_2)\cdot p_{ex\to ex}(t_4-t_3)\cdot 2D_{ex}\delta(t_4-t_3)+\\
&p_{ex\to ex}(t_1-0)\cdot p_{ex\to in}(t_2-t_1)\cdot 2D_{in}\delta(t_2-t_1)\cdot p_{in\to in}(t_3-t_2)\cdot p_{in\to in}(t_4-t_3)\cdot 2D_{in}\delta(t_4-t_3)+\\
&p_{ex\to ex}(t_1-0)\cdot p_{ex\to in}(t_2-t_1)\cdot 2D_{in}\delta(t_2-t_1)\cdot p_{in\to in}(t_3-t_2)\cdot p_{in\to ex}(t_4-t_3)\cdot 2D_{ex}\delta(t_4-t_3)+\\
&p_{ex\to ex}(t_1-0)\cdot p_{ex\to in}(t_2-t_1)\cdot 2D_{in}\delta(t_2-t_1)\cdot p_{in\to ex}(t_3-t_2)\cdot p_{ex\to in}(t_4-t_3)\cdot 2D_{in}\delta(t_4-t_3)+\\
&p_{ex\to ex}(t_1-0)\cdot p_{ex\to in}(t_2-t_1)\cdot 2D_{in}\delta(t_2-t_1)\cdot p_{in\to ex}(t_3-t_2)\cdot p_{ex\to ex}(t_4-t_3)\cdot 2D_{ex}\delta(t_4-t_3)+\\
&p_{ex\to ex}(t_1-0)\cdot p_{ex\to ex}(t_2-t_1)\cdot 2D_{ex}\delta(t_2-t_1)\cdot p_{ex\to in}(t_3-t_2)\cdot p_{in\to in}(t_4-t_3)\cdot 2D_{in}\delta(t_4-t_3)+\\
&p_{ex\to ex}(t_1-0)\cdot p_{ex\to ex}(t_2-t_1)\cdot 2D_{ex}\delta(t_2-t_1)\cdot p_{ex\to in}(t_3-t_2)\cdot p_{in\to ex}(t_4-t_3)\cdot 2D_{ex}\delta(t_4-t_3)+\\
&p_{ex\to ex}(t_1-0)\cdot p_{ex\to ex}(t_2-t_1)\cdot 2D_{ex}\delta(t_2-t_1)\cdot p_{ex\to ex}(t_3-t_2)\cdot p_{ex\to in}(t_4-t_3)\cdot 2D_{in}\delta(t_4-t_3)+\\
&p_{ex\to ex}(t_1-0)\cdot p_{ex\to ex}(t_2-t_1)\cdot 2D_{ex}\delta(t_2-t_1)\cdot p_{ex\to ex}(t_3-t_2)\cdot p_{ex\to ex}(t_4-t_3)\cdot 2D_{ex}\delta(t_4-t_3)\big]
\end{aligned} \tag{B.25}$$

Similarly, inserting B.15 provides:

$$\begin{aligned}
\langle v(t_1)v(t_2)v(t_3)v(t_4)\rangle_{ex} = 3\cdot 4\cdot\delta(t_4-t_3)\cdot(f_{in}f_{ex}(D_{in}-D_{ex})^2\cdot e^{-k(t_4-t_2)}-\\
f_{in}(D_{in}-D_{ex})(f_{in}D_{in}+f_{ex}D_{ex})\cdot e^{-kt_2}-f_{in}(D_{in}-D_{ex})\cdot(f_{ex}D_{in}+f_{in}D_{ex})\cdot e^{-kt_4}+\\
(f_{in}D_{in}+f_{ex}D_{ex})^2\cdot\delta(t_2-t_1))
\end{aligned}$$

The mean fourth-order VA function becomes:

$$\begin{aligned}\langle v(t_1)v(t_2)v(t_3)v(t_4)\rangle &= f_{in}\langle v(t_1)v(t_2)v(t_3)v(t_4)\rangle_{in} + f_{ex}\langle v(t_1)v(t_2)v(t_3)v(t_4)\rangle_{ex} \\ &= f_{in}\cdot 3\cdot 4\cdot \delta(t_4-t_3)\cdot(f_{in}f_{ex}(D_{in}-D_{ex})^2\cdot e^{-k(t_4-t_2)}+ \\ f_{ex}(D_{in}-D_{ex})(f_{in}D_{in}+f_{ex}D_{ex})\cdot e^{-kt_2} &+ f_{ex}(D_{in}-D_{ex})\cdot(f_{ex}D_{in}+f_{in}D_{ex})\cdot e^{-kt_4}+ \\ &(f_{in}D_{in}+f_{ex}D_{ex})^2\cdot\delta(t_2-t_1))+ \\ f_{ex}\cdot 3\cdot 4\cdot\delta(t_4-t_3)\cdot(f_{in}f_{ex}(D_{in}-D_{ex})^2\cdot e^{-k(t_4-t_2)}- \\ f_{in}(D_{in}-D_{ex})(f_{in}D_{in}+f_{ex}D_{ex})\cdot e^{-kt_2} &- f_{in}(D_{in}-D_{ex})\cdot(f_{ex}D_{in}+f_{in}D_{ex})\cdot e^{-kt_4}+ \\ &(f_{in}D_{in}+f_{ex}D_{ex})^2\cdot\delta(t_2-t_1)) \\ &= 3\big[4\cdot f_{in}f_{ex}(D_{in}-D_{ex})^2\cdot\delta(t_2-t_1)\delta(t_4-t_3)e^{-k(t_4-t_2)}+ \\ &\quad 4\cdot(f_{in}D_{in}+f_{ex}D_{ex})^2\cdot\delta(t_2-t_1)\delta(t_4-t_3)\big]\end{aligned} \tag{B.26}$$

Define the variance of compartment diffusivities as $\mathrm{Var}(D) := f_{in}f_{ex}(D_{in}-D_{ex})^2$ and recall the definition of the mean diffusivity: $\overline{D} = f_{in}D_{in}+f_{ex}D_{ex}$. The mean VA can then be written

$$\langle v(t_1)v(t_2)v(t_3)v(t_4)\rangle = 12\cdot\mathrm{Var}(D)\cdot\delta(t_2-t_1)\delta(t_4-t_3)e^{-k(t_4-t_2)}+12\cdot\overline{D}^2\cdot\delta(t_2-t_1)\delta(t_4-t_3) \tag{B.27}$$

**Evaluating the fourth-order moment of the phase distribution**

$$\begin{aligned}\langle\phi(T)^4\rangle &= \int_0^T\int_0^T\int_0^T\int_0^T q(t_1)q(t_2)q(t_3)q(t_4)\langle v(t_1)v(t_2)v(t_3)v(t_4)\rangle dt_1dt_2dt_3dt_4 \\ &= \int_0^T\int_0^T\int_0^T\int_0^T q(t_1)q(t_2)q(t_3)q(t_4)[12\cdot\mathrm{Var}(D)\cdot\delta(t_2-t_1)\delta(t_4-t_3)e^{-k(t_4-t_2)}+ \\ &\quad 12\cdot\overline{D}^2\cdot\delta(t_2-t_1)\delta(t_4-t_3)]dt_1dt_2dt_3dt_4 \\ &= 12\cdot\mathrm{Var}(D)\int_0^T e^{-k(t_4-t_2)}\int_0^T q(t_2)q(t_4)\int_{-\infty}^{\infty}q(t_1)\delta(t_2-t_1)dt_1\int_{-\infty}^{\infty}q(t_3)\delta(t_4-t_3)dt_3dt_2dt_4 \\ &\quad + 12\cdot\overline{D}^2\int_0^T q(t_2)\int_0^T q(t_4)\int_{-\infty}^{\infty}q(t_1)\delta(t_2-t_1)dt_1\int_{-\infty}^{\infty}q(t_3)\delta(t_4-t_3)dt_3dt_2dt_4 \\ &= 12\cdot\mathrm{Var}(D)\int_0^T e^{-k(t_4-t_2)}\int_0^T q(t_2)^2q(t_4)^2dt_2dt_4 + 12\cdot\overline{D}^2\int_0^T q(t_2)^2dt_2\int_0^T q(t_4)^2dt_4\end{aligned}$$

$$= 12 \cdot \mathrm{Var}(D) \int_0^T e^{-k(t_4-t_2)} \int_0^T q(t_2)^2 q(t_4)^2 dt_2 dt_4 + 12 \cdot \overline{D}^2 b^2 \tag{B.28}$$

where $\int_0^T q(t)dt = \int_{-\infty}^{\infty} q(t)dt$ because $q(t) = 0 \; \forall \; t \notin [0 \quad T]$. Define $t := t_4 - t_2, t \in [-T, T]$, then

$$\begin{aligned} \langle \phi(T)^4 \rangle &= 12 \cdot \mathrm{Var}(D) \int_{-T}^T e^{-kt} \int_0^T q(t_2)^2 q(t_2+t)^2 dt_2 dt + 12 \cdot \overline{D}^2 \cdot b^2 \\ &= 12 \cdot \mathrm{Var}(D) \int_{-T}^T e^{-kt} q_4(t) dt + 12 \cdot \overline{D}^2 \cdot b^2 \end{aligned} \tag{B.29}$$

where $q_4(t) = \int_0^T q(t_2)^2 q(t_2+t)^2 dt_2$ is the fourth-order autocorrelation function of $q(t)$. The fourth order moment of the phase distribution can be expressed:

$$\begin{aligned} \langle \phi(T)^4 \rangle &= 12 \cdot \mathrm{Var}(D) \int_{-T}^T e^{-k|t|} q_4(|t|) dt + 12 \cdot \overline{D}^2 \cdot b^2 \\ &= 12 \cdot \mathrm{Var}(D) \cdot 2 \int_0^T e^{-kt} q_4(t) dt + 12 \cdot \overline{D}^2 \cdot b^2 \end{aligned} \tag{B.30}$$

**Final signal representation**

The final signal equation is now given by

$$\begin{aligned} \ln(S) &\approx -\frac{1}{2}\langle \phi^2 \rangle + \frac{1}{24}(\langle \phi^4 \rangle - 3\langle \phi^2 \rangle^2) \\ &= -\frac{1}{2} \cdot 2\overline{D}b + \frac{1}{24}\left[12 \cdot \mathrm{Var}(D) \cdot 2 \int_0^T e^{-kt} q_4(t) dt + 12 \cdot \overline{D}^2 \cdot b^2 - 3 \cdot (2\overline{D}b)^2\right] \\ &= -\overline{D}b + \frac{1}{2}\mathrm{Var}(D) \cdot 2 \int_0^T e^{-kt} q_4(t) dt \end{aligned} \tag{B.31}$$

In other words,

$$\ln(S) \approx -\overline{D}b + \frac{1}{2}\mathrm{Var}(D) h(\cdot) b^2 \tag{B.32}$$

where

$$h(\cdot) = \frac{2}{b^2} \int_0^T e^{-kt} q_4(t) dt \tag{B.33}$$

is the exchange-weighting term.

Done.

## Appendix B3: General exchange-restriction theory

The derivations in this section are an extension (generalisation) of the theory presented in Appendix B2.

Definition of the velocity-autocorrelation function:

$$\langle v(t_1)v(t_2)\rangle = \begin{cases} \frac{1}{\pi}\int_{-\infty}^{\infty} D(\omega)\mathrm{e}^{i\omega(t_2-t_1)}d\omega & ; \quad \text{if intracellular} \\ \\ 2D_{ex}\delta(t_2-t_1) & ; \quad \text{if extracellular} \end{cases} \tag{B.34}$$

**Evaluating the second-order moment of the phase distribution**

$$\langle \phi(T)^2\rangle = \int_0^T \int_0^T q(t_1)q(t_2)\langle v(t_1)v(t_2)\rangle dt_1 dt_2 \tag{B.35}$$

Since $q(t) = 0 \; \forall \; t \notin [0 \quad T]$, $\int_0^T q(t)dt = \int_{-\infty}^{\infty} q(t)dt$. This allows the reformulation:

$$\langle \phi(T)^2\rangle = \int_{-\infty}^{\infty} \int_{-\infty}^{\infty} q(t_1)q(t_2)\langle v(t_1)v(t_2)\rangle dt_1 dt_2 \tag{B.36}$$

The mean second-order velocity autocorrelation function obtained from the Maple script in Appendix B1 is:

$$\langle v(t_1)v(t_2)\rangle = \left(2 \cdot f_{in} \cdot \frac{1}{2\pi}\int_{-\infty}^{\infty} D(\omega)e^{i\omega(t_2-t_1)}d\omega\right) + 2 \cdot f_{ex} \cdot D_{ex}\delta(t_2-t_1) \tag{B.37}$$

The second-order moment of the phase distribution then becomes

$$\begin{aligned} \langle \phi(T)^2\rangle &= \int_{-\infty}^{\infty}\int_{-\infty}^{\infty} q(t_1)q(t_2)\Bigg[\left(2f_{in} \cdot \frac{1}{2\pi}\int_{-\infty}^{\infty} D(\omega)e^{i\omega(t_2-t_1)}d\omega\right) \\ &\quad + 2 \cdot f_{ex} \cdot D_{ex}\delta(t_2-t_1)\Bigg]dt_1 dt_2 \\ &= 2 \cdot f_{in} \cdot \int_{-\infty}^{\infty}\int_{-\infty}^{\infty} q(t_1)q(t_2)\left(\frac{1}{2\pi}\int_{-\infty}^{\infty} D(\omega)e^{i\omega(t_2-t_1)}d\omega\right)dt_1 dt_2 + \\ &\quad 2 \cdot f_{ex} \cdot D_{ex} \cdot \int_{-\infty}^{\infty}\int_{-\infty}^{-\infty} q(t_1)q(t_2) \cdot \delta(t_2-t_1)dt_1 dt_2 \\ &= 2 \cdot f_{in} \cdot \left(\frac{1}{2\pi}\int_{-\infty}^{\infty} D(\omega)\left[\int_{-\infty}^{\infty} q(t_1)e^{-i\omega t_1}dt_1\right]\left[\int_{-\infty}^{\infty} q(t_2)e^{i\omega t_2}dt_2\right]\right) + \end{aligned}$$

$$
\begin{aligned}
&2 \cdot f_{ex} \cdot D_{ex} \cdot \int_{-\infty}^{\infty} q(t_1) \cdot \left[ \int_{-\infty}^{\infty} q(t_2)\delta(t_2 - t_1)dt_2 \right] dt_1 \\
&= 2 \cdot f_{in} \cdot \left( \frac{1}{2\pi} \int_{-\infty}^{\infty} D(\omega)[Q(\omega)] \cdot [Q^*(\omega)]dw \right) + 2 \cdot f_{ex} \cdot D_{ex} \cdot \int_0^T q(t_1)[q(t_1)]dt_1 \\
&= 2 \cdot f_{in} \cdot \left( \frac{1}{2\pi} \int_{-\infty}^{\infty} D(\omega) \cdot Q(\omega) \cdot Q^*(\omega)d\omega \right) + 2 \cdot f_{ex} \cdot D_{ex} \cdot \int_0^T q(t_1)^2 dt_1
\end{aligned}
$$

where $Q(\omega)$ is the Fourier transform of $q(t)$ and * denotes complex conjugate.
The second-order moment of the phase distribution can now be written:

$$
\langle \phi(T)^2 \rangle = 2 \left( \frac{f_{in}}{2\pi} \int_{-\infty}^{\infty} D(\omega) \cdot |Q(\omega)|^2 d\omega + f_{ex} \cdot D_{ex} \cdot b \right) \tag{B.38}
$$

**Evaluating the fourth-order moment of the phase distribution**

$$
\langle \phi(T)^4 \rangle = \int_0^T \int_0^T \int_0^T \int_0^T q(t_1)q(t_2)q(t_3)q(t_4)\langle v(t_1)v(t_2)v(t_3)v(t_4)\rangle dt_1 dt_2 dt_3 dt_4 \tag{B.39}
$$

Since $q(t) = 0 \; \forall \; t \notin [0 \quad T]$, $\int_0^T q(t)dt = \int_{-\infty}^{\infty} q(t)dt$, an equivalent expression of the fourth-order moment is

$$
\langle \phi(T)^4 \rangle = \int_{-\infty}^{\infty} \int_{-\infty}^{\infty} \int_{-\infty}^{\infty} \int_{-\infty}^{\infty} q(t_1)q(t_2)q(t_3)q(t_4)\langle v(t_1)v(t_2)v(t_3)v(t_4)\rangle dt_1 dt_2 dt_3 dt_4 \tag{B.40}
$$

Similar to the long-time limit case, the fourth-order velocity autocorrelation function is factorised into two second-order terms:

$$
\begin{aligned}
\langle v(t_1)v(t_2)v(t_3)v(t_4)\rangle = \langle v(t_1)v(t_2)\rangle \cdot \langle v(t_3)v(t_4)\rangle + \langle v(t_1)v(t_3)\rangle \cdot \langle v(t_2)v(t_4)\rangle + \\
\langle v(t_1)v(t_4)\rangle \cdot \langle v(t_2)v(t_3)\rangle \\
\approx 3 \cdot \langle v(t_1)v(t_2)\rangle \cdot \langle v(t_3)v(t_4)\rangle
\end{aligned}
$$

The mean fourth-order velocity autocorrelation function obtained from the Maple script in Appendix B1 is

$$
\begin{aligned}
\langle v(t_1)v(t_2)v(t_3)v(t_4)\rangle = 4 \cdot \Bigg[ &\frac{f_{in}f_{ex}}{4\pi^2} \left( \int_{-\infty}^{\infty} D(\omega)e^{i\omega(t_4 - t_3)}d\omega \right) \cdot \left( \int_{-\infty}^{\infty} D(\omega)e^{i\omega(t_2 - t_1)}d\omega \right) \\
&- f_{in}f_{ex} \cdot D_{ex}\delta(t_4 - t_3) \cdot \left( \frac{1}{2\pi} \int_{-\infty}^{\infty} D(\omega)e^{i\omega(t_2 - t_1)}d\omega \right)
\end{aligned}
$$

$$- f_{in}f_{ex} \cdot D_{ex}\delta(t_2 - t_1) \cdot \left(\frac{1}{2\pi}\int_{-\infty}^{\infty} D(\omega)e^{i\omega(t_4-t_3)}d\omega\right) + f_{in}f_{ex} \cdot D_{ex}\delta(t_4 - t_3) \cdot \delta(t_2 - t_1)\Bigg]$$
$$\cdot e^{-k(t_4-t_2)} + 4 \cdot \Bigg[\frac{f_{in}f_{in}}{4\pi^2}\left(\int_{-\infty}^{\infty} D(\omega)e^{i\omega(t_4-t_3)}d\omega\right) \cdot \left(\int_{-\infty}^{\infty} D(\omega)e^{i\omega(t_2-t_1)}d\omega\right)$$
$$+ f_{in}f_{ex} \cdot D_{ex}\delta(t_4 - t_3) \cdot \left(\frac{1}{2\pi}\int_{-\infty}^{\infty} D(\omega)e^{i\omega(t_2-t_1)}d\omega\right) +$$
$$f_{in}f_{ex} \cdot D_{ex}\delta(t_2 - t_1) \cdot \left(\frac{1}{2\pi}\int_{-\infty}^{\infty} D(\omega)e^{i\omega(t_4-t_3)}d\omega\right) + f_{ex}f_{ex} \cdot D_{ex} \cdot \delta(t_4 - t_3) \cdot D_{ex}\delta(t_2 - t_1)\Bigg] \tag{B.41}$$

The colour-coding above is meant to enhance readability. Its meaning is provided below. The fourth-order moment of the phase distribution is now given by:

$$\langle\phi(T)^4\rangle = \int_{-\infty}^{\infty}\int_{-\infty}^{\infty}\int_{-\infty}^{\infty}\int_{-\infty}^{\infty} q(t_1)q(t_2)q(t_3)q(t_4)\langle v(t_1)v(t_2)v(t_3)v(t_4)\rangle dt_1dt_2dt_3dt_4$$
$$= 12 \cdot \int_{-\infty}^{\infty}\int_{-\infty}^{\infty}\int_{-\infty}^{\infty}\int_{-\infty}^{\infty} q(t_1)q(t_2)q(t_3)q(t_4)\Bigg(\Bigg[\frac{f_{in}f_{ex}}{4\pi^2}\left(\int_{-\infty}^{\infty} D(\omega)e^{i\omega(t_4-t_3)}d\omega\right) \cdot$$
$$\left(\int_{-\infty}^{\infty} D(\omega)e^{i\omega(t_2-t_1)}d\omega\right) - f_{in}f_{ex} \cdot D_{ex}\delta(t_4 - t_3) \cdot \left(\frac{1}{2\pi}\int_{-\infty}^{\infty} D(\omega)e^{i\omega(t_2-t_1)}d\omega\right)$$
$$- f_{in}f_{ex} \cdot D_{ex}\delta(t_2 - t_1) \cdot \left(\frac{1}{2\pi}\int_{-\infty}^{\infty} D(\omega)e^{i\omega(t_4-t_3)}d\omega\right) + f_{in}f_{ex} \cdot D_{ex}\delta(t_4 - t_3) \cdot \delta(t_2 - t_1)\Bigg]$$
$$\cdot e^{-k(t_4-t_2)} + \Bigg[\frac{f_{in}f_{in}}{4\pi^2}\left(\int_{-\infty}^{\infty} D(\omega)e^{i\omega(t_4-t_3)}d\omega\right) \cdot \left(\int_{-\infty}^{\infty} D(\omega)e^{i\omega(t_2-t_1)}d\omega\right)$$
$$+ f_{in}f_{ex} \cdot D_{ex}\delta(t_4 - t_3) \cdot \left(\frac{1}{2\pi}\int_{-\infty}^{\infty} D(\omega)e^{i\omega(t_2-t_1)}d\omega\right) +$$
$$f_{in}f_{ex} \cdot D_{ex}\delta(t_2 - t_1) \cdot \left(\frac{1}{2\pi}\int_{-\infty}^{\infty} D(\omega)e^{i\omega(t_4-t_3)}d\omega\right) +$$
$$f_{ex}f_{ex} \cdot D_{ex} \cdot \delta(t_4 - t_3) \cdot D_{ex}\delta(t_2 - t_1)\Bigg]\Bigg)dt_1dt_2dt_3dt_4 \tag{B.42}$$

Above, the blue, green and red expressions are the variance terms and violet expressions are the mean terms. All these terms will be handled one at a time below. The terms are labelled below for ease of reference:

$$\langle\phi(T)^4\rangle = V_1 + V_2 + V_3 + V_4 + M_1 + M_2 + M_3 + M_4 \tag{B.43}$$

where $V$ and $M$ denote variance and mean, respectively. The colour-coding presented above will be maintained throughout the derivations in this section.

***Evaluating*** $V_1$ :

$$V_1 = 12 \cdot \int_{-\infty}^{\infty}\int_{-\infty}^{\infty}\int_{-\infty}^{\infty}\int_{-\infty}^{\infty} q(t_1)q(t_2)q(t_3)q(t_4) \cdot \left[\left(\frac{f_{in}f_{ex}}{4\pi^2}\left(\int_{-\infty}^{\infty} D(\omega)e^{i\omega(t_4-t_3)}d\omega\right)\cdot \left(\int_{-\infty}^{\infty} D(\omega)e^{i\omega(t_2-t_1)}d\omega\right)\right)\cdot e^{-k(t_4-t_2)}\right] dt_1dt_2dt_3dt_4$$

$$= 12 \cdot \frac{f_{in}f_{ex}}{4\pi^2}\int_{-\infty}^{\infty}\int_{-\infty}^{\infty}\int_{-\infty}^{\infty}\int_{-\infty}^{\infty} q(t_1)q(t_2)q(t_3)q(t_4)\cdot e^{-k(t_4-t_2)}\int_{-\infty}^{\infty} D(\omega)e^{-i\omega(t_4-t_3)}d\omega$$

$$\cdot \int_{-\infty}^{\infty} D(\omega_1)e^{-i\omega_1(t_2-t_1)}d\omega_1dt_1dt_2dt_3dt_4$$

$$= 12 \cdot \frac{f_{in}f_{ex}}{4\pi^2}\int_{-\infty}^{\infty}\int_{-\infty}^{\infty}\int_{-\infty}^{\infty}\int_{-\infty}^{\infty} q(t_1)q(t_2)q(t_3)q(t_4)\cdot e^{-k(t_4-t_2)}\int_{-\infty}^{\infty} D(\omega)\cdot D(\omega_1)e^{i\omega t_4}e^{-i\omega t_3}\cdot$$

$$\cdot e^{i\omega_1 t_2}e^{-i\omega_1 t_1}d\omega d\omega_1 dt_1dt_2dt_3dt_4$$

$$= 12 \cdot \frac{f_{in}f_{ex}}{4\pi^2}\int_{-\infty}^{\infty}\int_{-\infty}^{\infty} q(t_2)q(t_4)\cdot e^{-k(t_4-t_2)}\int_{-\infty}^{\infty}\int_{-\infty}^{\infty} D(\omega)\cdot D(\omega_1)\left[\int_{-\infty}^{\infty} q(t_3)e^{-i\omega t_3}dt_3\right]\cdot$$

$$\cdot \left[\int_{-\infty}^{\infty} q(t_1)e^{-i\omega_1 t_1}dt_1\right]\cdot e^{i\omega t_4}\cdot e^{i\omega_1 t_2}d\omega d\omega_1 dt_2dt_4$$

$$= 12 \cdot \frac{f_{in}f_{ex}}{4\pi^2}\int_{-\infty}^{\infty} e^{-k(t_4-t_2)}\int_{-\infty}^{\infty}\int_{-\infty}^{\infty} D(\omega)\cdot D(\omega_1)[Q(\omega)]\cdot[Q(\omega_1)]\cdot\left[\int_{-\infty}^{\infty} q(t_2)q(t_4)\cdot e^{i\omega_1 t_2}\cdot e^{i\omega t_4}\right]d\omega d\omega_1 dt_2dt_4$$

where $Q(\omega)$ is the Fourier transform of $q(t)$. Now let $t := t_4 - t_2$, $t \in [-T \quad T]$. Then

$$V_1 = 12 \cdot \frac{f_{in}f_{ex}}{4\pi^2}\int_{-\infty}^{\infty} e^{-kt}\int_{-\infty}^{\infty}\int_{-\infty}^{\infty} D(\omega)\cdot D(\omega_1)Q(\omega)\cdot Q(\omega_1)\cdot\left[\int_{-\infty}^{\infty} q(t_2)q(t_2+t)\cdot e^{i\omega_1 t_2}\cdot e^{i\omega(t_2+t)}dt_2\right]d\omega d\omega_1 dt$$

Final expression for $V_1$ :

$$V_1 = 12 \cdot \frac{f_{in}f_{ex}}{4\pi^2}\int_{-\infty}^{\infty} e^{-kt}\int_{-\infty}^{\infty}\int_{-\infty}^{\infty} D(\omega)\cdot D(\omega_1)Q(\omega)\cdot Q(\omega_1)\cdot Q_2(t,\omega,\omega_1)d\omega d\omega_1 dt \tag{B.44}$$

where $Q_2(t,\omega,\omega_1)$ is the correlation:

$$Q_2(t,\omega,\omega_1) := \int_{-\infty}^{\infty} q(t_2)\cdot q(t_2+t)\cdot e^{i\omega_1 t_2}\cdot e^{i\omega(t_2+t)}dt_2$$

***Evaluating*** $V_2$:

$$\begin{aligned}
V_2 &= 12\cdot\int_{-\infty}^{\infty}\int_{-\infty}^{\infty}\int_{-\infty}^{\infty}\int_{-\infty}^{\infty} q(t_1)q(t_2)q(t_3)q(t_4)\cdot\Bigg[\Bigg(-f_{in}f_{ex}\cdot D_{ex}\delta(t_4-t_3)\cdot \\
&\frac{1}{2\pi}\int_{-\infty}^{\infty} D(\omega)e^{i\omega(t_2-t_1)}d\omega\Bigg)\cdot e^{-k(t_4-t_2)}\Bigg]dt_1dt_2dt_3dt_4 \\
&= -12\cdot\frac{f_{in}f_{ex}D_{ex}}{2\pi}\int_{-\infty}^{\infty}\int_{-\infty}^{\infty}\int_{-\infty}^{\infty}\int_{-\infty}^{\infty} q(t_1)q(t_2)q(t_3)q(t_4)\cdot e^{-k(t_4-t_2)}\cdot \\
&\cdot\Bigg(\delta(t_4-t_3)\cdot\int_{-\infty}^{\infty} D(\omega)e^{i\omega(t_2-t_1)}d\omega\Bigg)dt_1dt_2dt_3dt_4 \\
&= -12\cdot\frac{f_{in}f_{ex}D_{ex}}{2\pi}\int_{-\infty}^{\infty}\int_{-\infty}^{\infty} q(t_2)q(t_4)\cdot e^{-k(t_4-t_2)}\left[\int_{-\infty}^{\infty} q(t_3)\delta(t_4-t_3)dt_3\right]\cdot \\
&\cdot\int_{-\infty}^{\infty} D(\omega)\left[\int_{-\infty}^{\infty} q(t_1)e^{-i\omega t_1}dt_1\right]\cdot e^{i\omega t_2}d\omega dt_2dt_4 \\
&= -12\cdot\frac{f_{in}f_{ex}D_{ex}}{2\pi}\int_{-\infty}^{\infty}\int_{-\infty}^{\infty} q(t_2)q(t_4)\cdot e^{-k(t_4-t_2)}\left[q(t_4)\right]\cdot\int_{-\infty}^{\infty} D(\omega)[Q(\omega)]\cdot e^{i\omega t_2}d\omega dt_2dt_4
\end{aligned}$$

Defining $t := t_4 - t_2$, $t \in [-T \quad T]$ gives:

$$\begin{aligned}
V_2 &= -12\cdot\frac{f_{in}f_{ex}D_{ex}}{2\pi}\int_{-\infty}^{\infty}\int_{-\infty}^{\infty} q(t_2)q(t_2+t)^2\cdot e^{-k(t)}\cdot\int_{-\infty}^{\infty} D(\omega)Q(\omega)\cdot e^{i\omega t_2}d\omega dt_2dt \\
&= -12\cdot\frac{f_{in}f_{ex}D_{ex}}{2\pi}\int_{-\infty}^{\infty} e^{-kt}\int_{-\infty}^{\infty} D(\omega)Q(\omega)\int_{-\infty}^{\infty} q(t_2)\cdot q(t_2+t)^2\cdot e^{i\omega t_2}dt_2d\omega dt
\end{aligned}$$

Final expression for $V_2$ :

$$V_2 = -12\cdot\frac{f_{in}f_{ex}D_{ex}}{2\pi}\int_{-\infty}^{\infty} e^{-kt}\int_{-\infty}^{\infty} D(\omega)\cdot Q(\omega)\cdot Q_3(t,\omega)d\omega dt \tag{B.45}$$

where $Q_3(t,\omega)$ is given by the correlation

$$Q_3(t,\omega) := \int_{-\infty}^{\infty} q(t_2)\cdot q(t_2+t)^2 \cdot e^{i\omega t_2} dt_2$$

***Evaluating*** $V_3$ *:*

$$\begin{aligned}
V_3 &= 12 \cdot \int_{-\infty}^{\infty}\int_{-\infty}^{\infty}\int_{-\infty}^{\infty}\int_{-\infty}^{\infty} q(t_1)q(t_2)q(t_3)q(t_4)\cdot\Bigg[\Bigg(-f_{in}f_{ex}\cdot D_{ex}\delta(t_2-t_1)\cdot \\
&\frac{1}{2\pi}\int_{-\infty}^{\infty} D(\omega)e^{i\omega(t_4-t_3)}d\omega\Bigg)\cdot e^{-k(t_4-t_2)}\Bigg]dt_1dt_2dt_3dt_4 \\
&= -12\cdot\frac{f_{in}f_{ex}D_{ex}}{2\pi}\int_{-\infty}^{\infty}\int_{-\infty}^{\infty}\int_{-\infty}^{\infty}\int_{-\infty}^{\infty} q(t_1)q(t_2)q(t_3)q(t_4)\cdot e^{-k(t_4-t_2)}\cdot \\
&\cdot\Bigg(\delta(t_2-t_1)\cdot\int_{-\infty}^{\infty} D(\omega)e^{i\omega(t_4-t_3)}d\omega\Bigg)dt_1dt_2dt_3dt_4 \\
&= -12\cdot\frac{f_{in}f_{ex}D_{ex}}{2\pi}\int_{-\infty}^{\infty}\int_{-\infty}^{\infty} q(t_2)q(t_4)\cdot e^{-k(t_4-t_2)}\left[\int_{-\infty}^{\infty} q(t_1)\delta(t_2-t_1)dt_1\right]\cdot \\
&\cdot\int_{-\infty}^{\infty} D(\omega)\left[\int_{-\infty}^{\infty} q(t_3)e^{-i\omega t_3}dt_3\right]\cdot e^{i\omega t_4}d\omega dt_2dt_4 \\
&= -12\cdot\frac{f_{in}f_{ex}D_{ex}}{2\pi}\int_{-\infty}^{\infty}\int_{-\infty}^{\infty} q(t_2)q(t_4)\cdot e^{-k(t_4-t_2)}\left[q(t_2)\right]\cdot\int_{-\infty}^{\infty} D(\omega)[Q(\omega)]\cdot e^{i\omega t_4}d\omega dt_2dt_4
\end{aligned}$$

Defining $t := t_4 - t_2$, $t \in [-T \quad T]$ gives:

$$\begin{aligned}
V_3 &= -12\cdot\frac{f_{in}f_{ex}D_{ex}}{2\pi}\int_{-\infty}^{\infty}\int_{-\infty}^{\infty} q(t_2)q(t_2+t)^2\cdot e^{-k(t)}\cdot\int_{-\infty}^{\infty} D(\omega)Q(\omega)\cdot e^{i\omega(t_2+t))}d\omega dt_2dt \\
&= -12\cdot\frac{f_{in}f_{ex}D_{ex}}{2\pi}\int_{-\infty}^{\infty} e^{-kt}\int_{-\infty}^{\infty} D(\omega)Q(\omega)\int_{-\infty}^{\infty} q(t_2)^2\cdot q(t_2+t)\cdot e^{i\omega(t_2+t)}dt_2d\omega dt
\end{aligned}$$

Final expression for $V_3$ :

$$V_3 = -12\cdot\frac{f_{in}f_{ex}D_{ex}}{2\pi}\int_{-\infty}^{\infty} e^{-kt}\int_{-\infty}^{\infty} D(\omega)\cdot Q(\omega)\cdot Q_3(t,\omega)d\omega dt \tag{B.46}$$

where $Q_3(t,\omega)$ is given by the correlation

$$Q_3(t,\omega) := \int_{-\infty}^{\infty} q(t_2)^2\cdot q(t_2+t)\cdot e^{i\omega(t_2+t)}dt$$

and corresponds to the same $Q_3$ defined for $V_2$.

***Evaluating*** $V_4$ *:*

$$
\begin{aligned}
V_4 &= 12 \cdot \int_{-\infty}^{\infty}\int_{-\infty}^{\infty}\int_{-\infty}^{\infty}\int_{-\infty}^{\infty} q(t_1)q(t_2)q(t_3)q(t_4) \cdot \big[f_{in}f_{ex} \cdot D_{ex}\delta(t_4-t_3) \cdot D_{ex}\delta(t_2-t_1)\cdot \\
&\cdot e^{-k(t_4-t_2)}\big] dt_1 dt_2 dt_3 dt_4 \\
&= 12 \cdot f_{in}f_{ex}D_{ex}^2 \cdot \int_{-\infty}^{\infty}\int_{-\infty}^{\infty}\int_{-\infty}^{\infty}\int_{-\infty}^{\infty} q(t_1)q(t_2)q(t_3)q(t_4) \cdot \big[\delta(t_4-t_3) \cdot \delta(t_2-t_1)\cdot \\
&\cdot e^{-k(t_4-t_2)}\big] dt_1 dt_2 dt_3 dt_4 \\
&= 12 \cdot f_{in}f_{ex}D_{ex}^2 \cdot \int_{-\infty}^{\infty}\int_{-\infty}^{\infty} e^{-k(t_4-t_2)} \cdot q(t_2)q(t_4) \cdot \left[\int_{-\infty}^{\infty} q(t_3)\delta(t_4-t_3)dt_3\right] \cdot \\
&\cdot \left[\int_{-\infty}^{\infty} q(t_1)\delta(t_2-t_1)dt_1\right] dt_2 dt_4 \\
&= 12 \cdot f_{in}f_{ex}D_{ex}^2 \cdot \int_{-\infty}^{\infty}\int_{-\infty}^{\infty} e^{-k(t_4-t_2)} \cdot q(t_2)q(t_4) \cdot [q(t_4)][q(t_2)] dt_2 dt_4 \\
&= 12 \cdot f_{in}f_{ex}D_{ex}^2 \cdot \int_{-\infty}^{\infty}\int_{-\infty}^{\infty} e^{-k(t_4-t_2)} \cdot q(t_2)^2 q(t_4)^2 dt_2 dt_4
\end{aligned}
$$

Defining $t := t_4 - t_2$, $t \in [-T \quad T]$ gives:

$$V_4 = 12 \cdot f_{in}f_{ex}D_{ex}^2 \cdot \int_{-\infty}^{\infty}\int_{-\infty}^{\infty} e^{-k(t)} \cdot q(t_2)^2 q(t_2+t)^2 dt_2 dt$$

Final expression for $V_4$ :

$$V_4 = 12 \cdot f_{in}f_{ex}D_{ex}^2 \cdot \int_{-\infty}^{\infty} e^{-kt} Q_4(t) dt \tag{B.47}$$

where $Q_4(t)$ is the correlation

$$Q_4(t) := \int_{-\infty}^{\infty} q(t_2)^2 q(t_2+t)^2 dt_2$$

It is instructive to collect the derived variance terms before proceeding to the mean terms. Recall the decomposition:

$$\langle \phi(T)^4 \rangle = V_1 + V_2 + V_3 + V_4 + M_1 + M_2 + M_3 + M_4 \tag{B.48}$$

The work presented so far has shown that

$$V_1+V_2+V_3+V_4 = 12\cdot\frac{f_{in}f_{ex}}{4\pi^2}\int_{-\infty}^{\infty}e^{-kt}\int_{-\infty}^{\infty}\int_{-\infty}^{\infty}D(\omega)\cdot D(\omega_1)Q(\omega)\cdot Q(\omega_1)\cdot$$
$$\cdot Q_2(t,\omega,\omega_1)d\omega d\omega_1 dt + -12\cdot\frac{f_{in}f_{ex}D_{ex}}{2\pi}\int_{-\infty}^{\infty}e^{-kt}\int_{-\infty}^{\infty}D(\omega)\cdot$$
$$\cdot Q(\omega)\cdot Q_3(t,\omega)d\omega dt + -12\cdot\frac{f_{in}f_{ex}D_{ex}}{2\pi}\int_{-\infty}^{\infty}e^{-kt}\int_{-\infty}^{\infty}D(\omega)\cdot$$
$$\cdot Q(\omega)\cdot Q_3(t,\omega)d\omega dt + 12\cdot f_{in}f_{ex}D_{ex}^2\cdot\int_{-\infty}^{\infty}e^{-kt}Q_4(t)dt$$

That is

$$V_1+V_2+V_3+V_4 = 12\cdot f_{in}f_{ex}\int_{-\infty}^{\infty}e^{-kt}\left[\frac{1}{4\pi^2}\int_{-\infty}^{\infty}\int_{-\infty}^{\infty}D(\omega)\cdot D(\omega_1)Q(\omega)\cdot Q(\omega_1)\cdot\right.$$
$$\cdot Q_2(t,\omega,\omega_1)d\omega d\omega_1 - 2\cdot D_{ex}\cdot\frac{1}{2\pi}\int_{-\infty}^{\infty}D(\omega)\cdot Q(\omega)\cdot Q_3(t,\omega)d\omega +$$
$$\left.D_{ex}^2\cdot Q_4(t)\right]dt$$

where

$$Q_2(t,\omega,\omega_1) := \int_{-\infty}^{\infty}q(t_2)\cdot q(t_2+t)\cdot e^{i\omega_1 t_2}\cdot e^{i\omega(t_2+t)}dt_2$$
$$Q_3(t,\omega) := \int_{-\infty}^{\infty}q(t_2)\cdot q(t_2+t)^2\cdot e^{i\omega t_2}dt_2$$
$$Q_4(t) := \int_{-\infty}^{\infty}q(t_2)^2 q(t_2+t)^2 dt_2$$

The next step is to evaluate the mean terms $M_1, M_2, M_3$ and $M_4$.

***Evaluating*** $M_1$ :

$$M_1 = 12\cdot\int_{-\infty}^{\infty}\int_{-\infty}^{\infty}\int_{-\infty}^{\infty}\int_{-\infty}^{\infty}q(t_1)q(t_2)q(t_3)q(t_4)\cdot\left[\frac{f_{in}f_{in}}{4\pi^2}\left(\int_{-\infty}^{\infty}D(\omega)e^{i\omega(t_4-t_3)}d\omega\right)\cdot\right.$$
$$\left.\cdot\left(\int_{-\infty}^{\infty}D(\omega)e^{i\omega(t_2-t_1)}d\omega\right)\right]dt_1dt_2dt_3dt_4$$

$$= 12 \cdot \frac{f_{in}^2}{4\pi^2} \int_{-\infty}^{\infty}\int_{-\infty}^{\infty}\int_{-\infty}^{\infty}\int_{-\infty}^{\infty} q(t_1)q(t_2)q(t_3)q(t_4) \cdot \left[ \left( \int_{-\infty}^{\infty} D(\omega) e^{i\omega(t_4-t_3)} d\omega \right) \cdot \right.$$
$$\left. \cdot \left( \int_{-\infty}^{\infty} D(\omega) e^{i\omega(t_2-t_1)} d\omega \right) \right] dt_1 dt_2 dt_3 dt_4$$
$$= 12 \cdot \frac{f_{in}^2}{4\pi^2} \int_{-\infty}^{\infty} D(\omega) \left[ \int_{-\infty}^{\infty} q(t_1) e^{-i\omega t_1} dt_1 \right] \left[ \int_{-\infty}^{\infty} q(t_2) e^{i\omega t_2} dt_2 \right] d\omega \cdot$$
$$\cdot \int_{-\infty}^{\infty} D(\omega) \left[ \int_{-\infty}^{\infty} q(t_3) e^{-i\omega t_3} dt_3 \right] \left[ \int_{-\infty}^{\infty} q(t_4) e^{i\omega t_4} dt_4 \right] d\omega$$
$$= 12 \cdot \frac{f_{in}^2}{4\pi^2} \int_{-\infty}^{\infty} D(\omega)[Q(\omega)][Q^*(\omega)] d\omega \cdot \int_{-\infty}^{\infty} D(\omega_1)[Q(\omega_1)][Q^*(\omega_1)] d\omega_1$$

Final expression for $M_1$ :

$$M_1 = 12 \cdot \frac{f_{in}^2}{4\pi^2} \int_{-\infty}^{\infty} D(\omega)|Q(\omega)|^2 d\omega \cdot \int_{-\infty}^{\infty} D(\omega_1)|Q(\omega_1)|^2 d\omega_1 \tag{B.49}$$

***Evaluating*** $M_2$ :

$$M_2 = 12 \cdot \int_{-\infty}^{\infty}\int_{-\infty}^{\infty}\int_{-\infty}^{\infty}\int_{-\infty}^{\infty} q(t_1)q(t_2)q(t_3)q(t_4) \cdot \left[ f_{in} f_{ex} \cdot D_{ex} \delta(t_4 - t_3) \cdot \right.$$
$$\left. \cdot \left( \frac{1}{2\pi} \int_{-\infty}^{\infty} D(\omega) e^{i\omega(t_2-t_1)} d\omega \right) \right] dt_1 dt_2 dt_3 dt_4$$
$$= 12 \cdot \frac{f_{in} f_{ex} D_{ex}}{2\pi} \int_{-\infty}^{\infty}\int_{-\infty}^{\infty}\int_{-\infty}^{\infty}\int_{-\infty}^{\infty} q(t_1)q(t_2)q(t_3)q(t_4) \cdot \left[ \delta(t_4 - t_3) \cdot \right.$$
$$\left. \cdot \left( \int_{-\infty}^{\infty} D(\omega) e^{i\omega(t_2-t_1)} d\omega \right) \right] dt_1 dt_2 dt_3 dt_4$$
$$= 12 \cdot \frac{f_{in} f_{ex} D_{ex}}{2\pi} \int_{-\infty}^{\infty} q(t_3) \cdot \left[ \int_{-\infty}^{\infty} q(t_4) \delta(t_4 - t_3) dt_4 \right] \int_{-\infty}^{\infty} D(\omega) \cdot$$
$$\cdot \left[ \int_{-\infty}^{\infty} q(t_1) e^{-i\omega t_1} dt_1 \right] \cdot \left[ \int_{-\infty}^{\infty} q(t_2) e^{i\omega t_2} dt_2 \right] d\omega dt_3$$
$$= 12 \cdot \frac{f_{in} f_{ex} D_{ex}}{2\pi} \int_{-\infty}^{\infty} q(t_3) \cdot [q(t_3)] \int_{-\infty}^{\infty} D(\omega) \cdot [Q(\omega)] \cdot [Q^*(\omega)] \, d\omega dt_3$$

$$= 12 \cdot \frac{f_{in} f_{ex} D_{ex}}{2\pi} \int_{-\infty}^{\infty} q(t_3)^2 dt_3 \cdot \int_{-\infty}^{\infty} D(\omega)|Q(\omega)|^2 d\omega$$

Final expression for $M_2$ :

$$M_2 = 12 \cdot \frac{f_{in} f_{ex} D_{ex}}{2\pi} \cdot b \cdot \int_{-\infty}^{\infty} D(\omega)|Q(\omega)|^2 d\omega \tag{B.50}$$

***Evaluating*** $M_3$ :

$$\begin{aligned}
M_3 = & 12 \cdot \int_{-\infty}^{\infty}\int_{-\infty}^{\infty}\int_{-\infty}^{\infty}\int_{-\infty}^{\infty} q(t_1)q(t_2)q(t_3)q(t_4) \cdot \Big[ f_{in} f_{ex} \cdot D_{ex}\delta(t_2 - t_1) \cdot \\
& \cdot \left( \frac{1}{2\pi} \int_{-\infty}^{\infty} D(\omega) e^{i\omega(t_4 - t_3)} d\omega \right) \Big] dt_1 dt_2 dt_3 dt_4 \\
= & 12 \cdot \frac{f_{in} f_{ex} D_{ex}}{2\pi} \int_{-\infty}^{\infty}\int_{-\infty}^{\infty}\int_{-\infty}^{\infty}\int_{-\infty}^{\infty} q(t_1)q(t_2)q(t_3)q(t_4) \cdot \Big[ \delta(t_2 - t_1) \cdot \\
& \cdot \left( \int_{-\infty}^{\infty} D(\omega) e^{i\omega(t_4 - t_3)} d\omega \right) \Big] dt_1 dt_2 dt_3 dt_4 \\
= & 12 \cdot \frac{f_{in} f_{ex} D_{ex}}{2\pi} \int_{-\infty}^{\infty} q(t_2) \cdot \left[ \int_{-\infty}^{\infty} q(t_1)\delta(t_2 - t_1) dt_1 \right] \int_{-\infty}^{\infty} D(\omega) \cdot \\
& \cdot \left[ \int_{-\infty}^{\infty} q(t_3) e^{-i\omega t_3} dt_3 \right] \cdot \left[ \int_{-\infty}^{\infty} q(t_4) e^{i\omega t_4} dt_4 \right] d\omega dt_2 \\
= & 12 \cdot \frac{f_{in} f_{ex} D_{ex}}{2\pi} \int_{-\infty}^{\infty} q(t_2) \cdot [q(t_2)] \int_{-\infty}^{\infty} D(\omega) \cdot [Q(\omega)] \cdot [Q^*(\omega)] \, d\omega dt_2 \\
= & 12 \cdot \frac{f_{in} f_{ex} D_{ex}}{2\pi} \int_{-\infty}^{\infty} q(t_2)^2 dt_2 \cdot \int_{-\infty}^{\infty} D(\omega)|Q(\omega)|^2 d\omega
\end{aligned}$$

Final expression for $M_3$ :

$$M_3 = 12 \cdot \frac{f_{in} f_{ex} D_{ex}}{2\pi} \cdot b \cdot \int_{-\infty}^{\infty} D(\omega)|Q(\omega)|^2 d\omega \tag{B.51}$$

***Evaluating*** $M_4$ :

$$\begin{aligned}
M_4 &= 12 \cdot \int_{-\infty}^{\infty}\int_{-\infty}^{\infty}\int_{-\infty}^{\infty}\int_{-\infty}^{\infty} q(t_1)q(t_2)q(t_3)q(t_4)\cdot[f_{ex}f_{ex}D_{ex}\delta(t_4-t_3)\cdot \\
&\cdot D_{ex}\delta(t_2-t_1)]dt_1dt_2dt_3dt_4 \\
&= 12 \cdot f_{ex}^2 D_{ex}^2 \int_{-\infty}^{\infty}\int_{-\infty}^{\infty}\int_{-\infty}^{\infty}\int_{-\infty}^{\infty} q(t_1)q(t_2)q(t_3)q(t_4)\cdot[\delta(t_4-t_3)\cdot \\
&\cdot\delta(t_2-t_1)]dt_1dt_2dt_3dt_4 \\
&= 12 \cdot f_{ex}^2 D_{ex}^2 \int_{-\infty}^{\infty} q(t_1)\left[\int_{-\infty}^{\infty} q(t_2)\delta(t_2-t_1)dt_2\right]dt_1\cdot \\
&\int_{-\infty}^{\infty} q(t_3)\left[\int_{-\infty}^{\infty} q(t_4)\delta(t_4-t_3)dt_4\right]dt_3 \\
&= 12 \cdot f_{ex}^2 D_{ex}^2 \int_{-\infty}^{\infty} q(t_1)\left[q(t_1)\right]dt_1\cdot\int_{-\infty}^{\infty} q(t_3)\left[q(t_3)\right]dt_3 \\
&= 12 \cdot f_{ex}^2 D_{ex}^2 \int_{-\infty}^{\infty} q(t_1)^2dt_1\cdot\int_{-\infty}^{\infty} q(t_3)^2dt_3
\end{aligned}$$

Final expression for $M_4$ :

$$M_4 = 12 \cdot f_{ex}^2 D_{ex}^2 \cdot b^2 \tag{B.52}$$

The mean terms will be gathered here before presenting a final signal representation. Recall

$$\langle\phi(T)^4\rangle = V_1 + V_2 + V_3 + V_4 + M_1 + M_2 + M_3 + M_4$$

where the mean terms are now given by

$$\begin{aligned}
M_1 + M_2 + M_3 + M_4 = 12 \cdot \frac{f_{in}^2}{4\pi^2}\int_{-\infty}^{\infty} D(\omega)|Q(\omega)|^2d\omega \cdot \int_{-\infty}^{\infty} D(\omega_1)|Q(\omega_1)|^2d\omega_1 \\
+ 12 \cdot \frac{f_{in}f_{ex}D_{ex}}{2\pi}\cdot b\cdot\int_{-\infty}^{\infty} D(\omega)|Q(\omega)|^2d\omega \\
+ 12 \cdot \frac{f_{in}f_{ex}D_{ex}}{2\pi}\cdot b\cdot\int_{-\infty}^{\infty} D(\omega)|Q(\omega)|^2d\omega \\
+ 12 \cdot f_{ex}^2 D_{ex}^2 \cdot b^2
\end{aligned}$$

It is important to notice that the expression above can also be written

$$M_1 + M_2 + M_3 + M_4 = 3 \cdot \left[2 \cdot \left(\frac{f_{in}}{2\pi}\int_{-\infty}^{\infty} D(\omega)|Q(\omega)|^2d\omega + f_{ex}D_{ex}\cdot b\right)\right]^2 \tag{B.53}$$

In other words

$$M_1 + M_2 + M_3 + M_4 = 3 \cdot \langle \phi(T)^2 \rangle^2 \tag{B.54}$$

The second- and fourth-order cumulants of the phase distribution ($c_2 = \langle \phi(T)^2 \rangle$ and $c_4 = \langle \phi(T)^4 \rangle - 3 \cdot \langle \phi(T)^2 \rangle^2$, respectively) can now be evaluated to arrive at the final signal equation describing exchange and restriction. $c_2$ has already been evaluated since it is equal to the second-order moment of the phase distribution. $c_4$ can be obtained by considering that

$$\begin{aligned} c_4 &= \langle \phi(T)^4 \rangle - 3 \cdot \langle \phi(T)^2 \rangle^2 \\ &= [V_1 + V_2 + V_3 + V_4 + M_1 + M_2 + M_3 + M_4] - 3 \cdot \langle \phi(T)^2 \rangle^2 \\ &= V_1 + V_2 + V_3 + V_4 \end{aligned}$$

where the last equality comes from the finding that $M_1 + M_2 + M_3 + M_4 = 3 \cdot \langle \phi(T)^2 \rangle^2$.

## Final signal representation

The final signal equation can now be expressed:

$$\ln(S/S_0) \approx -\frac{1}{2} c_2 + \frac{1}{24} c_4 \tag{B.55}$$

where

$$c_2 = 2 \left( \frac{f_{in}}{2\pi} \int_{-\infty}^{\infty} D(\omega) \cdot |Q(\omega)|^2 d\omega + f_{ex} \cdot D_{ex} \cdot b \right)$$

and

$$\begin{aligned} c_4 = 12 \cdot f_{in} f_{ex} \int_{-\infty}^{\infty} e^{-kt} \Bigg[ & \frac{1}{4\pi^2} \int_{-\infty}^{\infty} \int_{-\infty}^{\infty} D(\omega) \cdot D(\omega_1) Q(\omega) \cdot Q(\omega_1) \cdot \\ & \cdot Q_2(t, \omega, \omega_1) d\omega d\omega_1 - 2 \cdot D_{ex} \cdot \frac{1}{2\pi} \int_{-\infty}^{\infty} D(\omega) \cdot Q(\omega) \cdot Q_3(t, \omega) d\omega + \\ & D_{ex}^2 \cdot Q_4(t) \Bigg] dt \end{aligned}$$

where

$$\begin{aligned} Q_2(t, \omega, \omega_1) &:= \int_{-\infty}^{\infty} q(t_2) \cdot q(t_2 + t) \cdot e^{i\omega_1 t_2} \cdot e^{i\omega(t_2 + t)} dt_2 \\ Q_3(t, \omega) &:= \int_{-\infty}^{\infty} q(t_2) \cdot q(t_2 + t)^2 \cdot e^{i\omega t_2} dt_2 \\ Q_4(t) &:= \int_{-\infty}^{\infty} q(t_2)^2 q(t_2 + t)^2 dt_2 \end{aligned}$$

We are done.

## Appendix B4: On the validity of $\langle v(t_1)v(t_2)v(t_3)v(t_4)\rangle \approx 3\cdot\langle v(t_1)v(t_2)\rangle\cdot\langle v(t_3)v(t_4)\rangle$

This section evaluates the validity of the approximation:

$$\begin{aligned}\langle v(t_1)v(t_2)v(t_3)v(t_4)\rangle &= \langle v(t_1)v(t_2)\rangle\cdot\langle v(t_3)v(t_4)\rangle + \langle v(t_1)v(t_3)\rangle\cdot\langle v(t_2)v(t_4)\rangle + \\ &\quad \langle v(t_1)v(t_4)\rangle\cdot\langle v(t_2)v(t_3)\rangle \\ &\approx 3\cdot\langle v(t_1)v(t_2)\rangle\cdot\langle v(t_3)v(t_4)\rangle \end{aligned} \tag{B.56}$$

by comparing the fourth-order phase moment ($\langle\phi(T)^4\rangle$) evaluated using

$$\langle v(t_1)v(t_2)v(t_3)v(t_4)\rangle \approx 3\cdot\langle v(t_1)v(t_2)\rangle\cdot\langle v(t_3)v(t_4)\rangle$$

to that obtained using the full expression:

$$\begin{aligned}\langle v(t_1)v(t_2)v(t_3)v(t_4)\rangle =& \langle v(t_1)v(t_2)\rangle\cdot\langle v(t_3)v(t_4)\rangle + \langle v(t_1)v(t_3)\rangle\cdot\langle v(t_2)v(t_4)\rangle + \\ & \langle v(t_1)v(t_4)\rangle\cdot\langle v(t_2)v(t_3)\rangle\end{aligned}$$

This is done for the long-time limit where there is exchange and Gaussian diffusion. The Maple script in Appendix B1 gives segments of the mean velocity autocorrelation function corresponding to the factors $\langle v(t_1)v(t_2)\rangle\cdot\langle v(t_3)v(t_4)\rangle$, $\langle v(t_1)v(t_3)\rangle\cdot\langle v(t_2)v(t_4)\rangle$ and $\langle v(t_1)v(t_4)\rangle\cdot\langle v(t_2)v(t_3)\rangle$ as

$$\begin{aligned}\langle v(t_1)v(t_2)v(t_3)v(t_4)\rangle_a &= 4\cdot f_{in}f_{ex}(D_{ex}-D_{in})^2\cdot\delta(t_2-t_1)\delta(t_4-t_3)e^{-k(t_4-t_2)} + \\ &\quad 4\cdot(f_{in}D_{in}+f_{ex}D_{ex})^2\cdot\delta(t_2-t_1)\delta(t_4-t_3),\end{aligned} \tag{B.57}$$

$$\begin{aligned}\langle v(t_1)v(t_2)v(t_3)v(t_4)\rangle_b &= 4\cdot f_{in}f_{ex}(D_{ex}-D_{in})^2\cdot\delta(t_3-t_1)\delta(t_4-t_2)e^{-k(t_4-t_2)} + \\ &\quad 4\cdot(f_{in}D_{in}+f_{ex}D_{ex})^2\cdot\delta(t_3-t_1)\delta(t_4-t_2)\end{aligned} \tag{B.58}$$

and

$$\begin{aligned}\langle v(t_1)v(t_2)v(t_3)v(t_4)\rangle_c &= 4\cdot f_{in}f_{ex}(D_{ex}-D_{in})^2\cdot\delta(t_3-t_2)\delta(t_4-t_1)e^{-k(t_4-t_2)} + \\ &\quad 4\cdot(f_{in}D_{in}+f_{ex}D_{ex})^2\cdot\delta(t_3-t_2)\delta(t_4-t_1)\end{aligned} \tag{B.59}$$

respectively. Note the similarity between all three terms. The subscripts $a, b, c$ are meant to indicate that the three terms above are components of the mean fourth-order velocity autocorrelation function, such that $\langle v(t_1)v(t_2)v(t_3)v(t_4)\rangle = \langle v(t_1)v(t_2)v(t_3)v(t_4)\rangle_a + \langle v(t_1)v(t_2)v(t_3)v(t_4)\rangle_b + \langle v(t_1)v(t_2)v(t_3)v(t_4)\rangle_c$. Components of the fourth-order phase

moment can now be evaluated for all three terms above.

***Deriving*** $\langle\phi(T)^4\rangle_a$

Component $a$ was derived in Appendix B2 and is provided below for ease of comparison:

$$\langle\phi(T)^4\rangle_a = 4\cdot\mathrm{Var}(D)\int_0^T e^{-k(t_4-t_2)}\int_0^T q(t_2)^2q(t_4)^2dt_2dt_4 + 4\cdot\overline{D}^2b^2$$

***Deriving*** $\langle\phi(T)^4\rangle_b$

$$\begin{aligned}
\langle\phi(T)^4\rangle_b &= \int_0^T\int_0^T\int_0^T\int_0^T q(t_1)q(t_2)q(t_3)q(t_4)\langle v(t_1)v(t_2)v(t_3)v(t_4)\rangle dt_1dt_2dt_3dt_4\\
&= \int_0^T\int_0^T\int_0^T\int_0^T q(t_1)q(t_2)q(t_3)q(t_4)[4\cdot\mathrm{Var}(D)\cdot\delta(t_3-t_1)\delta(t_4-t_2)e^{-k(t_4-t_2)}+\\
&\qquad 4\cdot\overline{D}^2\cdot\delta(t_3-t_1)\delta(t_4-t_2)]dt_1dt_2dt_3dt_4\\
&= 4\cdot\mathrm{Var}(D)\int_0^T e^{-k(t_4-t_2)}\int_0^T q(t_2)q(t_3)\int_{-\infty}^{\infty}q(t_1)\delta(t_3-t_1)dt_1\int_{-\infty}^{\infty}q(t_4)\delta(t_4-t_2)dt_4dt_2dt_3\\
&\quad + 4\cdot\overline{D}^2\int_0^T q(t_2)\int_0^T q(t_3)\int_{-\infty}^{\infty}q(t_1)\delta(t_3-t_1)dt_1\int_{-\infty}^{\infty}q(t_4)\delta(t_4-t_2)dt_4dt_2dt_3\\
&= 4\cdot\mathrm{Var}(D)\int_0^T e^{-k(t_4-t_2)}\int_0^T q(t_2)^2q(t_3)^2dt_3dt_2 + 4\cdot\overline{D}^2\int_0^T q(t_2)^2dt_2\int_0^T q(t_3)^2dt_3\\
&= 4\cdot\mathrm{Var}(D)\int_0^T e^{-k(t_4-t_2)}\int_0^T q(t_2)^2q(t_3)^2dt_3dt_2 + 4\cdot\overline{D}^2b^2
\end{aligned}$$

***Deriving*** $\langle\phi(T)^4\rangle_c$

$$\begin{aligned}
\langle\phi(T)^4\rangle_c &= \int_0^T\int_0^T\int_0^T\int_0^T q(t_1)q(t_2)q(t_3)q(t_4)\langle v(t_1)v(t_2)v(t_3)v(t_4)\rangle dt_1dt_2dt_3dt_4\\
&= \int_0^T\int_0^T\int_0^T\int_0^T q(t_1)q(t_2)q(t_3)q(t_4)[4\cdot\mathrm{Var}(D)\cdot\delta(t_4-t_1)\delta(t_3-t_2)e^{-k(t_4-t_2)}+\\
&\qquad 4\cdot\overline{D}^2\cdot\delta(t_4-t_1)\delta(t_3-t_2)]dt_1dt_2dt_3dt_4\\
&= 4\cdot\mathrm{Var}(D)\int_0^T e^{-k(t_4-t_2)}\int_0^T q(t_2)q(t_4)\int_{-\infty}^{\infty}q(t_1)\delta(t_4-t_1)dt_1\int_{-\infty}^{\infty}q(t_3)\delta(t_3-t_2)dt_3dt_2dt_4
\end{aligned}$$

$$+ 4 \cdot \overline{D}^2 \int_0^T q(t_2) \int_0^T q(t_4) \int_{-\infty}^{\infty} q(t_1)\delta(t_3 - t_1)dt_1 \int_{-\infty}^{\infty} q(t_3)\delta(t_3 - t_2)dt_3 dt_2 dt_4$$

$$= 4 \cdot \mathrm{Var}(D) \int_0^T e^{-k(t_4-t_2)} \int_0^T q(t_2)^2 q(t_4)^2 dt_2 dt_4 + 4 \cdot \overline{D}^2 \int_0^T q(t_2)^2 dt_2 \int_0^T q(t_4)^2 dt_4$$

$$= 4 \cdot \mathrm{Var}(D) \int_0^T e^{-k(t_4-t_2)} \int_0^T q(t_2)^2 q(t_4)^2 dt_2 dt_4 + 4 \cdot \overline{D}^2 b^2$$

The fourth-order moment is given by $\langle \phi(T)^4 \rangle = \langle \phi(T)^4 \rangle_a + \langle \phi(T)^4 \rangle_b + \langle \phi(T)^4 \rangle_c$:

$$\begin{aligned}\langle \phi(T)^4 \rangle =& 4 \cdot \mathrm{Var}(D) \int_0^T e^{-k(t_4-t_2)} \int_0^T q(t_2)^2 q(t_4)^2 dt_2 dt_4 + 4 \cdot \overline{D}^2 b^2 + \\ & 4 \cdot \mathrm{Var}(D) \int_0^T e^{-k(t_4-t_2)} \int_0^T q(t_2)^2 q(t_3)^2 dt_3 dt_2 + 4 \cdot \overline{D}^2 b^2 + \\ & 4 \cdot \mathrm{Var}(D) \int_0^T e^{-k(t_4-t_2)} \int_0^T q(t_2)^2 q(t_4)^2 dt_2 dt_4 + 4 \cdot \overline{D}^2 b^2 \end{aligned} \tag{B.60}$$

The simplification

$$\langle v(t_1)v(t_2)v(t_3)v(t_4) \rangle \approx 3 \cdot \langle v(t_1)v(t_2) \rangle \cdot \langle v(t_3)v(t_4) \rangle$$

is equivalent to assuming

$$\langle \phi(T)^4 \rangle \approx 3 \cdot \langle \phi(T)^4 \rangle_a$$

That is, assuming that the components $\langle \phi(T)^4 \rangle_b$ and $\langle \phi(T)^4 \rangle_c$ are both equal to $\langle \phi(T)^4 \rangle_a$. Note that $\langle \phi(T)^4 \rangle_a$ and $\langle \phi(T)^4 \rangle_c$ are identical in every respect, but exhibit a slight discrepancy from $\langle \phi(T)^4 \rangle_b$ in the terms in $q$. Thus, the assumption above is equivalent to assuming:

$$4 \cdot \mathrm{Var}(D) \int_0^T e^{-k(t_4-t_2)} \int_0^T q(t_2)^2 q(t_3)^2 dt_3 dt_2 \approx 4 \cdot \mathrm{Var}(D) \int_0^T e^{-k(t_4-t_2)} \int_0^T q(t_2)^2 q(t_4)^2 dt_2 dt_4$$

which reduces to

$$\int_0^T e^{-k(t_4-t_2)} \int_0^T q(t_2)^2 q(t_3)^2 dt_3 dt_2 \approx \int_0^T e^{-k(t_4-t_2)} \int_0^T q(t_2)^2 q(t_4)^2 dt_2 dt_4$$

or:

$$\int_0^T q(t_2)^2 q(t_3)^2 dt_3 \approx \int_0^T q(t_2)^2 q(t_4)^2 dt_4$$

Equivalently:

$$t_3 \approx t_4$$

The approximation in equation B.56 becomes an equality when the time points $t_3$ and $t_4$ are equal. A simple rearrangement of the integrals in $q(t)$ shows that the same is true when any two time points in the set $\{t_1, t_2, t_3, t_4\}$ are equal.